Advances in the use of biomass-derived carbons for sodium-ion batteries

SUN Mei-ci[1], QI Shuo-lin[1], ZHAO Yun-he[1], CHEN Chun-xia[1], TAN Li-chao[2], HU Zhong-li[3,*], WU Xiao-liang[1,*], ZHANG Wen-li[4,5,6,*]

(1. *Center for Innovative Research in Synthetic Chemistry and Resource Utilization, College of Chemistry, Chemical Engineering and Resource Utilization, Northeast Forestry University, Harbin* 150040, *China*;
2. *Institute of Carbon Neutrality, Zhejiang Wanli University, Ningbo*, 315100, *China*;
3. *College of Chemistry and Chemical Engineering, Chongqing University of Technology, Chongqing* 400054, *China*;
4. *Guangdong Provincial Key Laboratory of Plant Resources Biorefinery, School of Chemical Engineering and Light Industry, Guangdong University of Technology (GDUT), Guangzhou* 510006, *China*;
5. *Jieyang Branch of Chemistry and Chemical Engineering Guangdong Laboratory (Rongjiang Laboratory), Jieyang* 515200, *China*;
6. *School of Advanced Manufacturing, Guangdong University of Technology (GDUT), Jieyang* 522000, *China*)

Abstract: Sodium-ion batteries (SIBs) have emerged as a promising alternative to commercial lithium-ion batteries because of the similar properties of Li and Na as well as the abundance and accessibility of sodium resources. The development of anode materials with a high capacity, excellent rate performance, and long cycle life is the key to the industrialization of SIBs. Biomass-derived carbon (BDC) anode materials synthesized from resource-rich, low-cost, and renewable biomass have been extensively researched and their excellent sodium storage performance has been proven, making them the most promising new low-cost and high-performance anode material for SIBs. This review first introduces the sources of BDCs, including waste biomass such as plants, animals, and microorganisms, and then describes several methods for preparing BDC anode materials, including carbonization, chemical activation, and template methods. The storage mechanism and kinetic process of Na^+ in BDCs are then considered as well as their structure control. The electrochemical properties of sodium-ion storage in BDCs with different structures are examined, and suggestions for future research are made.

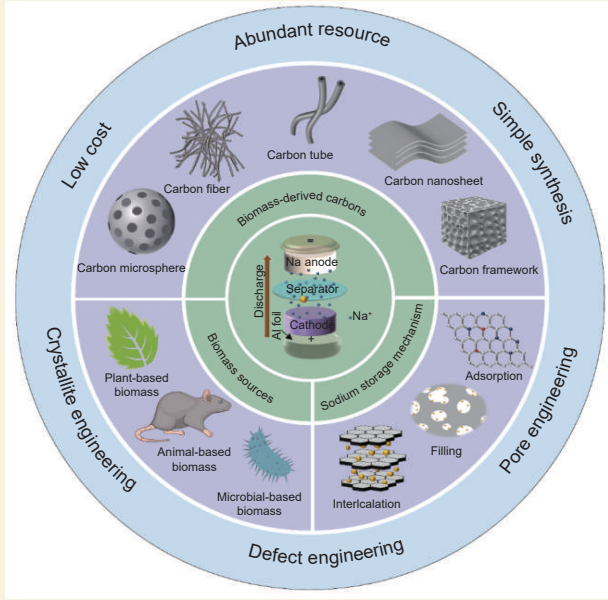

Key words: Biomass；Carbon；Anode materials；Sodium storage mechanism；Microstructure

1 Introduction

The depletion of fossil fuels and their environmental impact has become a major constraint on the global economy and modern industry, and the development of clean, non-polluting renewable energy sources is an effective solution to energy and environmental problems[1–2]. However, the widespread use of renewable energy exposes issues such as intermittency and instability, so it is particularly crucial to research safe and reliable new energy storage systems and devices[3–4]. In recent years, lithium-ion batteries (LIBs), a new type of energy storage device, have been widely used in 3C electronic products (communications, computers, and consumer), electric vehicles, and smart grids due to their unique advantages such as high capacity, long life, flexibility, and lightweight design[5–7]. Furthermore, due to geographical factors, lithium resources are unevenly distributed worldwide, increasing the cost of lithium-ion bat-

Received August 05, 2024
Revised December 13, 2024
Accepted December 15, 2024

tery production[8–9]. Therefore, to promote the diversification of the energy storage market, it is imperative to find a new and reliable energy storage device.

To address these issues, researchers have focused their attention on the development of low-cost, high-capacity, high-rate performance and long-cycle sodium-ion batteries (SIBs). Sodium is located in the same main group as lithium on the periodic table and shares similar physical and chemical properties. It has a concentration of 2.75% compared to 0.0065% for lithium. Additionally, sodium has a low development cost, meanwhile, SIBs offer several advantages, including high safety, no over-discharge, good interfacial reaction kinetics, and excellent performance at both high and low temperatures. Moreover, during charging and discharging, SIBs exhibit the intercalation/deintercalation mechanism similar to that of LIBs. Furthermore, it is worth noting that the standard potential of Na^+/Na (−2.7 V vs. SHE) is approximately 0.3 V higher than that of Li^+/Li (−3.04 V vs. SHE) and SIBs can use water-based electrolytes instead of organic electrolytes[10–12]. While SIBs may not have an advantage in energy density and are unlikely to replace LIBs as the mainstream energy storage devices in the short term, their significant low-cost characteristics make them a promising option for low-speed electric vehicles and large-scale energy storage systems[13–15].

SIBs are composed similarly to LIBs, comprising a cathode, electrolyte, separator, anode and cell case (Fig. 1a). The electrochemical performance of the battery is primarily contingent upon the cathode and anode materials. The SIBs operate on a working principle that is akin to the “rocking chair” lithium-ion battery, which was proposed by Armand et al. in 1972[16]. During the charging process, Na^+ ions are extracted from the cathode material and subsequently embedded into the anode material through the electrolyte. Simultaneously, compensating electrons are transferred to the anode via the external circuit to en-

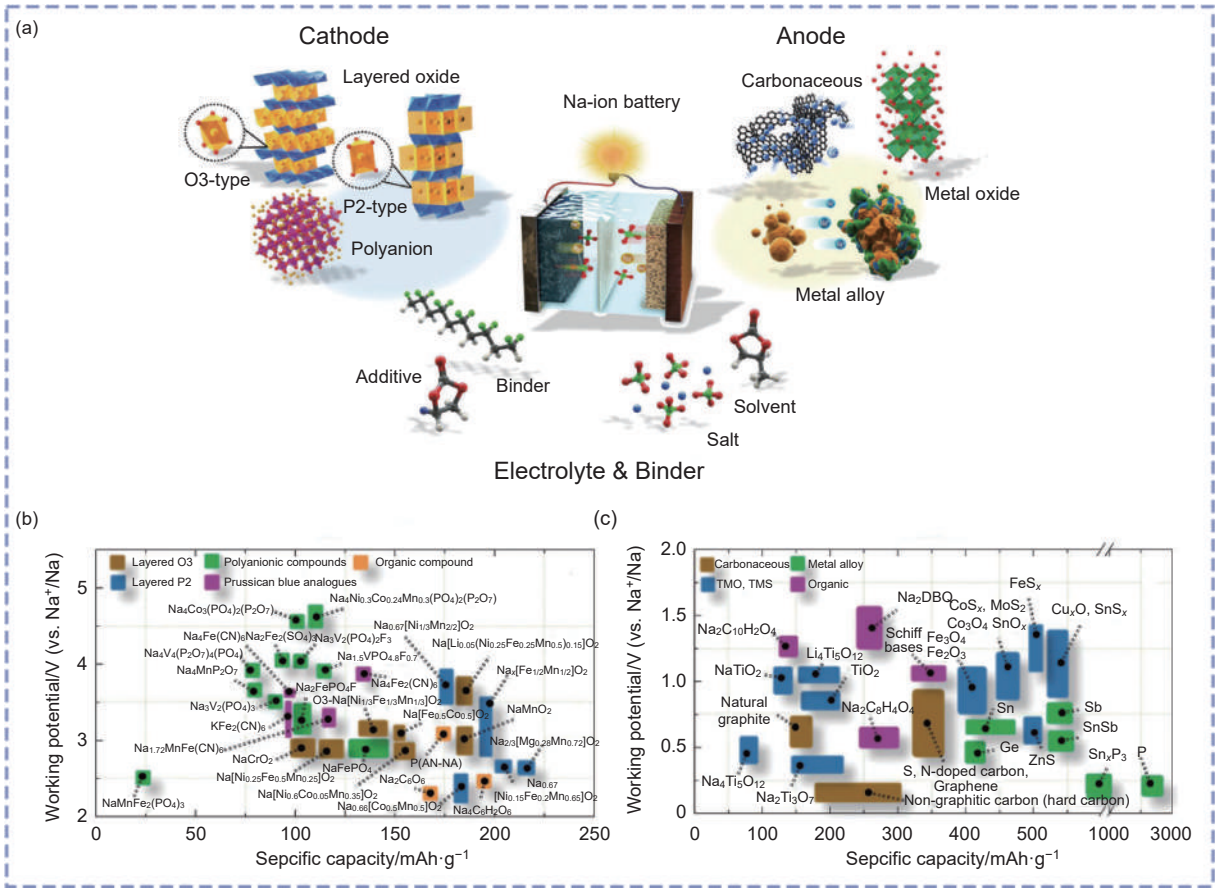

Fig. 1 (a) Working mechanism of SIBs[13]. (b, c) Comparison of reversible capacity and average voltage of the reported cathode materials for sodium ion half batteries[13]. Reprinted with permission

sure a balanced charge between the cathode and anode. Conversely, in the discharge process, Na^+ ions are removed from the anode material and re-embedded into the lattice of the cathode material via interaction within the sodium-ion-containing electrolyte. In the "rocking chair" charging and discharging process, the battery system relies on the reversible embedding of ions between the cathode and anode electrode materials to complete the charging and discharging, so the main key to research into the SIBs system is the development of high-performance electrode materials that can be embedded with Na^+. Fig. 1b presents typical cathode materials for SIBs. For cathode materials, such as transition metal oxide[17–18], Prussian blue analogs[19–21], polyanions[22–24], organic compounds[25–26], etc. have made great progress in recent years, the performances of many cathode materials are comparable to the level of commercial LIBs, the current research bottleneck is mainly focused on the development and design of advanced anode materials.

Various materials have been reported for use as main anodes in SIBs, including metals/alloys[27–29], metal oxides/sulfides/phosphides[30–32], titanium-based materials[33–35], and carbon-based materials[36–37] (Fig. 1c). Of the materials mentioned above, titanium-based materials exhibit lower conductivity, resulting in relatively low reversible capacity and initial Coulombic efficiency (ICE), which consequently reduces the energy density of the battery system. Although transition metal oxides and sulfides typically provide high reversible capacity, they have poor cycling stability, and low ICE and are associated with a large hysteresis phenomenon, all of which can adversely affect the practical use of the battery. Carbon-based materials are expected to be the first anode in large-scale sodium-ion energy storage devices due to their abundant resources, good stability, higher capacity, low cost and other technological advantages.

Conventional commercial graphite has been widely used as the anode material for LIBs, but the radius of Na^+ (0.102 nm) is larger than that of Li^+ (0.076 nm), resulting in more difficult transport and transfer of Na^+ during charging and discharging. The narrow interlayer spacing of graphite is not conducive to intercalation/deintercalation of Na^+ and has a lower reversible capacity (35 mAh g^{-1}) as SIB anode[38–39]. Thus, an immediate requirement is to create innovative and alternative carbon-based anode materials that can efficiently store Na^+. Carbon-based materials, including expanded graphite, nanocarbon, and amorphous carbon (soft carbon and hard carbon), have been demonstrated to ensure free insertion/extraction of Na^+ during charging and discharging[40]. In 2000, Stevens and Dahn[41] found that hard carbon has a reversible capacity close to 300 mAh g^{-1}. However, another amorphous carbon, soft carbon, as an SIB anode has a relatively low sodium storage capacity. For example, due to the insufficient interlayer distances for ion intercalation, the sodium storage capacities of anthracite and bitumen-derived soft carbons without additional treatment were only 222 mAh g^{-1} and less than 100 mAh g^{-1}, respectively[42–43]. Consequently, the researchers concentrated on hard carbon anodes. They discovered that hard carbon materials with large interlayer spacing and high disorder can achieve high specific sodium storage capacity, low sodium storage potential and excellent cycling stability. These findings suggest that non-graphitic carbon materials have great potential as anode materials for SIBs[44]. Common hard carbon precursors include biomass, carbohydrates and polymer, among which, polymer precursors such as phenolic resins, polyaniline and polyacrylonitrile can be used to synthesize high-purity carbon materials with adjustable microstructures and morphologies while guaranteeing high carbon yields (≈ 50%), and are therefore widely used for the production of hard carbon materials at the industrial level. However, most polymeric precursors have been found to have a detrimental impact on the environment, largely due to the use of petrochemical resources and the reliance on toxic precursors (such as phenol and formaldehyde) in their production processes, which hinders its sustainable mass production and application. Based on this, the biosourced precursors (biomass and carbohydrates) have become a research hotspot for advancing the commercialization of hard car-

bon anode materials, especially low-cost biomass precursors.

Various biomasses have been used to prepare anode materials for SIBs, such as banana peels[45], corn cobs[46], peanut skin[47], cotton[48], wood[49], etc., all of which show excellent electrochemical properties. However, when considering practical applications, biomass-derived carbon (BDC) may encounter issues such as a reduced number of effective storage sites, slower diffusion kinetics, and low electronic conductivity. To address these issues, it is necessary to optimize the intrinsic structure of carbon materials derived from biomasses. This can be achieved by regulating interlayer spacing and graphite microcrystalline domains, increasing reversible sodium storage active sites, and doping with heteroatoms to obtain BDC anode materials with unique microstructures. These measures can enhance the electrochemical performances of the materials in SIBs[50]. Furthermore, as the sodium storage mechanism of hard carbon materials is still a matter of debate and there are no established criteria for selecting and processing carbon material precursors, a comprehensive understanding of the sodium storage mechanism of BDCs can aid in the development of BDCs anode materials for sodium storage with appropriate structures.

With the increasing research on BDCs, researchers have published a large number of review articles on the application of biocarbon-based materials to SIBs in recent years, which mainly summarise the research progress on the synthesis methods, optimization strategies, electrochemical properties and sodium storage mechanisms of BDCs. For example, Zhao et al.[51] discussed the relationship between the properties of hard carbon obtained from biomass and sodium storage performance. Molaiyan et al.[52] summarised different synthesis strategies for BDC anode materials applied to high-performance SIBs. Konarov et al.[53] focused on the effect of the carbonization temperature and heteroatom doping on the physical and electrochemical properties of biowaste-derived hard carbon. Zhang et al.[54] discussed structural regulation strategies to improve the sodium storage performance of biomass-based carbon anodes. Wang et al.[55] reviewed the effect of different micromorphologies and compositions of biomass carbon used for SIBs on the electrochemical performance. Alvira et al.[9] provided an overview of the current state of research on plant-derived hard carbon anodes in SIBs, with a detailed description of the mechanisms and models proposed so far for the storage of Na^+ ions in hard carbon anodes. However, we believe that further elucidation of the correlation between the microstructural characteristics, sodium storage behaviors, functionalization modification strategies, and electrochemical performance of BDCs is equally important for the design of high-performance anodes. Therefore, it is time to conduct a systematic review of recent research advances on the structure-property relationships of BDCs for SIBs to provide strategic guidance for the rational design of BDC materials in next-generation energy storage systems. Firstly, the basic research background of BDCs, including sources, structural characteristics, and preparation methods, is introduced in this review. Secondly, the structural regulation engineering for optimizing the sodium storage performance of BDCs is summarized, starting from the sodium storage active sites and models of BDCs. On this basis, the structural design, and electrochemical properties of BDC anode materials with different morphologies are analyzed in detail. Finally, we highlight the challenges faced by BDCs as high-performance practical SIB anode materials in the application and look forward to prospective research directions for future development (Fig. 2).

2 Overview of BDCs

2.1 Sources and structural characteristics of biomass

Biomass is a kind of renewable organic material, which refers to organic matter produced directly or indirectly through photosynthesis, mainly carbohydrates, such as starch, protein, cellulose, lignin, etc. It is derived from a variety of sources, including plants, animals and microorganisms (Fig. 3a)[56]. Biomass is clean, renewable, low-cost, resource-rich, widely distributed, and environmentally friendly,

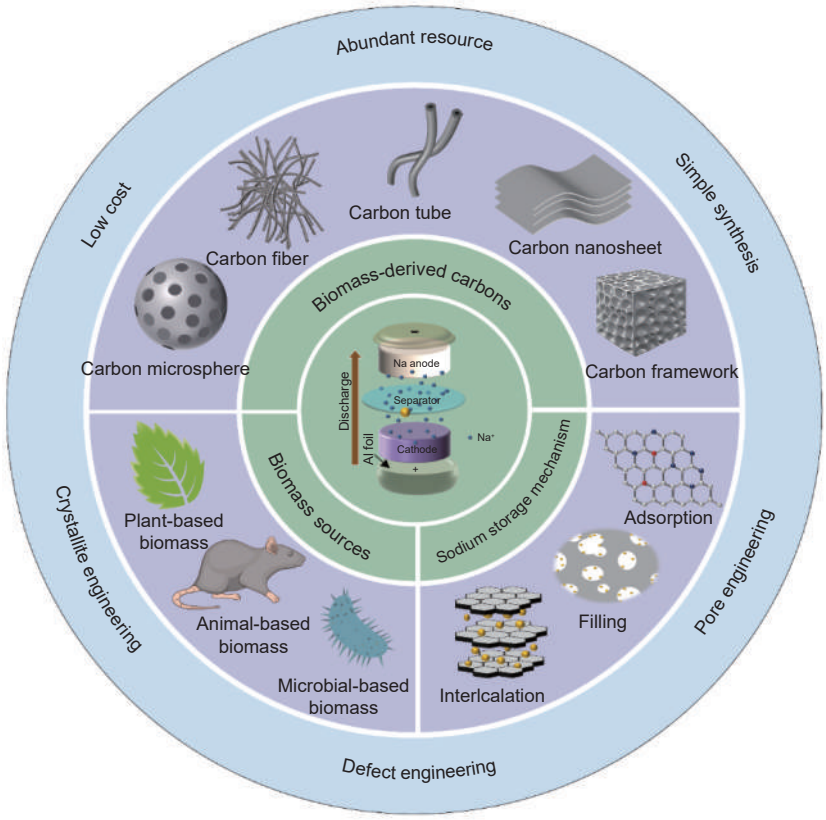

Fig. 2 Schematic illustration of sources and different morphologies of BDCs and their sodium storage mechanism

making it an excellent raw material for the preparation of carbon-based materials. The choice of biomass can directly determine the structure, morphology, and composition of the derived carbon and subsequently, the parameters such as pore size distribution and specific surface area (SSA) of the electrode material, which could ultimately affect the performance of the energy storage device.

Green plants, as producers in the food chain, can be found everywhere on earth, and agricultural wastes and by-products are the most widely used biomass due to their abundance and low price[58]. Plants contain significant amounts of organic compounds (40%–50% cellulose, 25% hemicelluloses, 20% lignin) and trace amounts of inorganic minerals. The structure of organic compounds is nonlinear, consisting of strong interconnections and chemical covalent bonding, which enables the carbon skeleton formed after carbonization to exhibit abundant nanovoids and randomly oriented graphene layers. The inorganic minerals, when removed, can be used as porogenic agents to form nanopores, including micropores and mesopores, which facilitates the rapid transport and diffusion of ions. The use of plant-derived carbon materials as energy storage materials is an effective strategy for achieving high-value utilization. For example, woody plants such as poplar wood[59], bamboo[60], and ginkgo[61] have been used as the precursors of hard carbon anode materials for high-performance SIBs. Various agricultural wastes, such as straw biomass (e.g., corn straw[62], wheat straw[63], etc.), seed biomass (e.g., oak seeds[64], pine pollen[65], etc.), shell biomass (e.g., peanut shells[66], coconut husks[67], etc.), and rind biomass (e.g., banana peel[68], orange peel[69] etc.), can also be used to produce biomass-derived carbon materials. The natural fiber structure of this kind of plant makes it easy to facilitate the formation of porous carbon materials directly after high-temperature heat treatment, which can promote the rapid transfer of charge and improve the storage and transportion of ions. In addition, aquatic plants such as lotus, duckweed, kelp and algae[70–72] are also potential biomass precursors for high-performance energy storage devices.

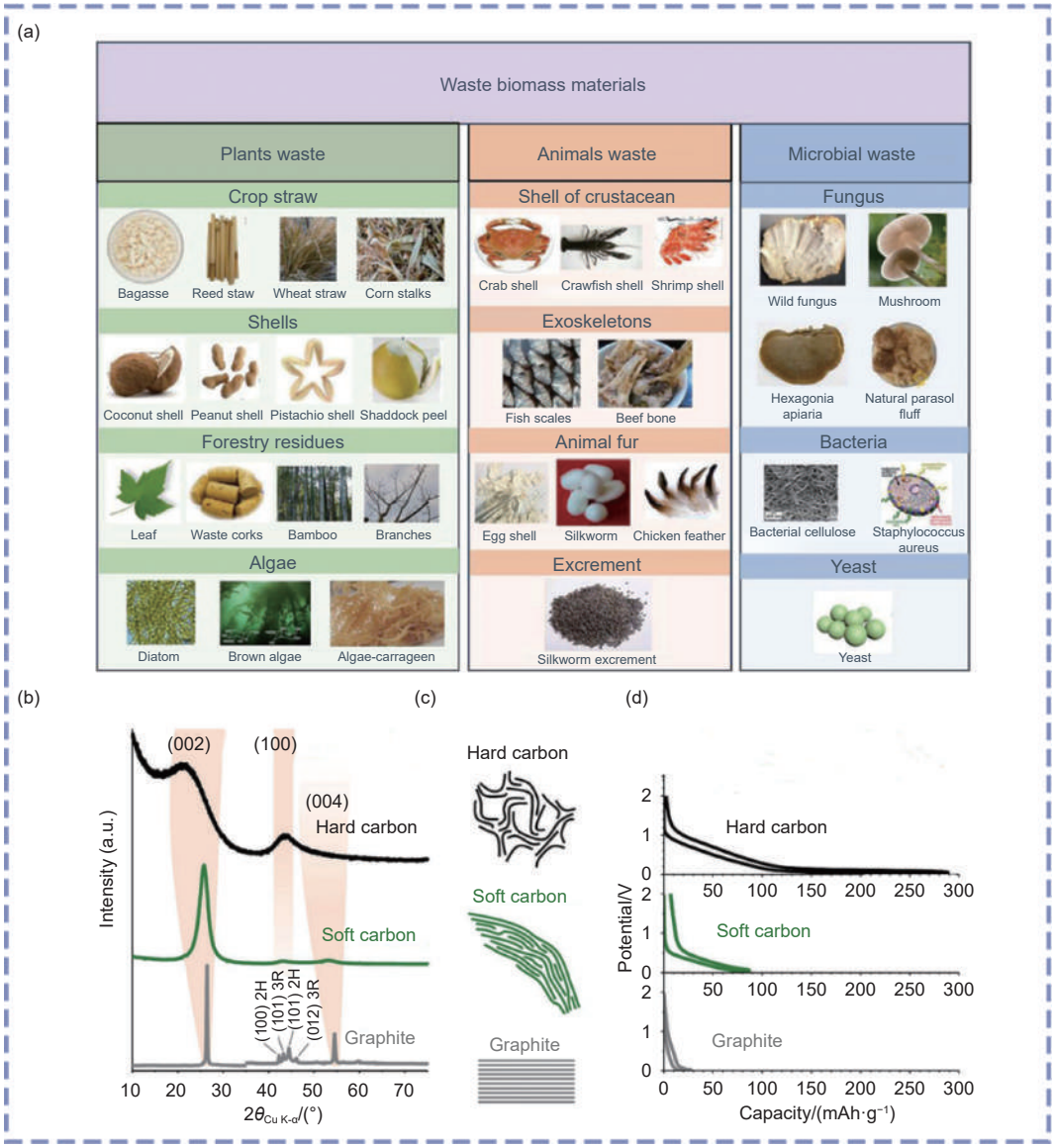

Fig. 3 (a) Classification of biomass sources[56]. (b) Typical XRD patterns of graphene, hard carbon, soft carbon, and graphite[57]. (c) Microstructure diagram of graphene, hard carbon, soft carbon, and graphite[57]. (d) Typical constant voltage-charge profiles for sodium storage of graphene, hard carbon, soft carbon, and graphite[57]. Reprinted with permission

The precursors of animal BDCs are primarily animal wastes, including crustacean shells (crab shells and shrimp shells), animal bones (cow horns, pig bones and fish bones), and animal furs and excrements (chicken feathers, wool and insect excrements)[73–75]. In contrast to plant-based biomass feedstocks, the organic compound components in animal biomass are typically fats, proteins and chitin, among other substances[76]. These often contain significant amounts of inorganic elements (e.g., N, O, S, P, etc.), rendering them particularly suitable for the preparation of heteroatom-doped carbon materials with enhanced charge storage capacity[76]. Furthermore, trace metal elements present in animal biomass can be employed as catalysts to facilitate the formation of carbon material structures, thereby yielding structurally complex new carbon materials. Chitin is a biopolymer extracted from crustaceans, which is the most abundant nitrogen-rich organic compound in nature.

In addition to plants and animals, microorganisms also have organic carbon structures as their basic components. Consequently, microbial waste can also be used as a carbon source. In recent years, carbon-based nanostructures derived from microbes have been widely used in electrochemical energy storage devices. Microbes consist mai

leic acids[77], including bacteria[78–80], fungus[81–83] and viruses[84–85]. Carbon materials prepared from various microbes exhibit unique structures, controllable porosities, and compositions. On the one hand, in-situ, heteroatom-doped nanostructures can be employed as high-capacity, multi-active-site active materials[86]. On the other hand, highly conductive skeletons can be utilized to support active materials, accelerate reaction kinetics, and enhance the contact between internal/external circuits[87].

Biomass is a thermoset precursor (oxygen-rich or hydrogen-poor material), which is difficult to graphitize at high temperature and ultimately converted to hard carbon due to the presence of more 3D cross-linked structures formed by sp^3 hybridization, which do not form colloidal bodies on high-temperature charring, and whose carbon layers are not able to grow in a rearranged manner, and form nanopores resulting from the escape of gases[88]. On the contrary, thermoplastic precursors (hydrogen-rich or oxygen-poor materials) undergo graphene layer rearrangement during high-temperature carbonization, with lamellar microcrystallites growing and arranging themselves in a more or less parallel manner, which results in their easy graphitization to soft carbon during high-temperature treatment[57]. In addition, soft carbon precursors such as petroleum coke, needle coke, anthracite, can be converted to artificial graphite by heating them to temperatures over 2000 °C.

BDCs belong to a kind of hard carbon, so they possess the basic microstructural characteristics of hard carbon that has a highly distorted structure formed by a large number of curved graphitized carbon layers stacked and connected with each other and contains a large number of pores (closed and open pores)[89–90]. In contrast, although soft carbon also exhibits short-range ordered and long-range disordered stacking characteristics, there are significantly fewer stacking faults. Unlike the amorphous carbon materials mentioned above, graphite exhibits an ordered layered structure. XRD patterns indicate the high crystallinity of graphite, while the soft carbon and hard carbon exhibit broad diffraction peaks and low-angle (002) peaks, indicating the degree of structural disorder and wider interlayer distances with respect to graphite, with the hard carbon having the highest degree of disorder (Fig. 3b). Typical charge/discharge curves of the three materials show that hard carbon exhibits a combination of high specific capacity, low average charge-discharge potential, and high Coulombic efficiency for sodium storage, with the best electrochemical performance and the most promising prospects for large-scale applications (Fig. 3d).

2.2 Synthesis methods of BDCs

Biomass materials must undergo thermal decomposition in an oxygen-free, high-temperature environment before being converted into BDCs for electrochemical energy storage. The complex composition of the biomass itself, its average electrical conductivity, and its low degree of graphitization all contribute to its limited electrochemical performance. To overcome the shortcomings of biomass raw materials and to obtain BDCs with excellent morphological, structural, electrical, and mechanical properties, researchers have explored and developed different synthetic methods to convert biomass materials into high-performance electrode materials in recent years, such as carbonization (pyrolysis and hydrothermal carbonization), activation (physical activation and chemical activation), and template methods (hard template and soft template)[91].

2.2.1 Pyrolysis carbonization

Pyrolysis carbonization is the simplest method of producing BDCs, requiring only direct pyrolysis of the biomass carbon source in inert gas (N_2, Ar, etc.) at high temperature in a tubular furnace to obtain carbon materials[92]. The product obtained by this method has relatively few surface functional groups, a relatively high degree of graphitization, and stable chemical properties. The pyrolysis process removes almost all substances that can be volatilized at high temperatures, including CO_2, CH_4, CO and some organics, leaving a solid carbon material. The preparation process of direct carbonization is straightforward and inexpensive, and the environmental pollution caused by the use of activators is av

method is adopted for the preparation of BDCs, the carbonization temperature has the most significant effect on the structure and elemental composition of BDCs. Pariyar et al.[93] investigated the variation of the SSA of pine saw dust, rice husk, food waste, poultry litter, and paper sludge at different pyrolysis temperatures and showed that the SSA of all the materials tended to increase with increasing temperature (350 to 650 °C). In addition, pyrolysis temperature also affects the heteroatom content in BDCs, which decreases with increasing carbonization temperature. For example, in their synthesis of buckwheat hull-derived carbon, Huang et al.[94] found that increasing the pyrolysis temperature from 700 to 1300 °C reduced the O content of the material from 5.79% to 3.97%.

2.2.2 Hydrothermal carbonization

Hydrothermal carbonization (HTC) has become one of the most widely used carbonization methods, with HTC-produced biomass carbon materials exhibiting coal-like properties. HTC is a chemical reaction process in which precursors are subjected to high temperature and pressure in a sealed vessel using water as a solvent and wet biomass as raw material to achieve carbonization of biomass through condensation, polymerization, hydrolysis, decarboxylation, dehydration, and aromatization processes[95]. Compared to other preparation methods of carbon materials, HTC offers advantages such as low reaction temperature (180–350 °C), an environmentally friendly process, and higher yield (approximately 70%–80%). It's worth mentioning that HTC can adjust the carbon product to create unique morphologies. For example, carbohydrates may be hydrothermally carbonized to form carbon microspheres with good thermochemical durability and thermal and electrical conductivity. Huang et al.[96] found that the hydrothermal temperature had a significant effect on the surface morphology and diameter of the prepared carbon microspheres during the hydrothermal treatment of wheat straw. When treated at 160 °C, the carbon microspheres were independently and uniformly distributed with diameters of 0.05–0.3 μm, but when treated at temperatures above 200 °C, the carbon microspheres appeared to be gradually agglomerated and reached diameters of 0.05–0.7 μm.

2.2.3 Physical activation

The pore structure of the BDCs obtained after the carbonization process is not fully developed, and the SSA is relatively small. Consequently, it is typically necessary to employ an activation process to enhance the porosity and pore volume of the carbon material, as well as to augment the SSA of the carbon material. In the activation process, biomass precursors in the action of activators gradually form pores and expand, and the pore walls between adjacent micropores are completely burned away to form larger pores, allowing mesopores and macropores to be generated, and ultimately the formation of the porous structure of the BDCs[97]. Depending on the activator used, the main common activation methods can be divided into physical activation and chemical activation. During physical activation, biomass precursors are first pyrolyzed in an inert atmosphere at low temperatures (<800 °C), which leads to partial carbonization and elimination of non-carbon elements[98]. This is followed by the activation of the sample in oxidizing gases (e.g. air, carbon dioxide, or water vapor) at 800–1100 °C, during which the oxidizing gases react with the carbon skeleton to produce CO and CO_2, as a result, pores are formed, which expand in depth to form new micropores, ultimately leading to the formation of a porous structure within the carbon material[99]. Zhong et al.[100] used vapor activation to convert rice into unique porous macrocellular carbon with cross-linked nano/micro sheets, where the water content of the feedstock plays a crucial role in the rapid transient expansion of the porous material. Since the reaction rate between carbon and water vapor is faster than the diffusion rate of water vapor, the reaction is limited to the surface of the carbon material. Using starch as a precursor, Fan et al.[101] developed a mild CO_2 etching and carbonization strategy capable of inducing a large number of closed nanopores. After CO_2 etching, the closed pore size of starch microspheres increased from 3.82 nm to 4.86 nm, and the corresponding pore volume increased from 0.045 to 0.117

2.2.4 Chemical activation

Chemical activation is generally a process in which precursors and activators are uniformly mixed in a certain ratio and then calcined at high temperatures in the range of 450–900 °C to undergo a series of cross-linking and condensation reactions to produce pores for forming porous carbon. The porous carbon materials with higher SSA, developed pore structure and controllable pore size can be produced by selecting suitable activators and controlling the appropriate reaction conditions. Chemical activation is currently the main preparation method for high-performance BDCs. Activators can be divided into three categories according to their properties: alkaline activators (KOH, NaOH, etc.), neutral activators ($ZnCl_2$, $FeCl_3$, etc.), and acidic activators (H_3PO_4, HNO_3, etc.), with KOH[102–104], $ZnCl_2$[105–107], and H_3PO_4[108–110] being the most commonly utilized. The process of activation using alkalis produces alkali metals and carbonates, which are responsible for stabilizing and enlarging the spaces between the layers of carbon atoms in the carbon matrix, thus altering the pore structure of BDCs. Researchers have successfully used KOH activators to prepare porous carbon materials with diverse pore structures and high SSA from various natural biomass source. Hou et al.[111] transformed rice bran into a porous carbon structure with micropores and mesopores embedded in each other by combining carbonization and KOH activation. The SSA of the obtained porous carbon material is 2475 $m^2\ g^{-1}$. The activation temperature required with $ZnCl_2$ as the activator is low (400–900 °C) and the SSA of the resulting BDCs is large (1000–2000 $m^2\ g^{-1}$). During the activation process, $ZnCl_2$ can act as a supporting skeleton for carbon, which leads to a better development of the pore structure. This is the main feature that makes it superior to other activators. The porous activated carbon formed after the removal of $ZnCl_2$ was predominantly mesoporous. Yu et al.[107] selected magnolia petals as a precursor and utilized $ZnCl_2$ as both a template and activator to synthesize coral-like magnolia-based porous carbon material (CMPC-2) through carbonization at 800 °C. CMPC-2 exhibits a substantial SSA of 903.1 $m^2\ g^{-1}$ and a well-developed pore volume of 1.09 $cm^{-3}\ g^{-1}$. H_3PO_4 is a common acid activator, and the H_3PO_4 activation process is characterized by a simple preparation process, low self-corrosion, low equipment and environmental hazard, and high carbon yield[112]. Porous carbon produced with H_3PO_4 as an activator typically features sizable mesopores or even macropores[113]. Furthermore, phosphoric acid can introduce phosphorus-based functional groups into the carbon structure during pore activation. Hong et al.[108] reported the preparation of 3D hierarchical porous carbon materials by phosphoric acid activation of grapefruit peel. The prepared material exhibits a high SSA (1272 $m^2\ g^{-1}$), and XPS analysis shows that there are many oxygen- and phosphorus-containing functional groups on the porous carbon surface.

2.2.5 Template method

The template method involves attaching precursor material to the surface of a template through a specific process and then removing the template to obtain nanomaterials with the same size and morphology[114–115]. The template material should have the characteristics of a special structure, controllable morphology, and low cost. The template method is classified into hard template methods and soft template methods according to the difference in the template composition. The hard template method generally uses inorganic materials with specific structure and morphology (e.g. silica, porous zeolite, metal-organic framework, inorganic salts, etc.) as templates, and fills the pores of the templates within the carbon precursors, which can be converted into target products by high-temperature heat treatment, and finally removes the templates to obtain the corresponding porous carbon[116]. Ou et al.[117] fabricated nitrogen-rich porous carbon material from buckwheat using a nano-$CaCO_3$ template, and its use as an anode for SIBs showed good sodium storage properties due to its inherent nitrogen content (3.14%) and interconnected porous structure with mesopores and macropores. The nano-$CaCO_3$ template was removed by a subsequent acid-washing step. Ji et al.[118] used a co-sacrificial template sequential pyrolysis method to prepare ordered

macroporous carbon-based framework material. With the pyrolysis process, the poly-methyl methacrylate (PMMA) template was partially converted into graphitic carbon (between ca. 290 and 300 °C), and the remaining PMMA was completely removed from the solid matrix in gaseous form (>350 °C). This method eliminates the step of removing the template using solvents such as strong acids and bases. The soft template method mainly involves mixing block copolymer (i.e. surfactant) and carbon precursor to form an ordered mesoporous structure precursor, forming macromolecular micelles between the precursor and the soft template by chemical bonding, and then obtaining ordered mesoporous carbon materials after removing the templates by high-temperature pyrolysis[119–121]. Using cassava as a precursor and triblock copolymers (F127) as a soft template, Zheng et al.[122] obtained a porous activated carbon material with a SSA of 286 $m^2\ g^{-1}$ and a total pore volume of 0.25 $cm^3\ g^{-1}$ by mixing, drying, and carbonizing, and the surface contained a large number of active groups. However, soft templates usually use polymers, most of which are non-renewable and made of expensive polymers, which limits their wide application.

In general, pyrolysis, hydrothermal carbonization, physical activation, chemical activation, and template methods can be used to produce biomass porous carbon, among which, high-temperature pyrolysis is simple to operate, but the SSA increase is not obvious and has limitations, and the HTC method does not require high activation temperature, but the SSA and porosity are lower. Physical activation has the advantages of safety and environmental protection and produces almost no by-products, but it requires high activation temperature, and relatively large energy consumption in the reaction process, and the activation effect is not obvious. On the contrary, chemical activation conditions are relatively mild, the reaction time is short, the activation temperature is low, and the product with an ideal SSA and hierarchical porous structure can be formed, but more by-products are produced in the activation process, and the waste treatment is more complicated in the subsequent process. The synthesis of biomass-based carbon materials using the template method can perfectly replicate the morphology and pore structure of the template, but the preparation process is relatively complex and requires additional post-treatment. Therefore, in practical applications, the choice of the appropriate preparation method should be based on the characteristics of the biomass precursor, the synthesis process technology, and the application area of the product. Table 1 lists the performance of different biomass sources derived carbon anodes for SIBs studied in recent years.

3 Sodium storage mechanism of BDCs

BDCs, as anode materials for SIBs, possess electrochemical properties superior to those of traditional carbon materials, such as graphite and soft carbons. On the one hand, BDCs exhibit a larger interlayer spacing than that of graphite, which is conducive to the insertion/extraction of sodium ions. On the other hand, the pore structure and larger SSA of BDCs are favorable for ion adsorption/desorption storage. Additionally, as mentioned above, new BDCs prepared by different methods using different biomass precursors have a variety of microstructures and there is no clear standard for the selection and handling of carbon material precursors, which can directly affect the electrochemical performance of SIBs and limit the standardization of sodium-ion battery technology for future commercial use[153–154]. Therefore, an in-depth understanding of the sodium-ion storage mechanism of hard carbon materials is essential for the rational design and optimization of hard carbon materials.

In SIBs, the storage of Na^+ by BDCs has been classified into various sodium storage methods, such as interlayer insertion, defect adsorption, and pore filling. The typical sodium storage process can be divided into two stages: the slope region at high voltage (> 0.1 V) and the plateau region at low voltage (0.1–0.01 V). The storage mechanisms are usually manifested in two ways, the capacity contribution in the slope region is mainly attributed to the insertion of

Table 1 A summary of performance comparison with different biomass sources derived carbon anodes for SIBs

Biomass precursor	Synthesis method	d_{002}/nm	S_{BET}/m^2 g^{-1}	ICE/%	Reversible capacity/mAh g^{-1}	Rate capability/ mAh g^{-1}	Ref.
Chitin	Hydrothermal carbonization (500–800 °C)	0.40	262	47 at 50 mA g^{-1}	140 of 2000th cycles at 5 A g^{-1}	102 at 10 A g^{-1}	[3]
Corn stalk	Hydrothermal carbonization (1000 °C)	0.407	9.24	65 at 60 mA g^{-1}	259.5 of 100th cycle at 60 mA g^{-1}	172 at 3 A g^{-1}	[62]
Oak seeds	Pyrolysis (900–1100 °C)	0.391	26.56	—	274.4 of 100th cycle at 50 mA g^{-1}	126.7 at 1 A g^{-1}	[64]
Pine pollen	Carbonization (900 °C)	0.41	171.54	59.8 at 100 mA g^{-1}	203.3 of 200th cycle at 200 mA g^{-1}	87.3 at 5 A g^{-1}	[65]
Starch	CO_2-Etching Carbonization (1300 °C)	0.396	2.29	90.56 at 25 mA g^{-1}	487.6 of 1st cycle at 25 mA g^{-1}	171 at 8 A g^{-1}	[101]
Magnolia petals	$ZnCl_2$ activation (800 °C)	0.354	903.0	—	161 of 4000th cycle at 1A g^{-1}	—	[107]
Buckwheat	Template method Carbonization (650–850 °C)	0.363	628	44.4 at 30 mA g^{-1}	185 of 100th cycle at 30 mA g^{-1}	75 at 2 A g^{-1}	[117]
Cow manure	Carbonization (800–1000 °C) HF solvothermal reaction	0.41	294.5	55.4 at 100 mA g^{-1}	372.2 of 1000th cycle at 100 mA g^{-1}	221.4 at 10 A g^{-1}	[123]
Hovenia dulcis	Carbonization (900–1200 °C)	0.382	195.32	72 at 100 mA g^{-1}	350.3 of 50th at 50 mA g^{-1}	108.4 at 2 A g^{-1}	[124]
Fallen leaves	H_3PO_4 activation (500 °C)	0.3714	601	63.9 at 100 mA g^{-1}	310.4 of 200th cycle at 100 mA g^{-1}	226.2 at 2 A g^{-1}	[125]
Lotus seedpod	Carbonization (1000–1400 °C)	0.386	140.7	50.4 at 50 mA g^{-1}	295 of 200th cycle at 50 mA g^{-1}	73.8 at 1 A g^{-1}	[126]
Waste woods	Carbonization (1300–1500 °C)	—	2.6	—	280 of 400th cycle at 500 mA g^{-1}	280 at 1 A g^{-1}	[127]
Waste corks	Carbonization (1200–2000 °C)	0.376	5.54	81 at 30 mA g^{-1}	312 of 200th cycle at 30 mA g^{-1}	—	[128]
Potato starch	Carbonization (800–1500 °C)	0.376	2.1	90.6 at 20 mA g^{-1}	250 of 50th cycle at 50 mA g^{-1}	73.8 at 1 A g^{-1}	[129]
Camellia shell	Hydrothermal treatment Carbonization (800 °C)	—	377.6	44.1 at 100 mA g^{-1}	215 of 100th cycle at 100 mA g^{-1}	123 at 1 A g^{-1}	[130]
Puffball	Carbonization (900–1100 °C)	0.354	131.24	57.6 at 100 mA g^{-1}	146.98 of 600th cycle at 2 A g^{-1}	102.12 at 10 A g^{-1}	[131]
Mushroom spore	Carbonization (1200–1600 °C)	0.364	5.5	81.2 at 20 mA g^{-1}	411.1 of 50th cycle at 20 mA g^{-1}	104.1 at 0.5 A g^{-1}	[132]
Onion wastes	Hydrothermal carbonization (700–1000 °C)	0.384	—	—	152 of 200th cycle at 50 mA g^{-1}	77.9 at 2.5 A g^{-1}	[133]
Porphyra	KOH activation (700–900 °C)	0.36	6.4	20.9 at 1 A g^{-1}	115 of 500th cycle at 1 A g^{-1}	60.2 at 10 A g^{-1}	[134]
Jute-fiber	Carbonization (800 °C)	0.379	210.9	66 at 30 mA g^{-1}	120 of 1000th cycle at 300 mA g^{-1}	56 at 3 A g^{-1}	[135]
Tea	Carbonization (1100 °C)	0.44	39.78	90 at 28 mA g^{-1}	262.4 100th cycle at 280 mA g^{-1}	224.5 at 1.4 A g^{-1}	[136]
Dandelion	Hydrothermal carbonization (800 °C)	0.35	1453	42 at 50 mA g^{-1}	97.51 of 1000th cycle at 5 A g^{-1}	115 at 5 A g^{-1}	[137]
Soybean roots	Carbonization (600–800 °C)	0.395	10.5	40.5 at 50 mA g^{-1}	288 of 1000th cycle at 1A g^{-1}	150 at 5 A g^{-1}	[138]
Cotton	Carbonization (1000 °C)	0.379	—	75.27 at 25 mA g^{-1}	272 of 100th cycle at 50 mA g^{-1}	69 at 0.5 A g^{-1}	[139]
Kapok fiber	$ZnCl_2$ assisted pyrolysis (1200 °C)	0.387	85.1	75.94 at 50 mA g^{-1}	185.7 of 500th cycles at 40 mA g^{-1}	128 at 3.2 A g^{-1}	[140]
Silver willow blossoms	Carbonization (600–1300 °C)	0.364	—	70 at 100 mA g^{-1}	301of 100th cycles at 100 mA g^{-1}	62 at 10 A g^{-1}	[141]
Pinecones	Template method Carbonization (900 °C)	0.404	552	63.5 at 100 mA g^{-1}	822.8 of 500th cycles at 100 mA g^{-1}	210 at 2 A g^{-1}	[142]
Mango-peel	Carbonization (1000 °C)	0.47	408.99	52.03 at 100 mA g^{-1}	350 of 250th cycles at 100 mA g^{-1}	128 at 4 A g^{-1}	[143]
Waste corncob	Carbonization (1150–1400 °C)	0.376	12.899	73.2 at 30 mA g^{-1}	250 of 100th cycles at 30 mA g^{-1}	90 at 0.6 A g^{-1}	[144]
Chickpea husk	KOH activation (1100 °C)	0.38	1599	—	316 of 200th cycles at 20 mA g^{-1}	70 at 2 A g^{-1}	[145]
Onion peel	Carbonization (750 °C)	0.4	756.5	23 at 50 mA g^{-1}	67 of 1000th cycles at 10 A g^{-1}	69.4 at 10 A g^{-1}	[146]
Rice husk	NaOH activation (600–1200 °C)	0.382	459.29	33.8 at 25 mA g^{-1}	328.4 of 100th cycles at 25 mA g^{-1}	185.71 at 0.5 A g^{-1}	[147]
Agar	Carbonization (750 °C)	0.391	706	42.1 at 100 mA g^{-1}	310 of 500th cycles at 100 mA g^{-1}	140 at 5 A g^{-1}	[148]
Sunflower seed hulls	K_2CO_3 activation (600–800 °C)	~ 0.3955	678.69	27.4 at 55.8 mA g^{-1}	468.9 of 100th cycles at 55.8 mA g^{-1}	104 at 1.395 A g^{-1}	[149]
Water-soluble starch	Template method Carbonization (800 °C)	0.387	221.8	33.7 at 80 mA g^{-1}	265 of 500th cycles at 2 A g^{-1}	154 at 8 A g^{-1}	[150]
Sugarcane bagasse	KOH activation (500–700 °C)	0.382	227.0	43.3 at 25 mA g^{-1}	304.1of 200th cycles at 25 mA g^{-1}	197.4 at 1 A g^{-1}	[151]
Camphor tree	Carbonization (700 °C)	0.43	—	70.74 at 40 mA g^{-1}	280 of 500th cycles at 2 A g^{-1}	282.3 at 2 A g^{-1}	[152]

Na^+ between the graphite microcrystalline layers, while the plateau region is dominated by the adsorption of Na^+ on reactive functional groups, defect sites, and pore structures. There are also a few sodium-ion storage mechanisms that show that the slope region corresponds to the adsorption of Na^+ at defect sites and on surfaces, while the plateau region is related to the filling of the nanopores with Na^+. However, the uncertainty and complexity of the structure of BDCs increase the difficulty of exploring the Na storage mechanism[155]. The limitations of existing characterization techniques allow researchers to remain controversial about the intrinsic charge storage mechanism behind their charging and discharging behavior, and different structural analyses generated by different characterization tools may provide inconsistent interpretations of the microstructure of carbon and the associated Na storage behavior.

3.1 Sodium storage active sites

BDCs exhibit excellent electrochemical performance as anode materials for SIBs, which can be attributed to their sodium storage structure, i.e. a small number of small-sized, curved graphite crystallites stacked in a short-range ordered, long-range disordered manner, as well as a large number of defects and nanopores inside (Fig. 4a)[156]. There are active sites providing additional diffusion pathways for Na^+ and storage sites for Na^+.

3.1.1 Crystallites

The crystallite structure is a unique structure of BDCs, which usually refers to disordered turbo-layered nanodomains containing a small number of randomly arranged defective graphite layers. It can be expressed by the carbon lateral size (L_a), stacking height (L_c), and interlayer distance (d_{002}) of the microcrystallites (Fig. 4b)[157], with different hard carbons having significantly different L_a and L_c. Typically, at low pyrolysis temperatures, the crystallite is highly disordered with low L_a and L_c. As shown in Fig. 4c, at higher temperatures the structure becomes progressively more ordered, with a slight increase in L_a and L_c for hard carbon[158]. In addition, the interlayer spacing of the hard carbon material has a great influence on the sodium ion storage and diffusion, and d_{002} of 0.37–0.40 nm is a more suitable layer spacing for Na^+ insertion[161–162]. When $d_{002} > 0.37$ nm, the insertion reaction of Na^+ is easier. When $d_{002} < 0.37$ nm, the energy barrier for Na^+ insertion is too high and the intercalation reaction is difficult to proceed[163]. In addition, if $d_{002} > 0.40$ nm, the Na^+ will be stored at this point of intercalation by adsorption behavior. Therefore, the microcrystalline structure greatly influences the storage sites and diffusion kinetics of BDCs. Increasing the interlayer spacing of the microcrystalline structure and increasing the content and order of disordered turbo-layered nanodomains can provide

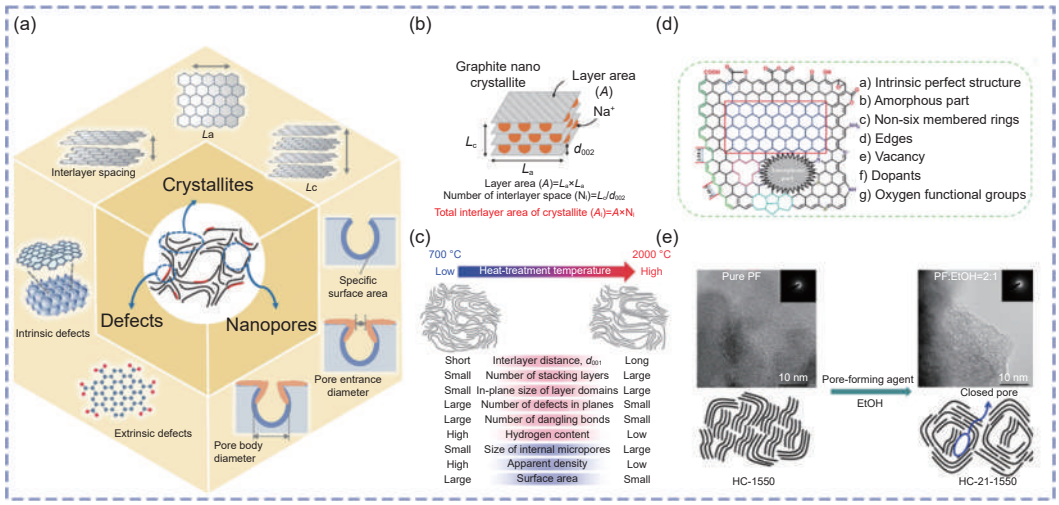

Fig. 4 (a) Illustration of the key structural features of hard carbons in SIBs[156]. (b) Structure Image of graphite nanocrystallite and crystallite interlayer area (Ai)[157]. (c) Schematic illustrations of structures of the hard carbon samples prepared at 700 and 2000 °C and the structural parameters[158]. (d) Illustration of carbon surface with different types of defects[159]. (e) Schematic diagram of pore formation by pore-forming agent[160]. Reprinted with permission

abundant ionic storage sites and diffusion pathways for ion transport, which can help to reduce the energetic barrier to sodium ion insertion/extraction, thereby improving the reversible capacity, rate performance and long cycling capability[164].

3.1.2 Defects

Many defects are present in BDCs, and the introduction of defects plays an important role in improving the effective storage sites and diffusion kinetics of Na^+. In general, defects include edge defects, vacancy defects, and heteroatom defects, which can be distinguished as intrinsic and non-intrinsic defects (Fig. 4d)[159]. Intrinsic defects are mainly vacancies, holes, and edges on the nanosheets, consisting mainly of dangling bonds and sp^3 hybridized carbon with other structural branches, such as pentagons, heptagons, octagons, and their combinations with various non-hexagon structures, leading to the bending of the graphene nanosheets. The sodium ion adsorption capacity increases with the concentration of intrinsic defects. The introduction of intrinsic defects gives the material a significantly higher sodium adsorption capacity. Non-intrinsic defects, i.e. impurity defects, mainly refer to heterogeneous atoms, the most common of which are oxygen-containing functional groups and heteroatoms such as P, S, F, N and B, which are usually found in vacancies and edges[165–166]. Based on the position of the heteroatoms, heterogeneous atom defects are classified into substitution-type doping and gap-type doping[167]. Substitution-type doping refers to the replacement of carbon on the hexagonal lattice in graphene-like sheets by exotic atoms, destroying the original structure. Gap-type doping refers to the introduction of exotic atoms into the center of the planar hexagonal sp^2 hybridized carbon. Defects enhance the electronic conductivity and provide a large number of electrochemically active sites, with important implications for surface adsorption and reversible surface redox reactions[168]. Surface adsorption processes and redox reactions can provide more sodium-ion storage sites and faster ion diffusion rates than ion intercalation reactions. Meanwhile, the surface-dominated electrochemical reaction is characterized by a short diffusion distance and a strong sodium-ion storage capacity, resulting in a low degree of destruction of the electrode structure during charging and discharging, which is conducive to improving the stability of the electrode and thus dramatically improving the reversible capacity and rate performance[169]. In recent years, there has been an increasing number of studies on the introduction of defects in hard carbon materials. However, not all defects are favorable for electrochemical performance, especially the trapping effect and the generation of irreversible solid electrolyte interface (SEI) layer, which leads to a reduction in ICE. Proper control of the defect type as well as the defect content in hard carbon is essential to reduce the irreversible Na^+ being trapped as well as to obtain a high sodium storage capacity.

3.1.3 Nanopores

BDCs have abundant pore structures, and the pores are mainly formed by random stacking of graphene sheets, and the number of pores is positively correlated with the SSA. There are mainly 2 types of pore structures, open and closed pores, where open pores store Na^+ through adsorption processes to increase the capacity of the slope region, thus a large SSA is beneficial for the open pore adsorption sodium-ion storage behavior, but it is worth noting that a large SSA likewise triggers more electrolyte decomposition to produce a thick SEI layer, which can lead to a low ICE. Closed pores are typically formed between bent graphene nanosheets, which are voids between the local crystallites and the local crystallites (Fig. 4e)[160]. During the cathodic reduction, Na^+ ions are deposited in the closed pores to form quasi-metallic clusters, and the behavior of the closed pore filling of Na^+ is a diffusion-dominant electrochemical process, so the construction of closed pores shortens the diffusion distance of Na^+ and improves the rate capacity[170–171].

3.2 Sodium storage models

Clarifying the constitutive relationship between hard carbon structure and performance can help guide the optimal design of hard carbon materials. Although the application of hard carbon materials in the

anodes of SIBs has been very extensive, there is still no clear conclusion on the sodium storage mechanism of hard carbon materials[172]. Researchers have proposed a variety of mechanism models based on the observed experimental phenomena. The existing controversy centers on the interpretation of the sodium storage mechanism corresponding to the high-voltage slope region and the low-voltage plateau region appearing in the charge/discharge curves. As shown in Fig. 5, the existing sodium storage models can be classified as follows: (1) "Insertion-filling" model, (2) "Adsorption-filling" model, (3) "Adsorption-insertion" model, and (4) "Multistage" model.

The "insertion-filling" ("house of cards") model was proposed by Stevens and Dahn in 2000 and is the first accepted model to describe the microstructure of hard carbon (Fig. 5a)[41]. The researchers conducted comprehensive in-situ small-angle X-ray scattering (SAXS) studies on glucose-derived hard carbon materials to elucidate the sodium-ion storage process in detail. They observed that the slope region above 0.1 V correlates with the insertion of Na^+ into the graphite domains in the hard carbon, whereas the plateau region below 0.1 V is associated with the filling of the hard carbon nanopores with Na^+, akin to the adsorption behavior. Subsequently, in 2012, Cao et al.[163] proposed an "adsorption–insertion" model to describe the sodium-ion storage behavior of polyaniline-based hollow carbon nanowires (Fig. 5b), where the high-potential slope region is related to the sodium-ion storage behavior of the surface defects of the hard carbon, while the low-potential plateau region is related to the sodium insertion between the carbon layers. Based on theoretical calculations, the minimum interlayer spacing for Na^+ insertion was indicated to be 0.37 nm. In contrast to the previous 2 theories, in 2015, Ji et al.[173] investigated the sodium-ion storage process in hard carbon by ex-in situ X-ray diffraction (XRD) and neutron scattering and then divided the voltage distribution into 3 regions and proposed the "adsorption-insertion-filling" mechanism (Fig. 5c). In this mechanism the capacity of the slope region corresponds to the adsorption of Na^+ at defects, and the capacity contribution of the plateau region originates from the insertion of Na^+ between carbon layers and the slight adsorption of Na^+ on the surface of the nanopores. In the same year, Tarascon et al.[177] used in-situ XRD and other technigues to investigate the

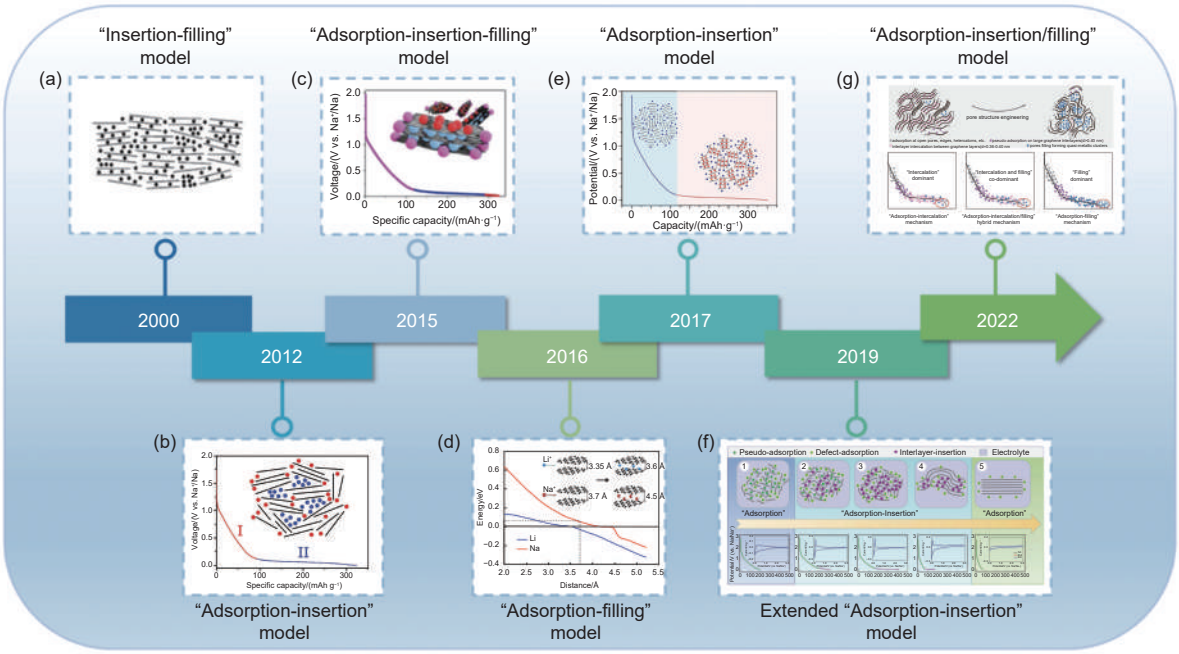

Fig. 5 (a) The "insertion-filling" model[41]. (b) The "adsorption-insertion" model[163]. (c) The "adsorption-insertion-filling" model[173]. (d) The "adsorption-filling" model[48]. (e) The "adsorption-insertion" model[174]. (f) The extended "adsorption-insertion" model[175]. (g) The "adsorption-insertion/filling" model[176]. Reprinted with permission

sodium storage mechanism of HC, and observed that the interlayer spacing of the carbon nanofiber electrodes did not change during the sodium insertion process of the graphene-like carbon layer. This indicated that there was no intercalation behavior during the charging and discharging, and combined with other characterizations, they proposed the "adsorption-filling" model. A similar experimental phenomenon was found by Hu et al.[48] The capacity of hard carbon microtubules (HCTs) decreased in the slope region and increased in the plateau region as the carbonization temperature increased. Characterization of the carbon structure using ex-in situ transmission electron microscopy revealed that the graphite-like layer spacing of the hard carbon anodes discharged to 0 V was found to be essentially unchanged compared to the initial state, further corroborating the mechanism, i.e., that the slope region corresponds to the adsorption of Na^+ at the defect site and on the surface; and the plateau region is associated with the filling of the nanopores with Na^+ (Fig. 5d). In 2017, Cao et al.[174] used in situ XRD, ex-in situ NMR, and electron paramagnetic resonance data to show that the high-voltage slope region is a process of Na^+ adsorption on the surface of the material, while the low-voltage plateau region is a process of Na^+ insertion into the carbon microcrystals, i.e. the "adsorption-insertion" model (Fig. 5e). In 2019, Sun et al.[175] proposed an extended "adsorption-insertion" model (Fig. 5f) and showed that sodium storage depends on the d_{002} of the hard carbon: when d_{002} is > 0.40 nm, Na^+ can freely enter the carbon layer with pseudocapacitive adsorption-storage behavior, and adsorption of Na^+ on graphite-like interlayers and defects jointly contribute to the capacity of the slope region. When d_{002} is between 0.36–0.40 nm, Na^+ contribute to the capacity of the plateau region by inserting into graphite-like interlayers. When d_{002} is < 0.36 nm, Na^+ cannot be inserted into the interlayer, and sodium intercalation storage cannot occur. In 2022, Cao et al.[176] proposed a mixed model of "adsorption-insertion/filling" (Fig. 5g), suggesting that the capacity of the low potential region comes from the insertion and pore-filling behavior of Na^+ and that the proportion of their contribution depends on the number of closed pores and graphite microcrystallites in the hard carbon microstructure.

From the above, it can be seen that the hard carbon material has low disorder and complex structure. The current understanding of hard carbon microstructure and sodium-ion storage mechanism is limited by the characterization technology. Furthermore, there is no unified scientific conclusion on the reaction mechanism of hard carbon anode for SIBs. A clear hard carbon microstructure and sodium storage mechanism is an important theoretical guide for the development of hard carbon anodes for high-performance SIBs, so studying the sodium storage mechanism and exploring the relationship between the internal microstructure of hard carbon and the electrochemical performance is the key to synthesizing and designing high performance hard carbon-based sodium storage anode materials.

3.3 Sodium storage kinetics

Three kinetic processes are involved in the movement of sodium ions from the electrolyte into the electrode bulk phase, namely the desolvation of solvated Na^+ between the electrolyte/electrode interface, the transport of Na^+ within the SEI and the diffusion of Na^+ into the electrode to undergo electrochemical reactions.

3.3.1 Desolvation process

When the sodium salt is dissolved in a certain solvent, anion dissociates and Na^+ are surrounded by solvent molecules to form a specific solvated structure[178]. Solvated Na^+ ions migrate in the electrolyte and subsequently undergo desolvation at the electrolyte/electrode interface, and the slower desolvation process undoubtedly drags down the performance output of the electrode, and the weakly coordinated solvated structure is usually beneficial to reduce the desolvation energy barrier and enhance the ion transport rate at the interface. Hong et al.[179] achieved the excellent rate properties of carbon materials using an ether electrolyte and attributed the improved performance to a lower desolvation barrier. Bai et al.[180] demonstrated that ether-based electrolytes can form

thermodynamically stable complexes with Na^+, a solvated Na^+ that somewhat avoids the slow desolvation process and improves kinetics. By studying the sodium-ion storage mechanism and interfacial behaviour of hard carbon in ether and ester electrolytes, Yan et al.[181] demonstrated that both the Na^+ transport process in SEI and the desolvation behavior have a profound effect on the multiplicity performance of hard carbon, and that the effect of the desolvation process is dominant.

3.3.2 Solid/liquid interface transport process

Due to the low sodium storage potential of hard carbon, which exceeds the reduction potential of the electrolyte components (including solvents, salts and additives), the electrolyte undergoes a reduction reaction during the first turn of the naturation process, and the organic and inorganic components generated by the decomposition of solvents and sodium salts build up on the surface of the anode electrode to form a solid electrolyte interface[182]. A stable SEI prevents the electrolyte from reacting further, whereas an unstable SEI continuously consumes the electrolyte, leading to a decrease in the coulombic efficiency of the device and a shorter service life, therefore, the composition, thickness, and densification of the SEI all critically affect the kinetic transport process of Na^+ ions. Ester electrolytes tend to decompose and form a thick and inhomogeneous SEI layer on the anode surface, resulting in a high solid-liquid interfacial energy and a slow rate of ion transport. The use of ether electrolytes effectively improves the rate performance of hard carbon, which is attributed to the more favorable solvation effect and a more stable and homogeneous SEI in ether electrolytes. Zhang et al.[183] investigated the electrochemical properties of high specific surface area carbon (HSSAC) in ether-based and ester-based electrolytes and found that the stable, compact, thin and homogeneous SEI formed in the ether-based electrolyte enabled the hard carbon to exhibit excellent sodium storage properties. Through molecular dynamics simulations and experimental characterization, Zhao et al.[184] found that Na^+ has more excellent reaction kinetics in ether-based electrolytes compared to ester-based electrolytes and that the thin SEI layer (4.6 nm vs. 12 nm) and low interfacial impedance (1.5 Ω vs. 24 Ω), as well as the low desolvation energy (0.248 eV), allow the hard carbon to exhibit excellent rate performance and cycling stability in ether-based electrolytes. Bai et al.[180] demonstrated experimentally and theoretically that fast sodium-ion diffusion coefficients in ether systems and thin SEI films with low internal resistance can promote the rate properties of hard carbon materials.

3.3.3 Solid-phase diffusion process

The microstructure of hard carbon has a significant effect on the sodium storage kinetic process, and the sodium storage kinetic properties of hard carbon can be improved by modulating the microcrystalline layer spacing, pore structure, and surface chemistry. Wang et al.[185] used bacterial cellulose and resin to prepare hard carbon with enlarged interlayer spacing, and the rapid diffusion and storage of Na^+ provided sufficient diffusion channels, the Na^+ diffusion coefficient at the plateau region can be readily improved from $10^{-10.2}$ to ~ $10^{-9.0}$ cm^2 s^{-1}. Zhao et al.[123] prepared N/F doped hard carbon nanospheres (CDC-F-900). The conjugation effect of N/F accelerates the ion transport rate and hence the electrochemical kinetics. As a result, CDC-F-900 exhibited excellent capacity and cycling performance at high currents. Zhang et al.[186] precisely tuned the closed-pore structure of natural bamboo cell-derived hard carbon by deep eutectic solvent cell-shearing strategy. Suitable pore size (2 nm), ultrathinness (1-3 layers), and disordered pore walls enable bamboo-derived hard carbon to have abundant sodium storage active sites, resulting in fast ion diffusion kinetics and high reaction reversibility. Excellent rate capacity (318.6 mAh g^{-1} at 6 A g^{-1}) was successfully achieved when used as a SIB anode. Bai et al.[124] synthesized Hovenia dulcis-derived hard carbon (HC-1100A) with precisely tuned microcrystalline and porous structures. The synergetic effect of dual-functionalized Ca enlarges the interlayer spacing of HC-1100A and induces intrinsic defects, which can thermodynamically and kinetically facilitate Na^+ storage and transport, thus exhibiting improved sodiation

kinetics, HC-1100A delivers an impressive rate ability (108.4 mAh g^{-1} at 2 A g^{-1}).

4 Structural regulation engineering of BDCs

By understanding the sodium storage sites, models and kinetics of BDCs, we can realize that the sodium storage performance of BDCs is closely related to the structure, defects, pores, and carbon interlayer spacing all have an impact on the electrochemical performance of the materials. However, biomass precursors all have structural limitations, such as uncontrollable crystal structure, single chemical structure, and irregular porous structure, which limit the improvement of the sodium storage performance of BDCs. Therefore it is necessary to design structural modulation and engineering methods to address the inherent structural limitations of biomass materials.

4.1 Microcrystallite engineering

The microcrystallite structure of BDCs is the main part for sodium ion intercalation, which can provide enough storage sites for Na^+ embedding. Reasonable optimization of the microstructural characteristic parameters (L_a, L_c, d_{002}) of microcrystallite is conducive to improving the overall sodium storage performance of BDCs. Firstly, the wider d_{002} interlayer spacing can reduce the energy barrier for the insertion of Na^+ and ensure the adequate embedding and diffusion of Na^+ between the graphite layers of the BDCs, thus the appropriate d_{002} interlayer spacing is the key to increasing the sodium storage capacity of BDCs. Secondly, the L_a and L_c values of BDCs are related to the degree of graphitization. The suitable L_a and L_c values can lead to more suitable adsorption storage so that sodium ions can be further stored in the defects.

Appropriate d_{002} interlayer spacing (0.37–0.4 nm) and degree of graphitization are crucial for high-capacity BDCs, and we expect the carbon structure to achieve a balance between graphite-like domain development and defect and pore content, and the use of temperature control and heteroatom doping is a reasonable means of optimizing the crystal structure. Elevated carbonization temperature increases the L_a and L_c values, decreases the d_{002} value, and reduces the pore size and defect location, which in turn has a great impact on the electrochemical properties of BDCs. Asfaw et al.[187] used oxidized cork as a precursor to pyrolyze and synthesize hard carbon nanosheets (HCNS) at different temperatures (1000–1500 °C), the d_{002} interlayer spacing decreased from 3.9 Å to 3.7 Å with increasing carbonation temperature. The results of Raman scattering tests reflected the decrease in defect concentration, and increase in graphitization and crystal size in HCNS by increasing from 1000 to 1500 °C. In addition, temperature affects the proportion of capacity contributed by tilted and flat regions, with increasing capacity contribution from the flat region and decreasing capacity contribution from the tilted region with increasing temperature (500–2000 °C).

In addition to regulating the carbonization temperature, the introduction of heteroatoms can also serve to optimize the microcrystalline structure. For example, doping of sulfur[188–190], phosphorus[125,191], and fluorine[192–193] can improve the interlayer spacing, provide more storage sites for ions, and improve diffusion kinetics, thus increasing the reversible capacity and rate performance. Kim et al.[162] synthesized P-doped hard carbon with a doping level of 1.10% at 1300 °C. Due to the increased interlayer spacing between graphite layers after P doping (0.3748–0.3868 nm), which enhances the intercalation effect of Na^+, the reversible capacity of the P-doped hard carbon was enhanced to 328 mAh g^{-1} at 50 mA g^{-1}, with ICE as high as 72%. Dai et al.[192] prepared F-doped (1.1%) carbon particles by pyrolysis of lotus leaf stalks. The introduction of F can form F—C bonds with high polarity and stability, and the F—C bonds are easy to increase the mutual repulsion between the carbon layers and widen the interlayer spacing, so they were used as an anode material for SIBs, and they exhibited an initial charging capacity of 230 mAh g^{-1} at a current density of 50 A g^{-1}. Even after 200 cycles at a high current density of 0.2 A g^{-1}, the capacity retention rate is still as high as 99%.

4.2 Defect engineering

Defect engineering methods can be used to enhance the electrochemical activity of carbon, adjust the surface wettability and electronic conductivity of materials, and thus improve their sodium storage properties. Exogenous defects doped with heteroatoms are the main strategy of defect engineering, and heteroatom doping can improve the electrochemical properties, surface wettability, electronic conductivity, porosity, and interlayer spacing of BDCs[194–195]. The effects of different doping atoms on the electrochemical properties of SIBs vary greatly, with nitrogen (N), sulfur (S), and phosphorus (P) being the most common heteroatom dopants.

Nitrogen (N) is one of the most widely studied heteroatoms in BDCs, and N is a substitutional dopant that enhances reactivity and conductivity by creating extrinsic defects in place of carbon atoms in the lattice[196–198]. There are two main methods to prepare N-doped BDCs, one is obtained by pyrolysis of N-containing biomass, and the other is pyrolytic synthesis of materials such as urea, melamine, and nitric acid with biomass. N can be introduced into the carbon skeleton in different doped configurations such as pyridinic-N, pyrrolic-N and graphite-N. The transformation between different N-doped configurations can be achieved by controlling the pyrolysis temperature, and pyridinic-N and pyrrolic-N can be gradually transformed into graphite-N at high temperatures[199]. The configuration of N has an important effect on the activity and structure of BDCs, and pyridinic-N and pyrrolic-N with high chemical activity can introduce chemically active sites and defects to improve the surface adsorption capacity, and the construction of pyridinic/pyrrolic-N-dominated carbons is of great significance for the design of high-activity anodes for SIBs. Xu et al.[200] directly pyrolyzed shrimp skin to produce nitrogen-rich mesoporous carbon materials. The resulting carbon materials had a large amount of pyrrolic-N and pyridinic-N, which introduced a number of electrochemically active sites and defects and improved the surface adsorption capacity. Therefore, when used as an anode for SIBs, it has a high capacity of 434.6 mAh g^{-1} at a current density of 30 mA g^{-1}. Even at a high current density of 2 A g^{-1}, it still has a reversible capacity of 110 mAh g^{-1}. Du et al.[201] prepared porous flexible nitrogen-rich carbon membranes by pyrolysis of chitosan. The carbon membrane (CS-1000) formed by pyrolysis at 1000 °C had a honeycomb porous structure with 6.3% nitrogen content, and the high proportion of pyridinic-N improved the adsorption and electrical conductivity of Na^+ on CS-1000. When used as anode material for SIBs, its sodium-ion storage remains 236 mAh g^{-1} after 70 cycles.

Sulfur (S) doping is also important for energy storage and conversion. S can react with Na^+ to provide storage sites, and introducing S into BDCs can improve their sodium storage capacity. Firstly, S has a higher covalent radius, and S-doping into BDCs can expand the interlayer spacing by a larger electrostatic repulsion[202–203], which is favorable for the insertion/extraction of Na^+. Secondly, S is an electrochemically active component of redox reactions, and S-doping can provide more active sites for Na^+ storage[204]. Thirdly, the binding energy of S-doped BDCs with Na^+ is stronger than that of pure carbon[205]. Finally, S doping helps to increase the electrical conductivity of carbon[206]. S-doped BDCs are usually obtained by high-temperature pyrolysis of mixtures of biomass precursors with sulfur sources (e.g., sulfur powder, sodium dodecyl sulfate, etc.) or by solvothermal reaction of sulfur-rich organic compounds with carbon precursors. Zhao et al.[190] used spring onion peel as a biomass precursor and S powder as a sulfur source, and prepared S-doped carbon nanosheets (S-CNS) by one-step pyrolysis after mixing, S doping effectively enhanced the sodium storage performance of the carbon materials, and the in situ generated C—S bond had a very good adsorption of polysulfides, which effectively enhanced the cycling performance of the materials. S-CNS has a super high reversible specific capacity (50 mA g^{-1}, 605.5 mAh g^{-1}), excellent rate performance (10 A g^{-1}, 605.5 mAh g^{-1}), and cycling stability (5 A g^{-1}, 2000 cycles, 94% retention). Wang et al.[207] synthesized S-doped carbon nanofibers (S-CNFs) by sulfide pyrolys-

is using the industrial waste product bacterial cellulose as a precursor and applied them in SIBs. The high content of S doping (15%) enlarged the layer spacing of the materials, and the C—S—C covalent bonding increased the electrochemical activity and facilitated the de-embedding and adsorption processes of sodium ions. The S-CNFs exhibit a high capacity of 460 mAh g^{-1} at a current density of 0.05 A g^{-1}. The capacity of 310 mAh g^{-1} could be maintained after 1100 cycles at 1 A g^{-1}.

Phosphorus (P) doping is another method for designing advanced carbon anodes, and P-doped BDCs also play a key role in enhancing and modifying the carbon structure. Firstly, P-doping enlarges the interlayer spacing of carbon, which promotes the insertion of Na^+ and increases the amount of Na^+ storage[208]. Secondly, P doping facilitates the enhancement of capacitive performance, which is due to the redox activity of the P=O functional group on the carbon surface, which increases the adsorption of Na^+ and can provide more active sites for Na^+ storage[209]. Finally, P doping facilitates the improvement of the wettability of the electrode materials, and the P doping process introduces P-containing functional groups on the surface of the BDCs, which facilitates the penetration of the electrolyte solution into the interior of the electrode materials. Wu et al.[210] prepared P-doped carbon cloth (FPCC) from cotton cloth, which showed excellent electrochemical properties when used as an anode for SIBs, with an ICE as high as 72% and a specific capacity of 123.1 mAh g^{-1} at a current density of 1 A g^{-1}. Huang et al.[125] synthesized P-doped porous carbon (PC-3) by pretreatment and phosphoric acid activation using fallen leaves of horse chestnuts as a carbon source. Phosphoric acid activation produced a large SSA and pore volume and increased the interlayer spacing of the carbon lattice, which facilitated the adsorption of Na^+. PC-3 has a high capacity, excellent cyclic stability, and rate performance. The capacity is 310.4 mAh g^{-1} after 200 cycles at 100 mA g^{-1} and 226.2 mAh g^{-1} at 2 A g^{-1}.

4.3 Pore engineering

Pore structure is an important and highly complex factor, due to the different chemical compositions of the biomass precursors, the pore structures of the prepared BDCs including surface pore distribution, size, shape, connectivity, and pore volume are different, and all these factors could affect the overall performance. As we mentioned earlier, Na^+ can be stored by filling into the pore structure of BDCs, i.e., the pore size will affect the capacity of the material. A suitable pore size should satisfy a size larger than that of the solvated ions, the diffusion rate of sodium ions within the pore determines the rate performance of the electrode[211]. The design of hierarchical porous structures containing interconnected micropores, mesopores, and macropores can increase the accessibility of the internal active sites and improve the diffusion kinetics of the electrolyte in the material[212]. In addition, compared with open pores, closed pore structures are more favorable for the storage of Na^+, which helps to increase the platform capacity of BDCs and effectively enhances the transport rate of sodium ions. Hence, the design of more closed pores is meaningful for improving sodium storage capacity.

Hierarchical porous carbons can shorten the diffusion distance of ions and charges and greatly expose the active sites, resulting in high activity, which is expected to be an ideal anode for high-magnification, high-power SIBs. Wu et al.[126] used one-step carbonization to prepare lotus seedpods-derived hard carbon with a hierarchical porous structure. The porous structure of the material collapsed with increasing temperature, leading to a further decrease in capacity, and hard carbon pyrolyzed at 1200 °C exhibits the optimal reversible capacity as an anode for SIBs due to its suitable pore distribution (328.8 mAh g^{-1}) with 90% capacity retention after 200 cycles. In addition, the hollow structure of the hierarchical porous carbons facilitates adequate contact between the electrode and the electrolyte, effectively shortens the diffusion distance of sodium ions, and inhibits the volume expansion of the carbon material, thus effectively improving its cycling stability[213]. Sun et al.[214] reported the synthesis of 3D hierarchical porous carbon nanocages (FCNCs) from onion peel, and the appropriate hollow structure of FCNCs mitigated the volume change due to Na^+ insertion, which results in

excellent reversible capacity and cycle life for SIBs, with a reversible capacity of 318.2 mAh g^{-1} at 50 mA g^{-1}, and the reversible capacity at 10 A g^{-1} is 81.6 mAh g^{-1}, with a retention rate of 92% after 1000 cycles.

The design of the closed pore structure helps to enhance the capacity of SIBs in the platform region, which further improves the overall sodium storage capacity and energy density of SIBs. Suitable biomass precursors and carbonization temperatures are important factors for the construction of BDCs with closed pore structures. At low carbonization temperatures (<1400 °C), the precursors pyrolyze to form carbon layers with many open pores. As the carbonization temperature is further increased (>1400 °C or even when it exceeds 2000 °C), graphitic microdomains can be rearranged to induce the closure of open pores to form closed pores. Wang et al.[127] found that increasing the pyrolysis temperature increases the length of graphite-like carbon layers of crystalline cellulose-derived hard carbon and promotes the formation of closed pores. The hard carbon anode prepared by pyrolysis of wood-based precursors with high crystalline cellulose content at 1500 °C could provide a sodium storage capacity of 430 mAh g^{-1} at a current density of 20 mA g^{-1} (plateau capacity of 293 mAh g^{-1}), as well as better rate performance and cycling stability (85.4% capacity retention for 400 cycles at 500 mA g^{-1}). Hu et al.[128] reported a waste cork-derived hard carbon materials (CCs), where the CC produced closed nanopores at 1600 °C, and the positive correlation between the plateau capacity and the closure rate confirmed the pore-filling mechanism. CC-1600 shows a reversible capacity of up to 358 mAh g^{-1} in a half-cell with up to 81% ICE.

5 Different morphologies of BDCs for SIBs

The morphological structure of carbon materials has a significant influence on the sodium storage properties. Due to the wide variety of biomass in nature, carbon materials made from different biomass precursors usually retain or inherit the microscopic morphology of their precursors in their morphology, such as carbon microspheres, carbon nanotubes, carbon nanofibers, carbon nanosheets, and carbon skeletons. Different dimensional morphology designs result in different structural features, such as hollow structure, porous structure, hierarchical structure, and so on. Designing the nanostructures of BDCs through dimensional adjustment can promote the rapid transport of ions and electrons, which is an effective development strategy to improve the sodium storage performance of electrode materials. A positive effect of certain morphological structures on the overall sodium storage capacity of carbon has been observed, and in this section, the structures, electrochemical properties, and recent advances of different sizes of BDCs for SIBs are discussed, with special emphasis on the effects of modification and optimization strategies, such as layer spacing control, heteroatom doping, defect introduction, and pore structure construction, etc., on improving the sodium storage performance of BDCs.

5.1 Biomass-derived carbon microspheres

Biomass-derived carbon microspheres have a regular geometry and can achieve excellent electrochemical performance as anode materials for SIBs due to their mechanical stability and ability to limit volume changes. In addition, carbon microspheres exhibit many significant advantages, such as great electrical conductivity, adjustable porosity, and controllable particle size distribution. Researchers have recently investigated the sodium storage properties of biomass-derived carbon microspheres. Hu et al.[215] reported a method for the synthesis of monodispersed hard carbon spherules (HCS) from sucrose. The HCS carbonized at 1600 °C has the highest plateau capacity (220 mAh g^{-1}), which is advantageous for obtaining higher energy densities in the full cell. Thus, the full cell has a high capacity of more than 300 mAh g^{-1} when coupled with a P2-$Na_{2/3}Ni_{1/3}Mn_{2/3}O_2$ cathode. Song et al.[129] synthesized hard carbon microspheres (PC-1400) by pyrolysis of potato starch at 1400 °C using controlled oxidation. The large carbon domain size and high structural order in PC-1400 provide a channel for Na^+ to fill the pores, and when used as an anode for SIBs, a reversible capacity of

303.5 mAh g^{-1} could be achieved at 0.02 A g^{-1}, with ICE as high as 90%.

Although the regular spherical morphology enables dense stacking of carbon microspheres, which is conducive to achieving good stability, the solid spherical structure at the same time faces the problem of unfavorable migration and diffusion of electrolyte ions within the electrode material. Therefore, some researchers have introduced porosity into carbon spheres, using biomass as carbon source and removable templates to design porous and hollow carbon spheres. Wu et al.[130] prepared porous carbon microspheres (CSHP2) from camellia shells by comminution ball milling and two-step hydrothermal treatment. CSHP2 displays the best cycling stability and rate performance for SIBs. It maintains an ultra-high capacity of 215 mAh g^{-1} after 100 cycles at 100 mA g^{-1} with 86% capacity retention. The specific capacity reaches 123 mAh g^{-1} at a high current density of 1000 mA g^{-1}. The excellent Na^+ storage capacity is attributed to its porous structure and spherical morphology. The ultramicropores (d<0.7 nm) can slow down the formation of the SEI film by reducing the contact between the carbon surface and the electrolyte, and the spherical morphology can buffer the mechanical stress during the charging and discharging process. Yu et al.[131] thermally treated low-cost puffball at high temperature and produced biomass-derived hard carbon (PB-1000) with a unique balloon-like porous structure. The abundant pore structure of PB-1000 helps to shorten the ionic transport distance and effectively increases the active centers and energy storage channels. Especially, the high content of macroporous structure in PB-1000 enhances its ion storage capacity in SIBs, thus, the reversible capacity of PB-1000 at 100 mA g^{-1} is 205.05 mAh g^{-1}. The discharge capacity reaches 82.23 mAh g^{-1} even after 2000 cycles at a high current density of 5 A g^{-1}. Furthermore, the hollow carbon microspheres are conducive to electrode-electrolyte contact due to their carbon shells and substantial internal cavities, thus facilitating ion diffusion. Liang et al.[132] found that hollow porous carbon spheres have great potential as high-capacity sodium storage anode materials. By precisely controlling the carbonization temperature, hollow porous carbon spheres (HPCS-1400) obtained from mushroom spores exhibit excellent electrochemical performance as an anode for SIBs, with a reversible discharge capacity of 411.1 mAh g^{-1} and an ICE of up to 81.2%, and the capacity is maintained at 384.5 mAh g^{-1} after 50 cycles at 20 mA g^{-1}. The unique hollow porous structure of HPCS-1400 helps to maintain the internal integrity of the material during a long charging/discharging process.

On the other hand, the conductivity, surface wettability, and surface active sites of biomass-derived carbon microspheres can be increased by introducing heteroatoms, thus providing additional redox capacity or pseudocapacitance capacity to the material. Introducing N atoms with higher electronegativity is favorable for improving electronic conductivity and interacting with Na^+. Lu et al.[216] prepared novel N-doped mesoporous carbon spheres (NMCSs) by using low-cost glucose and melamine (Fig. 6a). NMCSs-800 consists of interconnected ultrathin nanosheets with open hollow features (Fig. 6b). NMCSs-800 exhibits an ultra-high rate capacity of 93.9 mAh g^{-1} at 5 A g^{-1}. The reversible sodium storage capacity is maintained at 228.2 mAh g^{-1} after 300 cycles at 0.05 A g^{-1} (Fig. 6c). The unique structure and optimal N-doping provide an abundance of sodium storage active centers, defects, and vacancies, as well as a large number of channels to facilitate charge transfer, resulting in NMCSs-800 exhibiting optimal sodium storage capacity and fast diffusion kinetics. Yang et al.[133] utilized onion waste and urea to fabricate nitrogen-rich carbon nanospheres by a simple hydrothermal and annealing reaction (Fig. 6d). Nitrogen-rich carbon nanospheres (NC-800), obtained by carbonization at 800 °C, have the highest graphitic-N and pyrrolic-N content (Fig. 6e), which is beneficial for increasing the conductivity and active sites of carbon nanospheres, as well as enhancing the diffusion of Na^+. As a result, the NC-800 exhibits significant rate capability (Fig. 6f), delivering a high reversible specific capacity of 225.7 mAh g^{-1} at 0.05 C, and 77.9 mAh g^{-1} at

2.5 C, with the reversible capacity returning to 95.7% of the initial capacity when the current density returns to 0.05 C. Sulfur doping is also important for energy storage and conversion because sulfur is a high-capacity chemical element that is more reversible than oxygen and can react with sodium ions to provide storage sites. Tomas et al.[217] prepared S-doped hard carbon microspheres (S-GC) by HTC and chemical vapor deposition using glucose as a precursor. The sulfur doping is mainly present at edges or existing defect sites to provide a more accessible surface, thereby increasing the sodium adsorption energy and lowering the energy barrier for subsequent desorption. This behavior facilitates reversible sodium storage. The S-GC anode exhibits a higher ICE (73% vs. 52%) and superior sodium storage capacity than the undoped material. Compared to single heteroatom doping, which only improves one aspect of the properties, multi-atom co-doping can significantly improve the overall electrochemical properties of biomass-derived carbon microspheres through synergistic effects, providing effective storage sites and excellent diffusion kinetics. Zhao et al.[123] successfully prepared N/F-doped porous carbon nanospheres (CDC-F-900) with 3D interconnected microporous structure using cow manure cellulose. The conjugation effect of N/F appropriately reduces the adsorption energy and decreases the irreversible adsorption behavior of Na^+, reducing the irreversible capacity and accelerating the kinetic reaction process. Thus, a high capacity of 372.2 mAh g^{-1} at 0.1 A g^{-1} and excellent cycling stability of 214.2 mAh g^{-1} after 5000 cycles at 10 A g^{-1} were obtained for SIBs. Kang et al.[134] prepared N, O and P in-situ doped porous carbon microspheres (NOP-PCM800) by a high-temperature hydrothermal activation process using porphyra as a carbon source. As illustrated in Fig. 6g, the elements C, O, P and N are distributed uniformly across the porous micro-

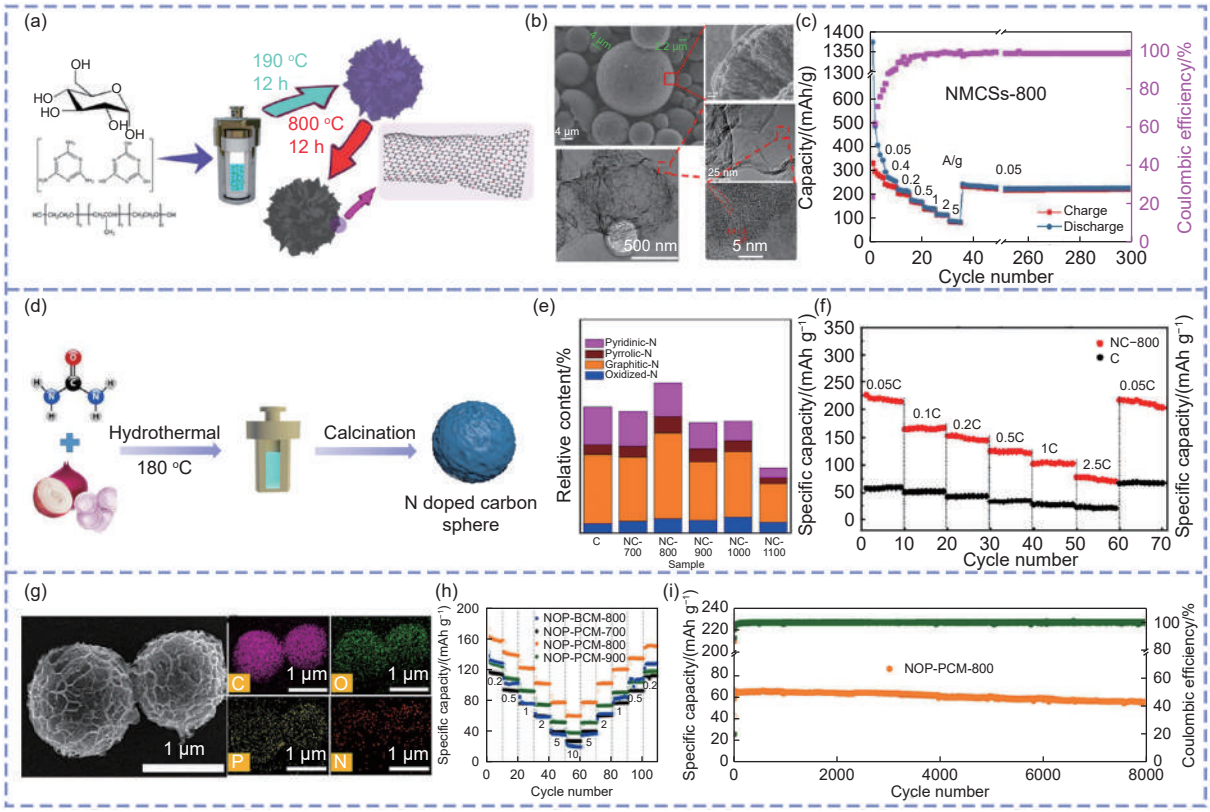

Fig. 6 (a) Schematic illustration for the synthesis of NMCSs[216]. (b) SEM and TEM images of the NMCSs-800[216]. (c) Rate and cycling performance at different current densities for NMCSs-800[216]. (d) Schematic illustration of the synthesis of N-doped carbon sphere[133]. (e) The content of different N species in the C and NC treated at different temperatures[133]. (f) The rate capability of C and NC-800/NC-2[133]. (g) SEM image and corresponds elemental mapping of NOP-PCM-800[134]. (h) Rate capacity at different currents of N, O and P-doped carbon microspheres[134]. (i) Long-term cycling performance at an ultra-high current of 5.0 A g^{-1} for the NOP-PCM-800[134]. Reprinted with permission

spheres. The doping of N, O and P can enhance the electrical conductivity, widen the interlayer spacing, and create active centers, respectively, therefore N, O, P doping can significantly improve the storage capacity of sodium. As a result, NOP-PCM-800 exhibits high rate capability (60.2 mAh g^{-1} at 10 A g^{-1}) and ultra-stable cycling stability (94.4% capacity retention at 5.0 A g^{-1} for 8000 cycles) as an anode material for SIBs (Fig. 6h, i).

The composite structure formed by compounding BDCs with high-capacity electrode materials can synergistically enhance diffusion kinetics and increase storage sites. By compounding BDCs with metal compounds, more high-speed ion diffusion and electron transport pathways can be provided, helping to improve the electrochemical performance of biomass-derived carbon microspheres. Xu et al.[218] used yeast cells as carbon templates and synthesized composites ($(Ni_{0.5}S_{0.5})S_2$@NPCS) by hydrothermal and sulfurization methods (Fig. 7a). The Ni, Co, S, C, N, and P elements coexist and are uniformly distributed in the spherical structure of the $(Ni_{0.5}Co_{0.5})S_2$@NPCS composite (Fig. 7b, c). The electrochemical performance of $(Ni_{0.5}Co_{0.5})S_2$@NPCS composites as SIBs anode was investigated. It can be inferred that the introduction of the bimetallic $(Ni_{0.5}Co_{0.5})S_2$ further improves the electrochemical performance through synergistic effects. $(Ni_{0.5}Co_{0.5})S_2$@NPCS has specific capacities of 407, 357, 325, 300, 260 and 243 mAh g^{-1} at current densities of 100, 200, 300, 500, 800 and 1000 mA g^{-1}, respectively (Fig. 7d), and could maintain a specific capacity of 370 mAh g^{-1} when the current density returned to 100 mA g^{-1} (Fig. 7e), confirming the good reversibility of $(Ni_{0.5}Co_{0.5})S_2$@NPCS. Pan et al.[219] prepared vanadium-modified hard carbon submicrospheres (HC/VC-1300) by HTC of glucose (Fig. 7f) and investigated its electrochemical performance for SIBs. Discharge-charge profiles (Fig. 7g) show that the discharge/charge capacities of the HC/VC-1300 in the first cycle are 379/278 mAh g^{-1}, corresponding to 68.7% of the ICE. The incorporation of vanadium serves to maintain the structural integrity of the electrode throughout the charge/discharge cycle. Furthermore, the introduction of V—O—C interfacial bonds enhances the stability of the interface, thereby facilitating the formation of a

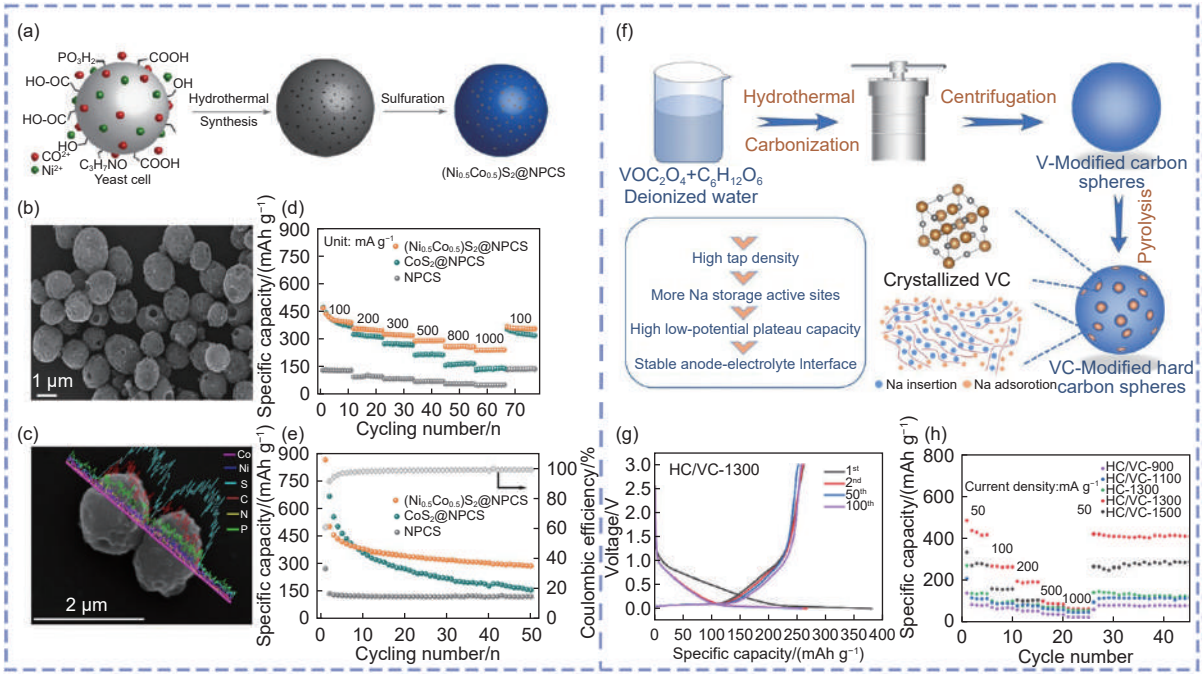

Fig. 7 (a) Schematic preparation of $(Ni_{0.5}Co_{0.5})S_2$@NPCS derived from yeast spheres[218]. (b) SEM image of $(Ni_{0.5}Co_{0.5})S_2$@NPCS[218]. (c) SEM/EDS images of $(Ni_{0.5}Co_{0.5})S_2$@NPCS[218]. (d) The rate capability of the $(Ni_{0.5}Co_{0.5})S_2$@NPCS[218]. (e) Cycling performance at 100 mA g^{-1} of the $(Ni_{0.5}Co_{0.5})S_2$@NPCS[218]. (f) Schematics of the formation process of uniform hard carbon spheres modified by vanadium carbide (HC/VC)[219]. (g) Selected discharge-charge voltage profiles of HC/VC-1300 at 100 mA g^{-1}[219]. (h) Rate capability at various current densities for HC/VC electrodes[219]. Reprinted with permission

stable SEI layer and optimizing the reaction kinetics. Therefore, HC/VC-1300 exhibits a high specific capacity of 420 mAh g^{-1} at 50 mA g^{-1} and a good rate capacity at 1 A g^{-1} (Fig. 7h).

5.2 Biomass-derived carbon fibers

Fibrous carbon precursors with one-dimensional (1D) nanostructures are widely distributed in nature[220–221]. Biomass-derived carbon fibers have excellent properties such as low cost, high aspect ratio, large SSA, high electrical conductivity, outstanding thermal stability, and lightweight, which facilitate the rapid transport of Na^+ and electrons and can effectively improve the electrochemical properties of carbon-based materials[222]. At the same time, carbon fibers have good mechanical stability and a special ability to resist external stress changes. In recent years, biomass-derived carbon fibers have been widely used in SIBs. Cao et al.[223] synthesized hard carbon microfibers by high-temperature carbonization using waste printed papers for the anode material of SIBs. The sample obtained at 1400 °C (HCF-1400) has a reversible charging capacity of up to 319.6 mAh g^{-1} and excellent cycling stability (capacity retention rate of 99.3% after cycling for 100 cycles at 0.2 C). The superior electrochemical performance of HCF-1400 is attributed to the suitable interlayer distance and proper amount of surface functional groups, which enhances capacitive behavior. Sun et al.[224] produced sustainable, stand-alone carbonized silk hard carbon fibers (CS_1300 °C) by pyrolysising silk biomass waste at 1300 °C. CS_1300 °C exhibits high capacity retention (nearly 100% after 100 cycles at 50 mAg^{-1}) and better rate performance (capacity at 12.5, 25, 50 and 125 mA g^{-1} is 216, 197, 180 and 144 mAh g^{-1}, respectively). The non-hollow fiber structure avoids excessive electrolyte consumption during the SEI formation cycle, favoring faster Na^+ migration kinetics and more outstanding ICE (75.6%). Wang et al.[225] developed free-standing flexible microfiber carbon papers (MFCPs) using renewable filter paper. The MFCPs display a layer-by-layer stacked and interwoven microfiber structure. As a practical additive-free anode for SIBs, the MFCP-1100 shows the best overall performance, exhibiting an excellent rate performance of 251.2 mAh g^{-1} at 1 A g^{-1} and a good cycle life of 217.3 mAh g^{-1} after 500 cycles. Similarly, thanks to the low SSA and porosity, MFCP-1100 has a high ICE of 95% when cycled at 20 mA g^{-1}. Accordingly, a reduction in the porosity of the material offers a promising avenue for the development of free-standing carbon anodes with high ICE.

Further design and construction of the internal structure of 1D carbon nanofibers can effectively improve the ions diffusion performance, such as hierarchical porous carbon nanofibers. Nagmani et al.[135] synthesized jute-based hard carbon fibers (JPC-D) by direct carbonization method, as shown in Fig. 8a, JPC-D has well-developed open pores in the cross-section and has the presence of both micropores and mesopores (Fig. 8b). The presence of this hierarchical porosity improves the ion diffusion path into the carbon lattice, providing more active centers for the adsorption/desorption of Na^+, allowing JPC-D to be used as an anode for SIBs with an excellent Na^+ storage capacity, and at 0.1 C (30 mA g^{-1}), with a reversible capacity of 328 mAh g^{-1} (ICE = 66%) and capacity retention of 84% after 100 cycles (Fig. 8c). Wang et al.[227] used a combination of electrostatic spinning and KOH chemical activation to prepare coal-based hierarchically porous carbon nanofibers (HPCCNFs). The suitable SSA (2236.43 m^2 g^{-1}) and interconnected carbon network increase the response sites, making HPCCNFs-1 a promising anode material for SIBs with excellent cycling stability (after 1000 cycles at 5 A g^{-1} can be maintained at 109 mAh g^{-1}) and good rate performance (121.7 mAh g^{-1} at 5 A g^{-1}). The porous structure allows for rapid diffusion of Na^+, effectively relieving the stress concentration caused by the expansion of the electrode material during the charging and discharging process. Chen et al.[226] prepared natural cotton radial porous carbon fibers (PCFs) using the biological swelling and dynamic graphitization process (Fig. 8d). SEM images (Fig. 8e) show that the PCF electrode has a hierarchical porous structure with a wide pore size of several hundred nanometers, and

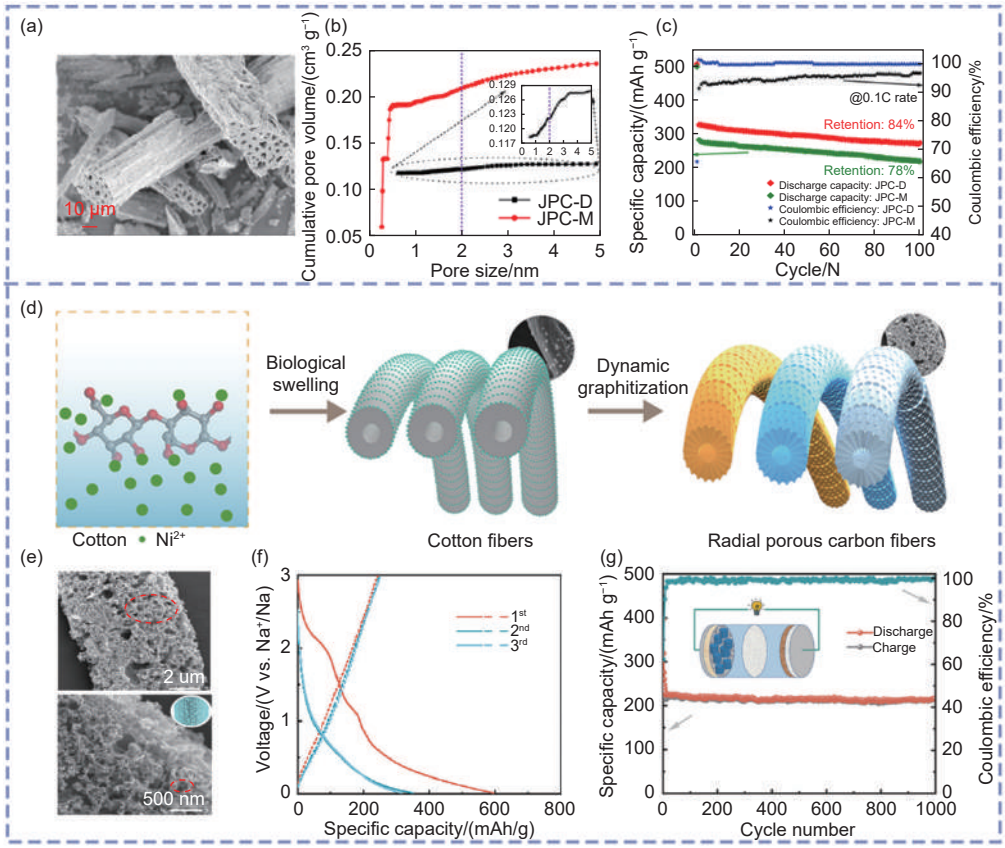

Fig. 8 (a) FE-SEM image of JPC-D[135]. (b) The porosity difference among jute-derived porous carbons[135]. (c) Cycling stability of JPC-D and JPC-M at 0.1 C rate (100 cycles)[135]. (d) Schematic illustration of the preparation process of PCFs[226]. (e) SEM images of PCFs[226]. (f) Galvanostatic discharge/charge curves at a current density of 50 mA g^{-1} [226]. (g) Long-term cycling capacity of the PCF electrode at a current density of 500 mA g^{-1} [226]. Reprinted with permission

the unique radial porosity gives the PCFs superior Na^+ storage properties. In the first cycle, the PCF exhibits a discharge/charge capacity of 546/319 mAh g^{-1} at 50 mA g^{-1} (Fig. 8f). At the same time, PCF provides good long-term cyclic stability, with a reversible capacity of 213 mAh g^{-1} after 1000 cycles at 0.5 A g^{-1} (Fig. 8g).

Surface modification of carbon fibers can improve their electronic conductivity and hydrophilicity, and enhance the chemisorption of Na^+, thus increasing the capacity properties of the device. Heteroatom doping is the most common methods of surface modification, which can change the electronic/ionic state of the reactive material, facilitating the reversible storage of sodium ions in biomass-derived carbon fiber materials through adsorption and redox reactions, and accelerating the reaction kinetics and is considered an effective way to achieve high electrochemical properties. Nitrogen as an electron-donating doping atom for carbon materials modifies the electronic structure of biomass-derived carbon fibers and reduces the energy barrier during ion adsorption and desorption. As shown in Fig. 9a, Qing et al.[228] prepared N-doped porous carbon fiber (N-PCF) by an in-situ sacrificial template-assisted hydrothermal method using natural biomass wood fibers as the carbon source. The sample (N-PCF-2), fabricated when the mass ratio of wood fiber to CN was 10∶2, exhibits a highly porous structure and a large interlayer spacing (0.38 nm). The elemental N is observed to be uniformly partitioned in the carbon skeleton (Fig. 9b). The high content of pyridinic-N and pyrrolic-N in N-PCF-2 facilitates the surface-induced capacitance process, which in turn achieves fast electrochemical kinetics. Consequently, the N-PCF-2 demonstrates a high specific capacity of 266 mAh g^{-1} following 300 cycles at 200 mA g^{-1} in SIBs (Fig. 9c). Additionally, the rate performance is also markedly superior (135 mAh g^{-1} retained at 1.6 A g^{-1}). S doping, a typical n-type doping, greatly improves the conductivity of the carbon material by

providing more free electrons. Yu et al.[207] prepared S-doped 3D interconnected carbon nanofibers (S-CNFs) from industrial waste bacterial cellulose, which showed great potential for use as anodes in SIBs. The excellent electrochemical performance exhibited by S-CNFS can be attributed to the fact that S-doped facilitates the increase of the carbon interlayer spacing (0.386–0.410 nm), which increases the adsorption of Na^+. The discharge capacity of S-CNFs at 0.05 A g^{-1} is 460 mAh g^{-1}, and after 1100 cycles at a current density of 1 A g^{-1}, the storage capacity stabilizes at 310 mAh g^{-1} with a Coulombic efficiency close to 100%. Mao et al.[229] prepared S-doped fibrous carbon (JFCS) by carbonizing biomass jute fiber mixed with sulfur powder. By adjusting the carbonization temperature and the doping amount, the $JFC_{700}S_{2.5}$ electrode, when applied in SIBs, demonstrates excellent reversible capacity (454.1 mAh g^{-1} at 0.05 A g^{-1}) and remarkable rate performance (234. 3 mAh g^{-1} at 2.0 A g^{-1}). The synergistic effect of co-doping multiple heteroatoms can improve the sodium storage properties of biomass-derived carbon fiber materials more effectively than single-atom doping[230–231]. Zhang et al.[136] prepared tea fluff-derived N, P co-

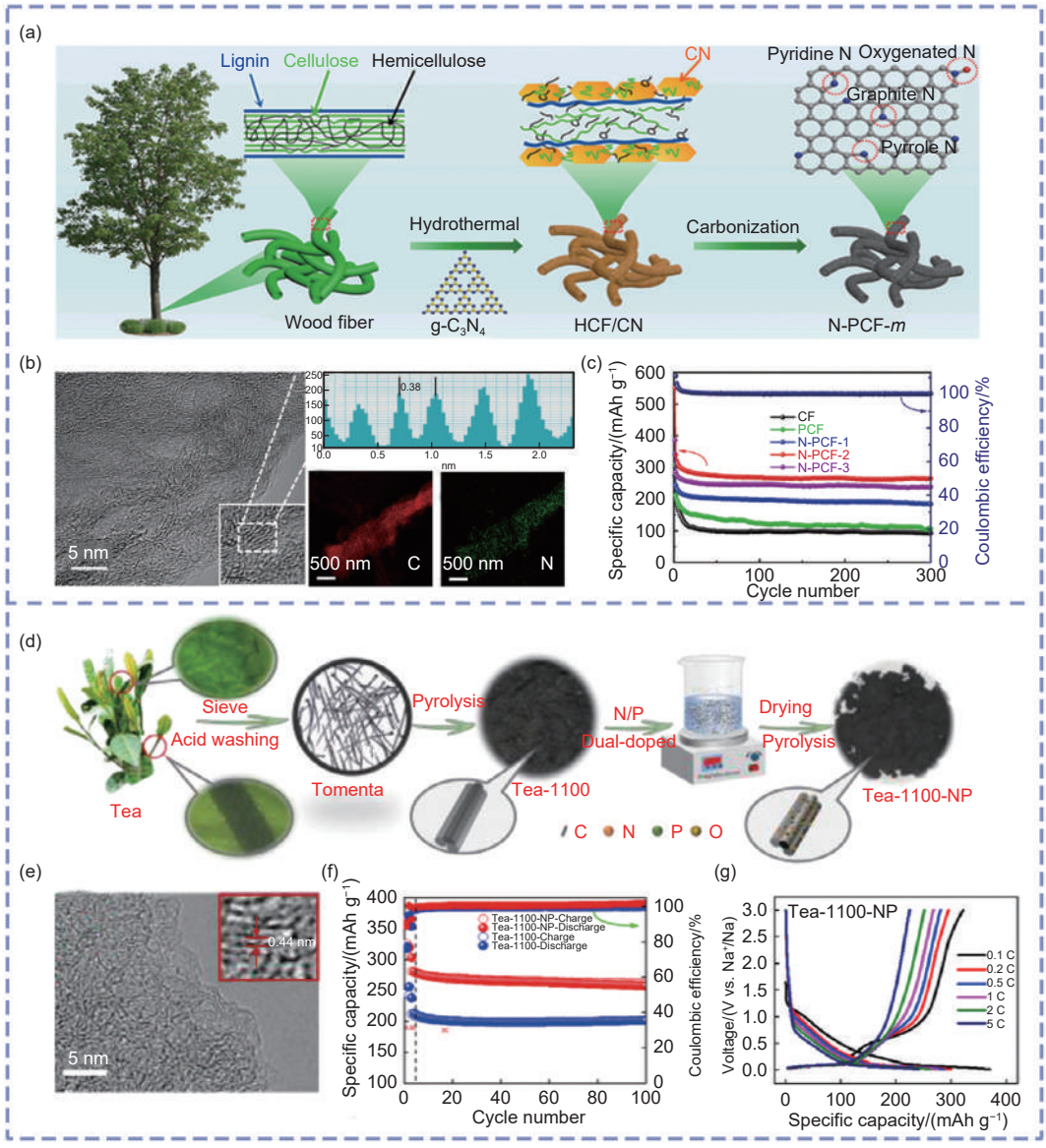

Fig. 9 (a) Schematic diagram of the synthetic procedure for N-PCF-m[228]. (b) HRTEM, the interlayer distances, and the elemental mapping images of N-PCF-2[228]. (c) Cycle performance of CF, PCF, and N-PCF-m electrodes at a current density of 200 mA g^{-1}[228]. (d) Schematic illustration of the material synthesis process of Tea-1100 and Tea-1100-NP[136]. (e) TEM image of Tea-1100-NP[136]. (f) Cycle performance at 1 C[136]. (g) GCD profiles at different current densities[136]. Reprinted with permission

doped hard carbon (Tea-1100-NP) by a simple carbonization and doping method. Tea-1100-NP exhibits a rod-like fiber morphology, as illustrated in Fig. 9d. The introduction of N and P atoms results in a larger carbon interlayer spacing (0.44 nm) (Fig. 9e), which facilitates the diffusion and transport of Na^+ and electrons, thereby ensuring the stability of the cycling life of Tea-1100-NP, which exhibit a specific capacity of 262.4 mAh g^{-1} after 100 cycles at a current density of 280 mA g^{-1} (Fig. 9f). The reversible capacity of 224.5 mAh g^{-1} can be maintained even at a high current density of 1400 mA g^{-1} (Fig. 9g).

In addition, carbon nanofibers can be used as an ideal substrate for metal/alloy nanomaterials, and by constructing high-performance composites it is possible to effectively improve the structural stability, as well as improve the sodium storage properties of biomass-derived carbon nanofibers[234–236]. Yang et al.[237] synthesized carbon fiber composites (TMS-HNP@CFs) embedded with transition metal sulfide hollow nanoparticles using sodium alginate as a template and raw material. When used as an anode for SIBs, CoS-HNP@CFs-900 shows superior rate performance with a capacity of 392.2 mAh g^{-1} after 100 cycles at 1 A g^{-1}. The reversible capacity of CoS-HNP@CFs-900 after 600 cycles at 5 A g^{-1} is 320.0 mAh g^{-1} with a capacity retention rate of 89.6%, demonstrating its outstanding cycling stability. The group also reported the preparation of 1D porous and micro/nano-structured FeS/carbon fibers composites (FeS/CFs-t) from ι-carrageenan by facile pyrolysis[238]. FeS/CFs-1 achieves excellent cycling stability (283 mAh g^{-1} at 1 A g^{-1} after 400 cycles) and rate performance (247 mAh g^{-1} at 5 A g^{-1}) for SIBs. Wang et al.[232] used the Metal-Aspergillus niger bioleaching approach to prepare a series of metal sulfide nanoparticles (MS/NCF (MS = ZnS, Co_9S_8, FeS, $Cu_{1.81}S$)) embedded in bio-derived nitrogen-rich carbon fibers. Taking ZnS/NCF as an example, it can be seen from Fig. 10a, b that ZnS nanoparticles are embedded in carbon fibers with interconnected porous channels and that the elements Zn, C, S and N are uniformly distributed inside and outside the fibers. ZnS/NCF has promising cycling performance (365.2 mAh g^{-1} capacity after 180 cycles at 1 A g^{-1}) and rate performance (reversible capacity of 231.7 mAh g^{-1} at 5A g^{-1}) as an anode for SIBs. The combination of metal sulfide nanoparticles with 1D carbon fibers greatly increased the diffusion rate of Na^+ and electrons, which solved the problems of MS/NCF volume expansion and low conductivity (Fig. 10c). Chen et al.[233] prepared N/P co-doped carbon fiber composites (MoS_2/NP-C) containing MoS_2 nanocrystals using waste leather as a precursor after sulfuration treatment (Fig. 10d). As demonstrated in Fig. 10e, the XRD patterns indicate that the diffraction peaks of MoS_2/NP-C-2 at 33.1°, 39.7° and 58.4° correspond to the (100), (103) and (110) crystal planes, respectively. This evidence substantiates the successful synthesis of molybdenum sulfide carbon composites. The encapsulation of MoS_2 crystals in leather-derived hard carbon can enhance the electrical conductivity of MoS_2/NP-C-2 material and mitigate the volume change that occurs during the charging and discharging processes, thereby improving the electrochemical performance of the material. The optimized MoS_2/NP-C-2 electrode displays remarkable cycling stability when employed as an anode for SIBs (Fig. 10f). The reversible capacity of the MoS_2/NP-C-2 electrode is 241 mAh g^{-1}, and the coulombic efficiency is approximately 100% after 2500 cycles at 1 A g^{-1}.

5.3 Biomass-derived carbon tubes

Carbon tubes consist of 1D cavities and graphite walls, which have high theoretical electrical conductivity, remarkable mechanical strength, and chemical stability, and a higher SSA and more electron-ion transport channels than carbon nanofibers, which can provide more active contact sites to ensure effective contact between the electrolyte and the electrode surface[48]. Most plant tissues with interconnected tubular structures can be used to prepare tubular carbon[137–138,239], and much previously reported work has demonstrated that biomass-derived carbon tubes facilitate the electrochemical conduction of electrons, thereby improving the rate performance of electrodes, and are a viable structure for high-performance Na^+

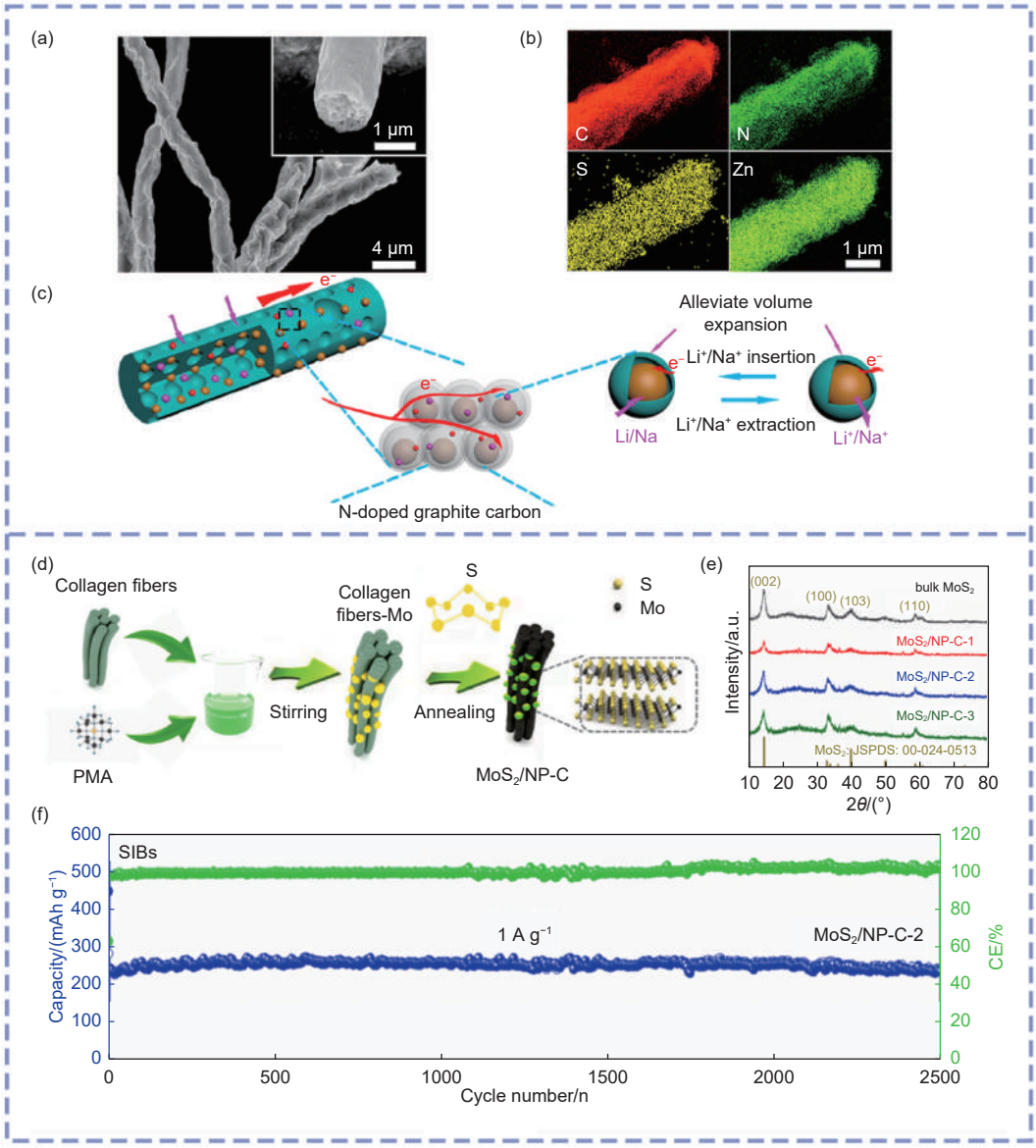

Fig. 10 (a) SEM image of ZnS/NCF[232]. (b) STEM mapping images of ZnS/NCF[232]. (c) Schematic illustration of the high storage performance of MS/NCF[232]. (d) Schematic synthesis of MoS_2/NP-C-2 composite[233]. (e) XRD patterns of MoS_2/NP-C and bulk MoS_2[233]. (f) Long-term cycling performance of the MoS_2/NP-C-2 electrode at 1 A g^{-1}[233]. Reprinted with permission

energy storage applications. Hu et al.[48] prepared hard carbon materials (HCTs) with uniform microtubular shapes by carbonizing natural cotton under the argon atmosphere, a structure that facilitates electrolyte transport and shortens the diffusion distance of Na^+. When used in SIBs, HCT1300 has the highest reversible capacity of 315 mAh g^{-1} at 0.03 A g^{-1}, 83% ICE, and good cycling stability, providing a stable specific capacity of 154 mAh g^{-1} after 1500 cycles at 400 mA g^{-1}. Guo et al.[240] prepared micro-nanotubes (HCMNT) by a two-step pyrolysis method using low-cost natural hollow cotton fibers as precursors. Benefiting from the micro-nano structure, 1400 HCMNT has the advantages of low SSA and short Na^+ diffusion paths and exhibits excellent sodium storage performance when used as the anode of SIBs, with a reversible capacity of 292.5 mAh g^{-1} at 0.1 C, with 80% ICE and a reversible specific capacity of 167 mAh g^{-1} at 2 C. Sun et al.[139] obtained carbonized cotton fabric-derived hard carbon (CF5min) self-supported electrodes by pyrolysis of waste cotton fabrics at 1000 °C for 5 min. CF5min exhibits a typical hollow morphology, which contributes to the improved wettability of the electrolyte on the material and reduces

the Na^+ diffusion distance, leading to faster Na^+ transfer kinetics. At 50 mA g^{-1}, CF5min exhibits a reversible capacity of 272 mAh g^{-1}, with 98% capacity retention after 100 cycles.

The porosity and pore size distribution of the electrode material are of great consequence concerning the transport and diffusion of electrolyte ions. Therefore, exploring carbon anode materials with a 1D porous structure is an effective way to improve the sodium storage properties of biomass-derived carbon tubes. Li et al.[241] proposed the use of natural parasol fluf as a biomass precursor to prepare interconnected porous carbon skeletons (NPF-500) with well-maintained tubular structures by KOH activation and Co^{2+}-assisted graphitization under a mild annealing temperature (500 °C) (Fig. 11a). Fig. 11b and 11c show that NPF-500 has an interconnected porous structure with a stripe spacing of 0.41 nm. Based on the large interlayer spacing, great pore structure, and the abundance of self-doped heteroatoms, NPF-500 provides a high reversible capacity of 359.0 mAh g^{-1} at 30 mA g^{-1}, excellent rate capacity (150 mAh g^{-1}) at 2 A g^{-1} as a SIB anode. Huang et al.[137] transformed dandelion into biomass carbon tubes with different nanopore sizes (non-porous carbon tube, micro-porous carbon tube, and meso-porous carbon tube), where the micro-porous carbon tube achieves the best rate performance (115 mAh g^{-1} at 5 A g^{-1}) and cycling stability (capacity retention is 84% after 430 cycles at 100 mA g^{-1}) as an anode for SIBs (Fig. 11d, e). The size of the nanopores affects the uniformity of the interlayer spacing of the carbon tubes, while the stability of the nanopore structure plays an essential role in the storage behavior of Na^+ during charging and discharging (Fig. 11f). Compared with non-porous and meso-porous carbon tubes, micro-porous carbon tube can re-

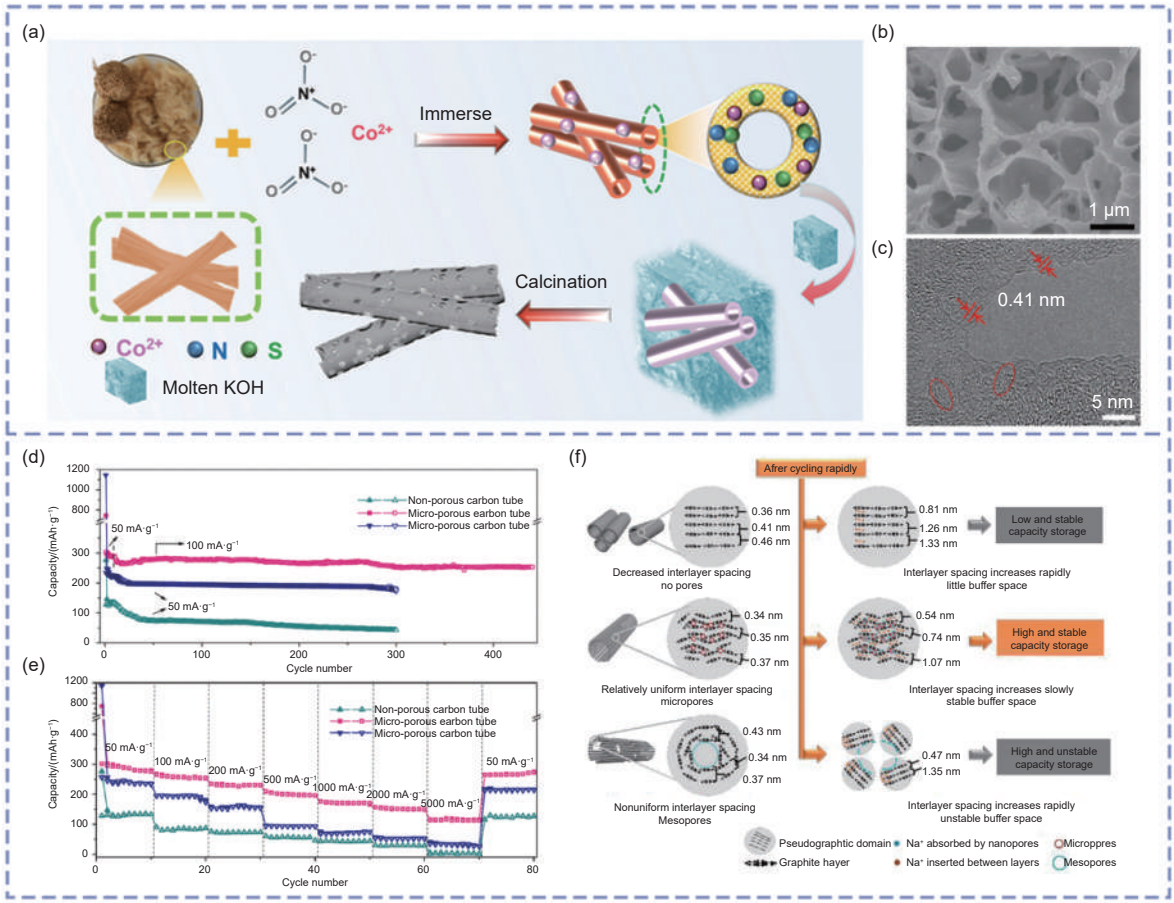

Fig. 11 (a) Illustration of the preparation process of the cross-linked porous NPF-500 sample[241]. (b) SEM image of NPF-500[241]. (c) HRTEM image of NPF-500[241]. (d) Cycling stability of all electrodes[137]. (e) Rate performances of all electrodes[137]. (f) Sodium-ion intercalation mechanism with different pore structures[137]. Reprinted with permission

duce the diffusion resistance and capacity loss due to the uniform distribution of interlayer spacing.

Heteroatom doping could enable excellent Na^+ storage capacity due to the introduction of pseudocapacitive effects. The role of sulfur, nitrogen, and phosphorus doping in carbon nanotubes has been extensively studied[242–244]. For example, Zhou et al.[245] fabricated high-performance sulfur-doped carbon microtubes (S-CMTs) from high-temperature sulfurizing cotton rolls. Due to the synergistic effect of high sulfur doping (10.2%) and favorable microporous structure, S-CMT as SIBs anode exhibits superior rate performance (140 mAh g^{-1} at 10 A g^{-1}) and excellent cycling performance (281 mAh g^{-1} at 1 A g^{-1} after 1000 cycles). The sulfurizing process provides additional Na^+ storage sites and enhances the sodium storage performance by expanding the SSA and increasing the conductivity. In contrast, the CMT electrode without sulfurization shows poor sodium storage performance, with the charging capacity of CMT rapidly decreasing to less than 10 mAh g^{-1} when the current rate is increased to 10 A g^{-1}. As shown in Fig. 12a, Zhang et al.[140] fabricated highly efficient nitrogen-doped kapok fiber-based hard carbon (N-ZAHC) with a tubular structure. Due to the large interlayer spacing, N-ZAHC exhibits excellent electrochemical performance in SIBs, with a reversible capacity as high as 401.7 mAh g^{-1} at 0.05 A g^{-1}. In addition, the high concentration of pyridinic-N enhances the defect sites and conductivity of N-ZAHC, which facilitates the diffusion of Na^+ during the insertion process, thus endowing it with favorable rate performance. Even at a high current density of 3.2 A g^{-1}, the reversible capacity is maintained at 128.2 mAh g^{-1} (Fig. 12b, c). Furthermore, multi-element co-doping can create more defects and active sites, increase the interlayer spacing of the carbon material, and further optimize the electron distribution around the carbon atoms, improving the conductivity of biomass-derived carbon tubes. Li et al.[141] constructed N, S and P co-doped hollow carbon microtubes (HCMTs) by direct high-temperature carbonization using silver willow blossoms composed of natural micrometer-scale fibers (Fig. 12d). As shown in Fig. 12e and 12f HCMT-1300 has nanoscale thin carbon wall (750 nm) and micrometer-sized hollow cavities, as well as suitable interlayer spacing (0.39 nm) that helps accelerate Na^+ transfer and optimize Na^+ embedding in the carbon layer. Meanwhile, the doped heteroatoms increase the conductivity and provide additional sites to accommodate the

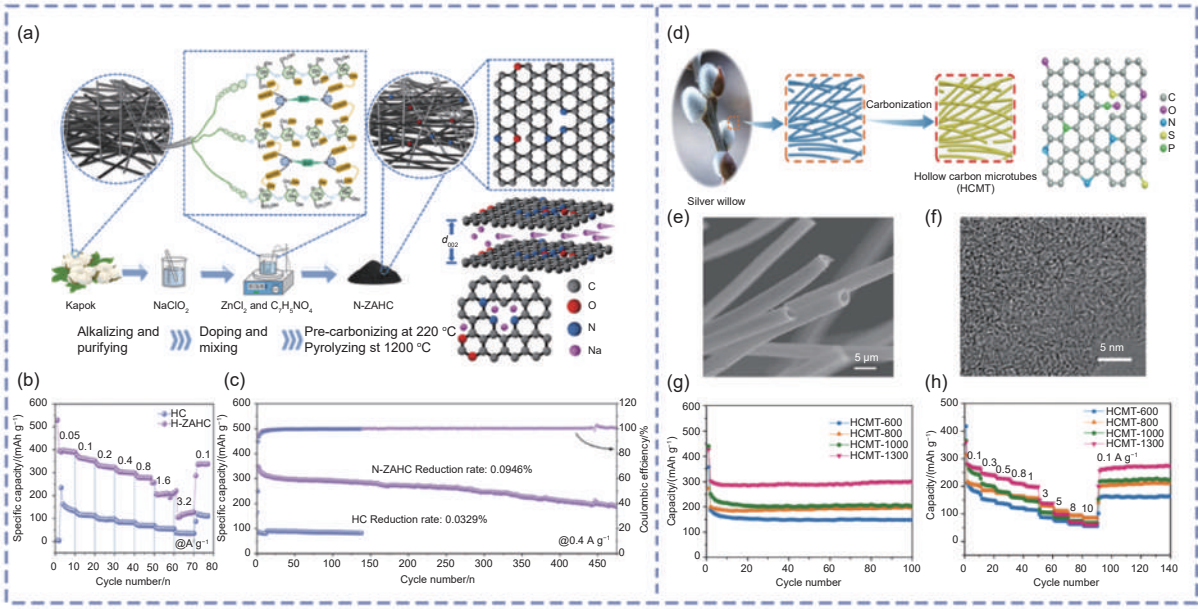

Fig. 12 (a) Schematic illustration of preparation for kapok fibers derived hard carbon[140]. (b) Rate performance of N-ZAHC and HC[140]. (c) Cyclic performance of N-ZAHC and HC at 0.4 A g^{-1}[140]. (d) Schematical illustration for the preparation of HCMTs[141]. (e) SEM image of HCMT-1300[141]. (f) Bright-field TEM image of HCMT-1300[141]. (g) Cycling performance of HCMT samples for 100 cycles with a current density of 0.1A g^{-1}[141]. (h) Rate performance of HCMT samples with different current densities ranging from 0.1 to 10 A g^{-1}[141]. Reprinted with permission

Na^+. Combining these specific structural advantages, the HCMT exhibits impressive sodium storage performance. The HCMT-1300 offers a remarkably high reversible capacity of 302 mAh g^{-1} at 0.1 A g^{-1} with no significant capacity loss during repeated charging/discharging (Fig. 12g). In addition, a high capacity of 201 mAh g^{-1} is still achieved at high current densities of up to 1 A g^{-1}, demonstrating desirable rate performance (Fig. 12h). Zhang et al.[246] prepared N, Fe co-doped carbon micron-tubes (NF-CMTs) from biomass for use in SIB anodes. The N-Fe defects provide multiple active centers for fast Na^+ storage, the open carbon skeleton enables capacitance-controlled capacity contribution, and the uniformly distributed N and Fe atoms facilitate the adsorption of Na^+, thus, the NF-CMTs exhibit excellent sodium ion storage performance, exhibiting excellent rate performance of 120 mAh g^{-1} at 2.0 A g^{-1} and 96.8% capacity retention over 200 cycles at 0.2 A g^{-1}.

The construction of composite electrode materials by combining biomass-derived carbon tubes with metal compounds that exhibit high SSA and excellent electrical conductivity represents a proven method for enhancing electrode performance. The composite electrode materials are capable of leveraging the distinctive attributes of each component, thereby facilitating a synergistic effect that enhances the storage capacity of Na^+ and the cycling stability of the electrode materials. Tong et al.[247] selected catkin-derived carbon (CDC) material with tubular morphology and Sb_2S_3 nanoparticles to form CDC/SbSxx (xx=0,10,15,20) composites. In particular, the CDC/SbS15 electrode, with its suitable Sb_2S_3 content (16.8%), low SSA, and improved conductivity, exhibits stable cycling performance as an anode for SIBs, even at high current densities. The hollow tubular morphology of the CDC effectively prevents the pulverization of Sb_2S_3 particles during cycling, thus improving the cycling stability of the electrode. Chen et al.[248] used natural herb juncus as a carbon source to obtain mesh-like FeS_2/carbon tube/FeS_2 composites (FCF-3) by uniformly immobilizing a large number of FeS_2 nanoparticles on the inner and outer surfaces of 3D interconnecting tubes through physical encapsulation and chemical bonding. The unique mesh structure accommodates volume changes and accelerates electron/ion transport, giving the FCF-3 electrode both a high capacity (542.2 mAh g^{-1}), superior cycling stability (95.4% capacity retention after 1000 cycles), and outstanding rate performance (426.2 mAh g^{-1} at 2 A g^{-1}) in SIBs. Qin et al.[249] successfully prepared few-layer 2D MoS_2 nanosheets (MoS_2/TSFC) composites grown vertically on TSFC microtubes by HTC using micro-nano-structured tubular sisal fiber carbon (TSFC) as the raw material. The free vertical growth of MoS_2 nanosheets on the TSFC carbon skeleton greatly improves the conductivity and structural stability, and the cross-linked network micro-nano-structure can provide more energy storage sites for Na^+, which helps to improve the sodium storage performance of TSFC. As an anode of SIBs, the reversible specific capacity of MoS_2/TSFC-2.5-180-12 is 243 mAh g^{-1} after 500 cycles at 0.1 A g^{-1} and a capacity retention rate of 97% between 200 and 500 cycles.

5.4 Biomass-derived carbon nanosheets

Two-dimensional sheet carbon materials are highly advantageous for energy storage and conversion applications due to their large SSA and volume ratios, excellent electrical conductivity, high ion diffusion efficiency, and an abundance of surface atoms and electroactive sites. Researchers have demonstrated the excellent electrochemical performance of synthetic carbon nanosheets from low-cost, renewable biomasses as anodes for SIBs[227,250–251]. Recently, Xiao et al.[252] used bagasse as a carbon source to prepare hard carbon materials (HC-*x*) with a sheet structure by simple pyrolysis. The medium SSA (92.3 m^2 g^{-1}) and suitable interlayer spacing (0.3768 nm) give HC-1000 outstanding sodium storage performance, exhibiting a high reversible capacity of 242.1 mAh g^{-1} and a high ICE of 73.1% at 25 mA g^{-1}, with a retention rate of 91.5% after 800 cycles at 1000 mA g^{-1}. Li et al.[253] used graphene oxides (GO) as catalysts to reconstruct lignin under hydrothermal conditions and obtained a composite ma-

terial (CRL10G) with a foam-like 3D network structure by adjusting the amount of GO. This material consisted of interconnected carbon nanosheets formed by the reconstitution of lignin on the surface of GO. CRL10G offeres significant capacity as an anode for SIBs, with a sodium storage capacity of 265 mAh g^{-1} at 0.05 A g^{-1} and 130 mAh g^{-1} at 2 A g^{-1}.

Porous carbon nanosheets with high SSA and abundant micro-mesopores can provide abundant interfacial active sites for ion accumulation. Especially the existence of the porous structure promotes the penetration of electrolytes and further shortens the diffusion distance of sodium ions, which can greatly improve the electrochemical performance of biomass-derived carbon nanosheets[254–255]. Yang et al.[142] synthesized pinecone-derived sheet-like mesoporous carbon (PDC-T) by a template-assisted method using mesoporous silica KIT-6 as a template. The interconnected mesoporous structure of PDC-T provides a shorter ion penetration path and expands the ion-accessible SSA for reversible ion adsorption and desorption. When used as an anode for SIBs, PDC-T possesses significant long-term cycling capacity (delivering 103.3 mAh g^{-1} after 1000 cycles) and rate capacity (average discharge capacity of 89.6 mAh g^{-1} at 1000 mA g^{-1}). Liang et al.[256] prepared porous flake biomass carbon (PFBC-700) from wheat straw. PFBC-700 has excellent cycling stability and rate performance as an anode for SIBs due to its maximum SSA (1192.5 m^2 g^{-1}), suitable interlayer spacing (0.421 nm), and the most abundant mesopores, which ensures that PFBC-700 is rich in active sites, but also promotes fast ion transport. A reversible specific capacity of 322 mAh g^{-1} is achieved after 300 cycles at 0.2 C. The high reversible specific capacity of 183 mAh g^{-1} is maintained after 600 cycles at 5 C. Rui et al.[257] fabricated hierarchical porous nanosheets structured carbon materials (HPNSCs) using agricultural waste-nelumbium seed-pods (NSP) as precursors and KOH as the activator. The hierarchical porous structure facilitates charge accommodation during the charge-discharge process, and the interconnectivity within the overall structure of the HPNSC material makes it conducive to energy conversion and storage. As an anode material for SIBs, HPNSC exhibits excellent rate performance with reversible capacities of 297.2, 248.5, 217.6, 184.7, 160, 139.2 and 115.3 mAh g^{-1} at current densities of 0.05, 0.1, 0.2, 0.5, 1, 2 and 5 A g^{-1}, respectively. After 3350 cycles, the capacity could still reach 160.5 mAh g^{-1}, indicating the excellent cycling stability of the HPNSC.

Altering the chemistry of carbon nanosheets through doping is an effective strategy for improving electrochemical activity and conductivity, and the preparation of heteroatom-doped carbon nanosheets derived from waste biomass has been extensively investigated[258–259]. For example, biomass-derived carbon nanosheets doped with N, S and P heteroatoms increase the interlayer spacing and active sites, which can store Na^+ more efficiently and enhance the electronic conductivity, thus effectively improving the specific capacity and rate performance. Liu et al.[260] prepared sulfur-doped camphor tree-derived hard carbon materials (S-Cmph-700) by a simple sublimation sulfur pyrolysis method. S-Cmph-700 exhibits a rough, wide sheet-like morphology and displays a loose and porous structure. S doping leads to an increase in the interlayer spacing of the Cmph-HC, facilitates the insertion/extraction of Na^+, and provides more active sites. Therefore, the SIB based on S-Cmph-700 offers a capacity of 616.7 mAh g^{-1} and an ICE of 66.61%. In addition, S-Cmph-700 exhibits good cycling performance with a reversible capacity of 145.6 mAh g^{-1} after 500 cycles at 2000 mA g^{-1}. Yang et al.[261] synthesized porous carbon nanosheets (ENPCNs-T) with controlled structure and composition enriched in marginal nitrogen (pyridinic-N and pyrrolic-N) by a simple pyrolysis process using glucose and g-C_3N_4 as the carbon and nitrogen sources, respectively. ENPCNs-T has ultrathin 2D graphene-like folds of a few microns in size (Fig. 13a, b). Due to the largest carbon interlayer spacing (0.487 nm), large SSA (690 m^2 g^{-1}), and abundant micro/mesoporous channels, ENPCN-800 exhibits excellent capacity (294.1 mAh g^{-1} at 0.1 A g^{-1}), superior rate performance (132.8 mAh g^{-1} at 10 A g^{-1}) and outstanding cycle life (180.6 mAh g^{-1} at 1 A g^{-1} after 1000 cycles)

as an anode material for SIBs. Fig. 13c shows that the good Na^+ storage performance of ENPCNs-800 is due to its high pyrrolic-N doping level (78.3%), which results in wider interlayer spacing and more Na^+ ion storage sites, facilitating the insertion/extraction of Na^+. Moreover, the co-doping of multiple elements has been demonstrated to significantly enhance the properties of biomass-derived carbon nanosheets. Tao et al.[138] selected rhizobia-rich soybean roots as precursors and constructed N, P co-doped mesoporous hard carbon (NPDCs) (Fig. 13d). NPDC-700 contains 6.82% and 3.64% of N and P, respectively, and shows good rate capacity as a SIBs anode (specific capacity at 5.0 A g^{-1} of 150 mAh g^{-1}) and cycling stability (197 mAg^{-1} at 1.0 A g for 2000 cycles) (Fig. 13e). Wang et al.[143] prepared a hard carbon material (NS-MPC) with flake-like morphology by modification with N and S using renewable waste biomass mango peels as raw material. N and S doping into hard carbon increases the interlayer spacing and defects, improves the diffusion coefficient of the material, and increases the contribution of surface-controlled capacity, thus facilitating the storage of Na^+. When used as an anode for SIBs, NS-MYC exhibits good reversible discharge capacity (400 mAh g^{-1} at 100 mA g^{-1}), superior rate performance (136 mAh g^{-1} at 4 A g^{-1}), and excellent cycling performance (155 mAh g^{-1} over 2500 cycles at 2 A g^{-1}). Zhang et al.[3] developed a top-down method to prepare N/O co-doped natural chitin-derived two-dimensional porous carbon nanosheets (CCNs) by HTC of chitin efficiently exfoliated into nanosheets. As an anode material for SIBs, high SSA, 2D porous nanostructure, and abundant N/O doping of CCNs-600 give it a high reversible capacity of 360 mAh g^{-1} at 50 mA g^{-1}, a good rate capacity of 102 mAh g^{-1} at 10 A g^{-1} and an excellent cycling stability of 140 mAh g^{-1} after 10 000 cycles at a high density of 5 A g^{-1}. Guo et al.[262] employed a microwave treatment, ion exchange, chemical etching, and hydrothermal selenization technique to prepare Co-Ni-Se nanosheets grown uniformly on a butterfly-wing carbon skeleton (BWCF) (Co-Ni-Se /BWCF-160), the Co-Ni-Se nanosheets expose more active sites and the ordered pore array ensures sufficient wetting between the electrolyte and the electrode material, allowing more efficient ion/electron transfer and

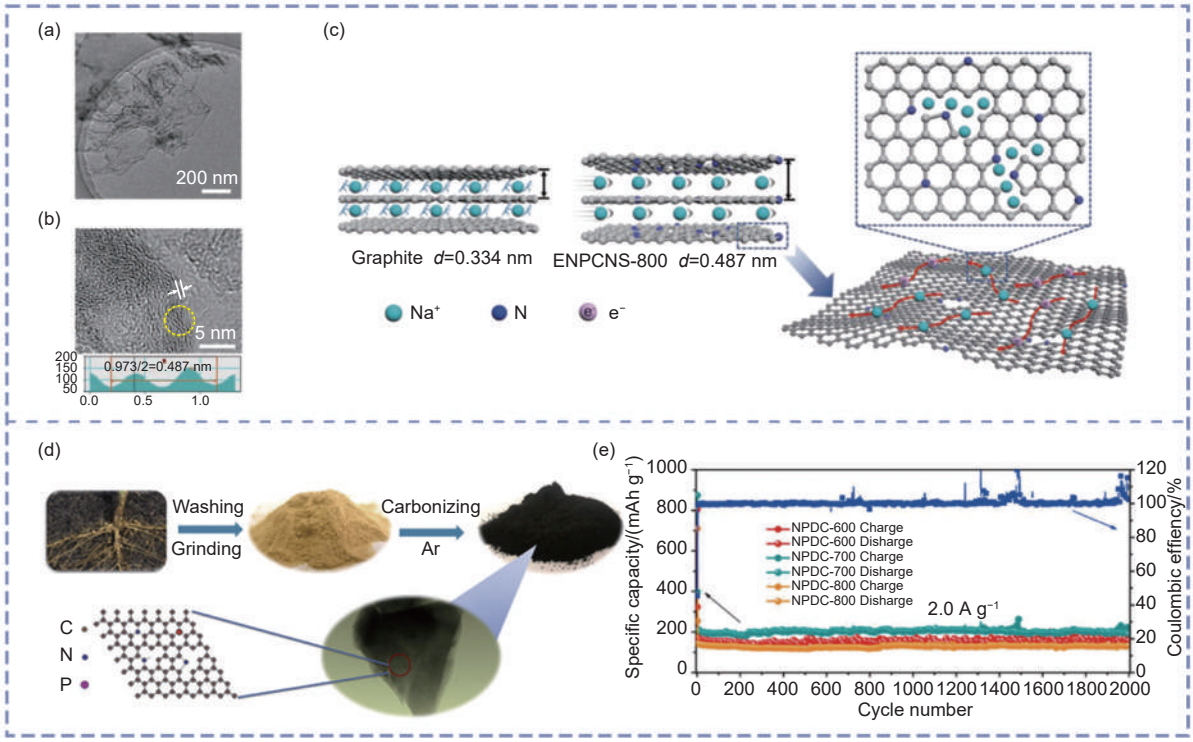

Fig. 13 (a) TEM image of ENPCNs-800[261]. (b) HRTEM image of ENPCNs-800[261]. (c) Schematic illustration of Na^+ storage mechanism of ENPCNs-T[261]. (d) Schematics of the synthesis process of NPDCs[138]. (e) Long cycle performance at 2.0 A g^{-1} of NPDCs[138]. Reprinted with permission

diffusion between the BWCF and Co-Ni-Se, accelerating the electrochemical reaction kinetics. In cycling performance tests, the Ni-Co-Se/BWCF electrode shows excellent electrochemical performance at SIBs, with an initial discharge specific capacity of up to 703 mAh g^{-1} at 0.1 A g^{-1}, maintaining 403 mAh g^{-1} after 100 cycles and at 1.0 A g^{-1} a good capacity of 211 mAh g^{-1} can still be achieved.

Meanwhile, the researchers found that compounding biomass-derived carbon nanosheets with metal compounds could also improve the material's sodium storage properties. Recently, Sun et al.[263] successfully synthesized P/N co-doped carbon nanosheets encapsulating Cu_3P nanoparticles (Cu_3P@P/N-C) through a feasible aqueous solution reaction using sodium alginate as a biomass carbon source followed by phosphorylation. Cu_3P nanoparticles are encapsulated in 2D carbon nanosheets, which buffer the volume change and prevent agglomeration of Cu_3P nanoparticles, enhance the electronic conductivity of the whole electrode as well as provide fast channels for electron/ion diffusion. Benefiting from these advantages, Cu_3P@P/N-C anode in SIBs exhibits a long cycle life (reversible capacity of 209.3 mAh g^{-1} after 1000 cycles at 1 A g^{-1}) and excellent rate performance (specific capacity of 118.2 mAh g^{-1} after 2000 cycles at a high current density of 5 A g^{-1}).

5.5 Biomass-derived carbon frameworks

3D carbon frameworks play a significant role in the application of electrode materials. They offer high SSA, a developed layered pore structure, and mechanical and chemical stability, which facilitate fast electron transfer and shorten the ion diffusion path. This provides more active reaction sites, which improves specific capacity and cycling stability. It is for these reasons that 3D carbon frameworks have been identified as a promising carbon anode, attracting significant interest from the scientific community in recent years. Biomass-derived carbon frameworks, with their inherent layered structure derived from natural sources and open channels with low tortuosity, have been shown to facilitate electrolyte penetration and transport, making them a promising material for SIBs[264–266]. Wang et al.[144] prepared corncob-derived hard carbon (CDHC). The hard carbon obtained by pyrolysis at 1300 °C (CDHC-1300) demonstrates the most excellent electrochemical performance, with a first discharge specific capacity of 391 mAh g^{-1} and an ICE of approximately 80% at 0.1 C. Even after 100 cycles, the discharge capacity remains at 250 mAh g^{-1}. Xie et al.[267] used acid etching to remove impurity elements and then calcined at high temperatures to obtain bamboo-based hard carbon, and the hard carbon particles show irregular bulk morphology, among which the hard carbon material prepared at 1300 °C (Bam-1300) obtains a high ICE (83.7%) and reversible specific capacity (up to 303.8 mAh g^{-1} at 30 mA g^{-1}). In addition, the plateau capacity of Bam-1300 is 208 mAh g^{-1} when cycled at 30 mA g^{-1}, which accounted for 57.3% of the total discharge capacity, which is closely related to its ordered structure and closed micropores. Yang et al.[268] employed freeze-drying treatment of onion biomass to synthesize nitrogen-doped porous carbon materials (FDOs) by KOH activation and pyrolysis at 900 °C. The FDO surface displays a wrinkled structure with macropores of micrometer diameter, which increases the contact area between the electrolyte and the electrode. This provides additional active sites for sodium storage and a wider electrode/electrolyte interface, which in turn facilitates rapid sodium ion storage. As a consequence, FOD exhibits remarkable rate performance as an anode for SIB, delivering 132.5, 124.2, 118.5, 113.5, 104.8, 93.4, 78.0, 65.6 and 116.7 mAh g^{-1} at 0.2, 0.5, 1, 2, 5, 10, 20, 30 and 0.5 A g^{-1}, respectively.

The hierarchical micro/meso/macroporous structure facilitates rapid sodium ion diffusion, while its substantial electrochemically active surface area enables high-capacity storage. The presence of micropores can effectively enhance the SSA and provide a substantial number of active sites for electrolyte ions. Meanwhile, meso- and macropores can reduce the ion transfer path and accelerate the diffusion of ions in the electrode material, which is pivotal to attaining optimal rate performance. Combining micro, meso, and macropores confers a distinctive advantage on hier-

archical porous carbon frameworks in energy storage[269–272]. As displayed in Fig. 14a, Zhao et al.[146] used onion peel as a biomass precursor and Na_2HPO_4 as an activator to produce 3D hierarchical porous carbon materials (HPCN) by a simple one-step activation method. The isotherms of the HPCN samples are typical of the combination of type I (characteristic of microporous carbon) and type IV (characteristic of mesoporous materials), with a large SSA of 756.5 m^2 g^{-1}, and the pore size mainly concentrates around 4 nm (Fig. 14b, c), indicating that the material containing abundant micropores and mesopores as well as a certain number of macropores, and this hierarchical porous structure not only provides more active surface sites for the storage of sodium ions but also can effectively shorten the diffusion distance of Na^+ ions. It can be demonstrated that HPCN exhibits excellent electrochemical performance in SIBs, with an ultra-high reversible capacity of 333.8 mAh g^{-1} at 50 mA g^{-1}, an exceptional rate performance of 69.4 mAh g^{-1} at 10 A g^{-1}, and a capacity retention rate of 91% after 1000 cycles. Yang et al.[147] prepared hierarchical porous hard carbon (HCRH) by carbonizing rice husks at different temperatures. Among them, the hard carbon treated at 1200 °C (HCRH-1200) shows superb sodium storage properties. As shown in Fig. 14d, HCRH-1200 has a hierarchical porous structure, and this special structure can adapt to the volume change of the electrode material during the charging/discharging cycle, which improves the Na^+ storage and cycling stability. Meanwhile, HCRH-1200 displays a suitable graphite layer spacing (0.382 nm), making Na^+ insertion/extraction easier and thus improving sodium storage performance. Therefore, as an anode for SIBs, HCRH-1200 exhibits excellent rate capacity (185.71 mAh g^{-1} at 500 mA g^{-1}) and cycling stability (324.8 mAh g^{-1} after 400 cycles at 100 mA g^{-1}) (Fig.14e, f). Zhang et al.[148] prepared

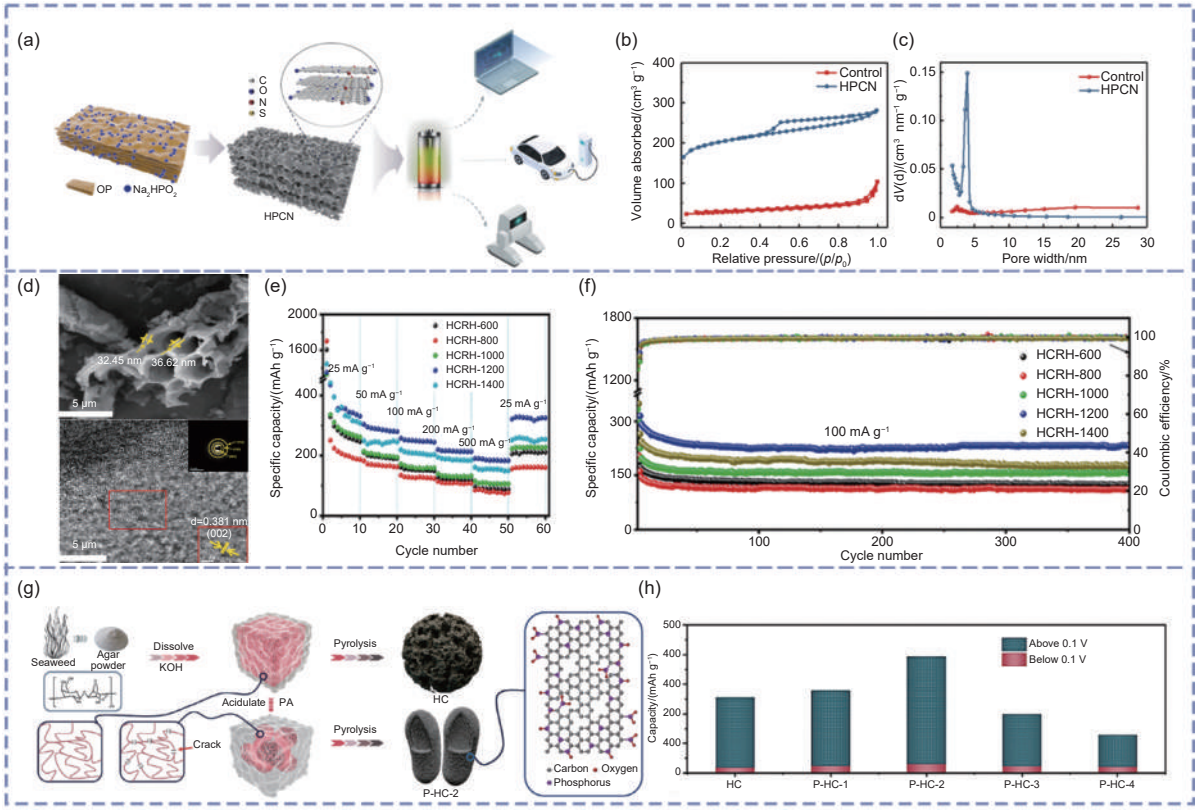

Fig. 14 (a) Illustration of the biomass-derived 3D hierarchical porous framework of carbon nanosheets as electrode materials in SIBs[146]. (b) Nitrogen adsorption-desorption isotherms of HPCN[146]. (c) Pore size distribution of HPCN[146]. (d) SEM and HRTEM micrographs of HCRH-1200[147]. (e) Rate capabilities of the HCRH-*x* composites at different rates[147]. (f) Cycling performance of the HCRH-*x* composites at a high rate of 100 mA g^{-1}[147]. (g) Synthesis and morphology characterization of HC and P-HC-*x*[148]. (h) Summary of the capacity above and below 0.1 V of the HC and P-HC-*x* electrodes[148]. Reprinted with permission

phosphor-doped agar-derived porous carbon (P-HC-2) (Fig. 14g) using agar as a precursor and phytic acid (PA) as a microscopic morphology-directing agent and dopant under low-temperature carbonization at 750 °C. Appropriate PA content can significantly adjust the pore size distribution and increase the defect concentration of the prepared carbon. Thus P-HC-2 exists in a hierarchical pore structure including micropores, macropores, and irregular mesopores. As shown in Fig. 14h, the P-HC-2 anode has a high slope capacity contribution of 363 mAh g^{-1} above 0.1 V, indicating that Na^+ storage is mainly achieved by filling nanopores and surface adsorption, which further leads to the excellent rate performance (discharge specific capacity remains 90 mAh g^{-1} at 10 A g^{-1}) and cycling stability (capacity stabilizes at 178 mAh g^{-1} after 10 000 cycles at 5 A g^{-1}).

To further improve the electronic conductivity, increase surface defects, and enlarge interlayer spacing of biomass-derived carbon frameworks and to improve their electrochemical properties, researchers have doped heteroatoms such as N, O, S and P into carbon frameworks through carbonization and activation processes, confirming that heteroatom doping has a positive effect on improving the sodium storage properties of 3D carbon frameworks[208,273]. Liang et al.[149] prepared honeycomb-shaped nitrogen-rich porous carbon (CPC) by simple impregnation-activation method using sunflower seed hulls as a precursor as shown in Fig. 15a. One of the samples at an activation temperature of 700 °C (CPC-700) has abundant micro/meso/macropores as well as interconnected network structures, which provides favorable conditions for Na^+ diffusion and transport. Moreover, the high N-doping content (3.93%) in CPC-700 leads to a large number of defects on the surface of the material, thus providing a large number of reaction sites for Na^+ adsorption, which is the key reason for the high capacity of the CPC-700 electrode. When used as active material in a SIB anode, CPC-700 provides a high reversible capacity of 609.15 mAh g^{-1} at 0.2 C, with a capacity retention of 77.77% after 100 cycles (Fig. 15b). It also exhibits a reversible capacity of 346 mAh g^{-1} and 243.9 mAh g^{-1} at 2 C and 5 C high rates, respectively (Fig. 15c). Alcántara et al.[188] treated olive stones with sulfuric acid solution and obtained S-doped porous carbon (SPC) after carbonization at 800 °C. During SPC synthesis, sulfuric acid acts not only as a simple impurity remover to increase the carbon yield and produce micropores, but also as an S dopant to induce C—S bond formation, enlarge the layer spacing, and improve electrochemical properties. Thus, as an SIB anode, AC provides higher reversible capacity (250 mAh g^{-1} at 200 mAh g^{-1}) and better rate performance (110 mAh g^{-1} at 185 mA g^{-1}) with the synergistic effect of sulfur doping and porous structure. The co-doping of multiple elements has the potential to significantly enhance the properties of materials, the overall properties of biomass-derived carbon frameworks can be optimized by the synergistic effect generated by multi-atom co-doping. In comparison to single-element doping, multi-element co-doping has the potential to create a greater number of defects and active sites. Furthermore, it can facilitate the optimization of the electron distribution around carbon atoms and enhance the electrical conductivity of the materials. Sun et al.[150] prepared biomass starch-based S/N co-doped hierarchical porous carbon materials (SN-HPCS) using an in situ template method. From the EDS image (Fig. 15d), it can be seen that the elements of C, O, N and S are uniformly distributed in the 3D network structure of SN-HPCS. The storage capacity of Na^+ is affected by the degree of graphitization and structural defects of the carbon material (Fig. 15e), and N and S doping not only enlarges the interlayer spacing but also provides more reactive sites for the storage of Na^+. Based on the synergistic effect of nitrogen and sulfur double doping, as an anode for SIBs, SN-HPCS shows superior storage capacity for Na^+, exhibiting a high capacity of 313 mAh g^{-1} at 0.8 A g^{-1} and cycling at a current density of 8 A g^{-1} for 3000 cycles possesses an excellent cycling stability of 156 mAh g^{-1} while maintaining 93% of its initial capacity. N, P co-doped porous carbon ($SBNP_K$) was prepared from sugarcane bagasse by Deng et al.[151] using melamine as a nitrogen

source, $NaH_2PO_4 \cdot 2H_2O$ as a phosphorus source, and KOH as an activator. As shown in Fig. 15f, N and P atoms were successfully incorporated into the carbon skeleton, enlarging interlayer distances. The special hierarchical porous structure can adapt to volume changes during cycling. Due to the synergistic effect of the property and structure of N and P doping, the material obtained at 600 °C ($SBNP_K$-600) shows superior electrochemical performance in SIBs, with a high reversible capacity of 304.1 mAh g^{-1} at 25 mA g^{-1}, and 225.7 mAh g^{-1} after 1000 cycles at 500 mA g^{-1}. Fig. 15g depicts the good rate performance of $SBNP_K$-600, with corresponding discharge capacities of 337.6 and 197.4 mAh g^{-1} at 25 and 1000 mA g^{-1}, respectively. In addition, the Nyquist plot (Fig. 15h) shows that the SBNP-600 electrode exhibits the smallest charge transfer resistance (96.0 Ω), which is also related to its proper doping with N and P atoms and large interlayer spacing. Deng et al.[152] synthesized P, N, S co-doped camphor wood-derived hard carbon (P-N-S-Cmph) by a simple pyrolysis process, and the synergistic effect of S, N, P heteroatom doping enlarged the interlayer spacing (0.430 nm) of the P-N-S-Cmph, reduces the irreversible depletion of Na^+ by surface functional groups. These advantages render P-N-S-Cmph an efficacious SIBs hard carbon anode, exhibiting an initial discharge capacity of 791 mAh g^{-1} at a current density of 40 mA g^{-1}, corresponding to an ICE of 70.74%. Upon 500 cycles at 2 A g^{-1}, the specific capacity of P-N-S-Cmph can still reach 280 mAh g^{-1}.

In addition to the direct use of biomass-derived 3D carbon skeletons as anode materials for SIBs, metals or metal oxides can be introduced without destroying the original structure of the carbon skeletons to establish composite electrode materials with good

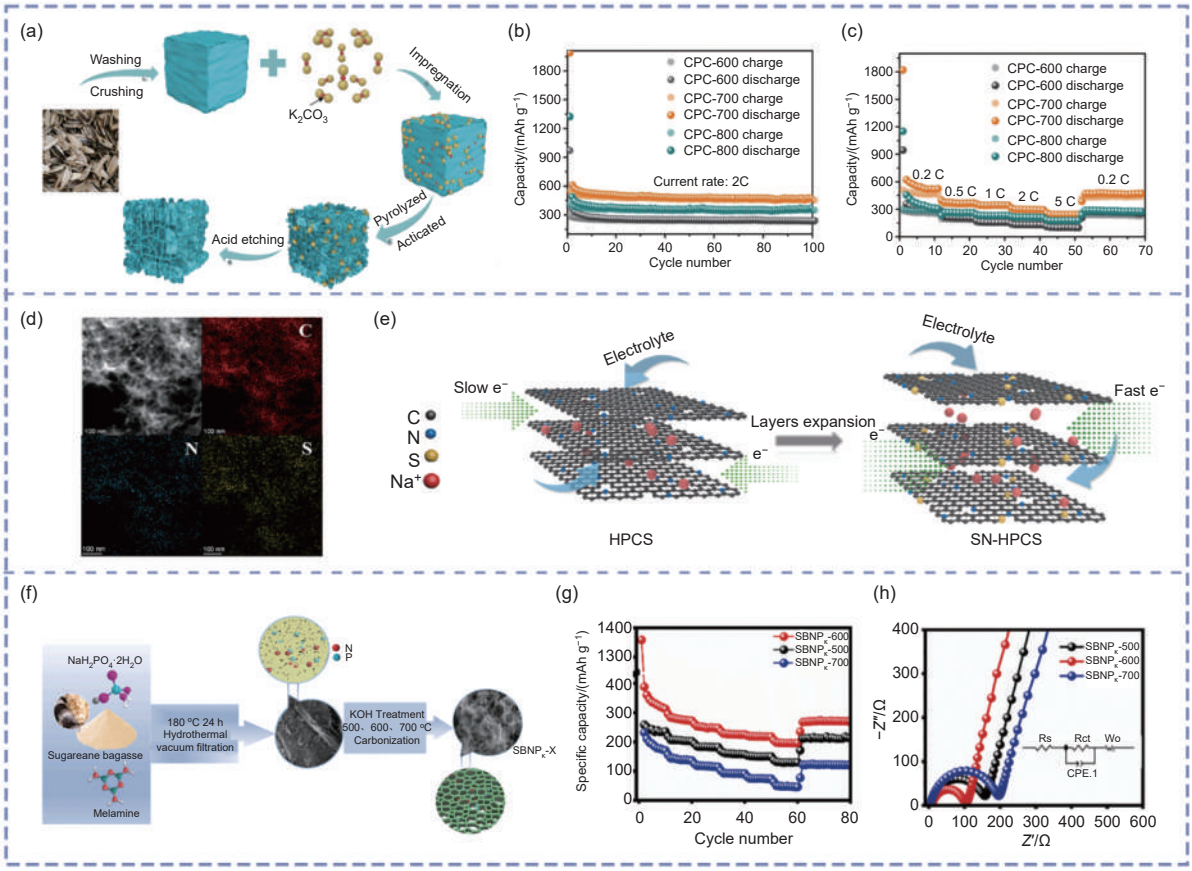

Fig. 15 (a) Schematic diagram of the synthesis mechanism of CPC[149]. (b) Cycling performance at 0.2 C[149]. (c) Rate capability from 0.2 C to 5 C of CPC-600, CPC-700 and CPC-800[149]. (d) EDS images of SN-HPCS and the corresponding elemental mapping of C, N, and S elements, respectively[150]. (e) Schematic illustration of the electrode structure change and the transport of Na^+ and electrons in SN-HPCS compared with HPCS[150]. (f) Schematic illustration of the preparation process of $SBNP_K$-X[151]. (g) Rate performances at different current densities[151]. (h) Nyquist plots of the $SBNP_K$-X anode[151]. Reprinted with permission

electrical conductivity and stable structure to further improve the sodium storage performance of BDCs[274]. Liu et al.[275] modified chickpea husk-derived hard carbon using carbonization and hydrothermal treatment to prepare MoS_2 nanopatterned porous hard carbon skeleton (HC@MoS_2-II). The modified HC@MoS_2-II electrode exhibits an initial reversible capacity of 469 mAh g^{-1} and 63% ICE at 50 mA g^{-1}, a stable average specific capacity of 398 mAh g^{-1} after 200 cycles, and an ultra-long cycling stability of 200 mAh g^{-1} after more than 3500 cycles at 1000 mA g^{-1}. The extraordinary electrochemical performances reveal the positive effects of the synergistic assembly of porous hard carbon skeleton and MoS_2 nanoflowers on the composite electrodes, i.e., the large interlayer spacing (0.650 nm) of MoS_2 is beneficial for the reversible embedding/de-embedding of the sodium ions. The high surface area of the porous hard carbon skeleton efficiently cushions the bulky swelling during charging/discharging. Chen et al.[276] used waste crab shells as a carbon source of low-cost 3D interconnected honeycomb hierarchical structure SnS_2/C and FeS_2/C composite anode materials by depositing SnS_2 nanosheets and FeS_2 nanosphere structures onto crab shell-derived carbon by a simple hydrothermal reaction. The SnS_2/C and FeS_2/C samples have a high capacity because of transition metal sulfides. When applied as anodes for SIBs, the capacities of SnS_2/C and FeS_2/C are 416.5 and 393.8 mAh g^{-1} after 200 cycles at a current density of 0.5 mA g^{-1}, respectively. Deng et al.[277] synthesized carbon-Fe-Co bimetallic composite (TS-2) from tapioca starch and $CoFe_2O_4$ by pyrolysis in one step. The introduction of bimetallic alloys facilitates the reaction kinetics, and the disordered carbon matrix effectively mitigates the volume expansion, prevents the aggregation of bimetallic alloys, and provides more accesses for the sodium ions shuttling, which enhances the cycling performance. The initial sodium storage capacity of TS-2 at 0.05 A g^{-1} is 712 mAh g^{-1} with 89.2% ICE, provides more than 419 mAh g^{-1} at a high current of 10 A g^{-1}, and the capacity after 200 cycles is stable at 325 mAh g^{-1} at 0.5 A g^{-1}.

6 Conclusions and outlooks

To achieve high energy density, high reversible capacity, and high cycling stability in SIBs, it is essential to develop anode materials suitable for Na^+ insertion/extraction. In this context, biomass, which is widely available, inexpensive, and rich in organic matter, has come to the forefront of researchers' minds. By treating biomass through various methods such as pyrolysis, activation, and templating, the SSA of BDCs can be effectively controlled, the pore structure can be improved and the surface functional groups can be increased, thus enabling the transformation from low-cost biomass to highly utilizable carbon-based anode materials for SIBs. Sodium storage active sites including graphite microcrystallites, defects, and nanopores enable BDCs to have multiple sodium storage methods. During charging and discharging, BDCs with different structures achieve reversible sodium insertion/extraction through sodium storage mechanisms such as sodium intercalation, active site sodium storage, and sodium storage in micropores, leading to the proposal of multiple mechanism models for sodium storage. At the same time, the good electrical conductivity of carbon-based materials and the structure to buffer the volume change of Na^+ insertion/extraction make the sodium ion battery have excellent capacity performance, rate performance, and cycle stability performance. However, the capacity of BDCs as anode materials for SIBs is generally low, and there is a lack of research on the compatibility with cathode materials. In addition, its application and promotion as an SIB anode for high-mass-loading have been less mentioned compared to cathode materials or other research areas[278–281].

In conclusion, to overcome the problems faced by BDCs as anode materials for SIBs, future research can include the following aspects: (1) So far, the sodium-ion storage mechanism is still controversial. In the future, researchers can further observe the storage process of sodium in BDCs through advanced testing techniques and characterization methods such as in-situ X-ray diffraction and in-situ electron microscopy. This will allow the mechanism of sodium storage in

BDCs can be further explored and analyzed from the structural point of view, which can provide theoretical support for the improvement of electrochemical performance of SIBs. (2) The choice of precursor is the primary factor in determining the sodium storage performance of BDCs. Plants, animals microorganisms can be used as precursors for BDCs. The ideal biomass precursor should have the advantages of low-cost, environmentally friendly properties, and excellent sodium storage performance at the same time. Therefore, the development of a suitable biomass precursor can help to design high-performance anode materials and promote the commercialization of SIBs in the field of smart grid and large-scale energy storage technologies. (3) Reasonable regulation of the microstructure of BDCs is an essential means to improve their sodium storage capacity. We can design optimized SIBs carbon anodes by purposely modifying BDCs based on their sodium storage active sites (graphite microcrystallites, defects, and nanopores), such as increasing the spacing of graphite layers, doping heteroatoms to produce abundant defect sites, introducing closed pores and designing the morphology, etc. It is worth noting that the effects of different modifications on materials are often not independent of each other, and therefore need to be precisely controlled to achieve a balance to ensure that the performance of the material is maximized. (4) To adjusting the microstructure of BDCs themselves, it is also necessary to focus on the research of electrolyte engineering and surface modification, pre-sodiation modification, etc. In addition, matching the appropriate cathode material for the high-performance BDC anode is an indispensable step in improving the energy density of the full battery, which will help promote the further application and development of SIBs. (5) Designing high-mass-loading BDC anodes is the most promising strategy to increase the energy density of SIBs in a limited space. We need to address the deteriorated electrolyte transport and electron transfer kinetics of conventional thick electrodes due to inactive binders and their severe cracking problems to satisfy the core requirements of practical/industrial production and applications. Therefore, extensive efforts are needed to optimize the design and configuration of high-mass-loading electrodes, e.g. developing self-supporting electrodes to avoid the introduction of electrochemically inert “dead mass” . In addition, the effect of the electrolyte on the charge storage on the surface of the high-mass-loading anode should be given sufficient attention, especially its penetration and filling process on the electrodes. Through continuous improvement and optimization, BDC anodes are expected to pave the way for the commercial development and integration of SIBs into various energy storage fields, enabling SIBs and making significant contributions to the global transition to sustainable energy technologies.

Acknowledgements

This work was supported by the Heilongjiang Province Excellent Youth Fund (YQ2023E002) and the National Natural Science Foundation of China (32370413, 22478083).

References

[1] Chombo P V, Laoonual Y. A review of safety strategies of a Li-ion battery[J]. Journal of Power Sources, 2020, 478: 228649.

[2] Liu W, Liu P, Mitlin D. Tutorial review on structure-dendrite growth relations in metal battery anode supports[J]. Chemical Society Reviews, 2020, 49(20): 7284-7300.

[3] Gao L, Ma J, Li S, et al. 2D ultrathin carbon nanosheets with rich N/O content constructed by stripping bulk chitin for high-performance sodium ion batteries[J]. Nanoscale, 2019, 11(26): 12626-12636.

[4] Li J, Yan D, Lu T, et al. An advanced CoSe embedded within porous carbon polyhedra hybrid for high performance lithium-ion and sodium-ion batteries[J]. Chemical Engineering Journal, 2017, 325: 14-24.

[5] Li M, Lu J, Chen Z, et al. 30 Years of Lithium-ion batteries[J].

Advanced Materials, 2018, 30(33): 1800561.

[6] Xu Z L, Park J, Yoon G, et al. Graphitic carbon materials for advanced sodium-ion batteries[J]. Small Methods, 2019, 3(4): 1800227.

[7] Wu Y, Huang X, Huang L, et al. Strategies for rational design of high-power lithium-ion batteries[J]. Energy & Environmental Materials, 2021, 4(1): 19-45.

[8] Zhen Y, Chen Y, Li F, et al. Ultrafast synthesis of hard carbon anodes for sodium-ion batteries[J]. Proceedings of the National Academy of Sciences of the United States of America, 2021, 118(42): e2111119118.

[9] Alvira D, Antorán D, Manyà J J. Plant-derived hard carbon as anode for sodium-ion batteries: A comprehensive review to guide interdisciplinary research[J]. Chemical Engineering Journal, 2022, 447: 137468.

[10] Lao M, Zhang Y, Luo W, et al. Alloy-based anode materials toward advanced sodium-ion batteries[J]. Advanced Materials, 2017, 29(48): 1700622.

[11] Fang C, Huang Y, Zhang W, et al. Routes to high energy cathodes of sodium-ion batteries[J]. Advanced Energy Materials, 2016, 6(5): 1501727.

[12] Wang T, Su D, Shanmukaraj D, et al. Electrode materials for sodium-ion batteries: Considerations on crystal structures and sodium storage mechanisms[J]. Electrochemical Energy Reviews, 2018, 1(2): 200-237.

[13] Hwang J Y, Myung S T, Sun Y K. Sodium-ion batteries: Present and future[J]. Chemical Society Reviews, 2017, 46(12): 3529-3614.

[14] Xiang X, Zhang K, Chen J. Recent advances and prospects of cathode materials for sodium-ion batteries[J]. Advanced Materials, 2015, 27(36): 5343-5364.

[15] Trotta F, Wang G J, Guo Z, et al. A comparative techno-economic and lifecycle analysis of biomass-derived anode materials for lithium- and sodium-Ion batteries[J]. Advanced Sustainable Systems, 2022, 6(6): 2200047.

[16] Armand M B. Intercalation electrodes[M]. Boston, MA: Springer US, 1980: 145-161.

[17] Liu Q, Hu Z, Chen M, et al. The cathode choice for commercialization of sodium-ion batteries: Layered transition metal oxides versus Prussian blue analogs[J]. Advanced Functional Materials, 2020, 30(14): 1909530.

[18] Oz E, Altin S, Avci S. Investigation of physical and electro-chemical properties of Ni-doped Tunnel/P2 hybrid $Na_{0.44}MnO_2$ cathode material for sodium-ion batteries[J]. Journal of Solid State Chemistry, 2023, 318: 123741.

[19] Qian J, Wu C, Cao Y, et al. Prussian blue cathode materials for sodium-ion batteries and other ion batteries[J]. Advanced Energy Materials, 2018, 8(17): 1702619.

[20] Zhou A, Xu Z, Gao H, et al. Size-, water-, and defect-regulated potassium manganese hexacyanoferrate with superior cycling stability and rate capability for low-cost sodium-ion batteries[J]. Small, 2019, 15(42): 1902420.

[21] Kjeldgaard S, Dugulan I, Mamakhel A, et al. Strategies for synthesis of Prussian blue analogues[J]. Royal Society Open Science, 2021, 8(1): 201779.

[22] Wei Y, Huang Y, Zhang Y, et al. Research progress of Na_2MSiO_4 (M = Fe, Mn, Co and Ni) sodium ion cathode materials[J]. Energy Reports, 2020, 6: 2191-2199.

[23] Thangavel R, Han D, Moorthy B, et al. Understanding the structural phase transitions in $Na_3V_2(PO_4)_3$ symmetrical sodium-ion batteries using synchrotron-based X-ray techniques[J]. Small Methods, 2022, 6(2): 2100888.

[24] Barman P, Jha P K, Chaupatnaik A, et al. A new high voltage alluaudite sodium battery insertion material[J]. Materials Today Chemistry, 2023, 27: 101316.

[25] Cariello M, Johnston B, Bhosale M, et al. Benzo-dipteridine derivatives as organic cathodes for Li- and Na-ion batteries[J]. ACS Applied Energy Materials, 2020, 3(9): 8302-8308.

[26] Kuan H C, Luu N T H, Ivanov A S, et al. A nitrogen- and carbonyl-rich conjugated small-molecule organic cathode for high-performance sodium-ion batteries[J]. Journal of Materials Chemistry A, 2022, 10(30): 16249-16257.

[27] Liu X, Si Y, Li K, et al. Exploring sodium storage mechanism of topological insulator Bi_2Te_3 nanosheets encapsulated in conductive polymer[J]. Energy Storage Materials, 2021, 41: 255-263.

[28] Yang K, Tang J, Liu Y, et al. Controllable synthesis of peapod-like Sb@C and corn-like C@Sb nanotubes for sodium storage[J]. ACS nano, 2020, 14(5): 5728-5737.

[29] Pfeifer K, Arnold S, Budak Ö, et al. Choosing the right carbon additive is of vital importance for high-performance Sb-based Na-ion batteries[J]. Journal of Materials Chemistry A, 2020, 8(12): 6092-6104.

[30] Zhang N, Han X, Liu Y, et al. 3D Porous γ-Fe_2O_3@C nanocomposite as high-performance anode material of Na-Ion batteries[J]. Advanced Energy Materials, 2015, 5(5): 1401123.

[31] Fang S, Bresser D, Passerini S. Transition metal oxide anodes for electrochemical energy storage in lithium- and sodium-ion batteries[J]. Advanced Energy Materials, 2020, 10(1): 1902485.

[32] Li S, Zhao Z, Li C, et al. SnS_2@C hollow nanospheres with robust structural stability as high-performance anodes for sodium ion batteries[J]. Nano-Micro Letters, 2019, 11(1): 14.

[33] Kannan K, Kouthaman M, Subadevi R, et al. Dual metal (Fe and Mg) substituted layered titanium-based P2 and O3-type negative electrodes for rechargeable sodium batteries[J]. Advanced Powder Technology, 2023, 34(6): 104038.

[34] Meng W, Dang Z, Li D, et al. Interface and defect engineered titanium-base oxide heterostructures synchronizing high-rate and ultrastable sodium storage[J]. Advanced Energy Materials, 2022, 12(40): 2201531.

[35] Cao Y, Zhang Q, Wei Y, et al. A water stable, near-zero-strain O3-Layered titanium-based anode for long cycle sodium-ion battery[J]. Advanced Functional Materials, 2020, 30(7): 1907023.

[36] Xia J L, Yan D, Guo L P, et al. Hard carbon nanosheets with uniform ultramicropores and accessible functional groups showing high realistic capacity and superior rate performance for sodium-

ion storage[J]. Advanced Materials, 2020, 32(21): e2000447.

[37] Sun F, Wang H, Qu Z, et al. Carboxyl-dominant oxygen rich carbon for improved sodium ion storage: Synergistic enhancement of adsorption and intercalation mechanisms[J]. Advanced Energy Materials, 2021, 11(1): 2002981.

[38] Zhang W, Zhang F, Ming F, et al. Sodium-ion battery anodes: Status and future trends[J]. EnergyChem, 2019, 1(2): 100012.

[39] Wang Y, Liu J, Chen X, et al. Structural engineering of tin sulfides anchored on nitrogen/phosphorus dual-doped carbon nanofibres in sodium/potassium-ion batteries[J]. Carbon, 2022, 189: 46-56.

[40] Hou H, Qiu X, Wei W, et al. Carbon anode materials for advanced sodium-ion batteries[J]. Advanced Energy Materials, 2017, 7(24): 1602898.

[41] Stevens D A, Dahn J R. High capacity anode materials for rechargeable sodium-ion batteries[J]. Journal of The Electrochemical Society, 2000, 147(4): 1271.

[42] Lu Y, Zhao C, Qi X, et al. Pre-oxidation-tuned microstructures of carbon anodes derived from pitch for enhancing Na storage performance[J]. Advanced Energy Materials, 2018, 8(27): 1800108.

[43] Li Y, Hu Y S, Qi X, et al. Advanced sodium-ion batteries using superior low cost pyrolyzed anthracite anode: Towards practical applications[J]. Energy Storage Materials, 2016, 5: 191-197.

[44] Bai Y, Wang Z, Wu C, et al. Hard carbon originated from polyvinyl chloride nanofibers as high-performance anode material for Na-ion battery[J]. ACS applied materials & interfaces, 2015, 7(9): 5598-5604.

[45] Lotfabad E M, Ding J, Cui K, et al. High-density sodium and lithium ion battery anodes from banana peels[J]. ACS nano, 2014, 8(7): 7115-7129.

[46] Liu P, Li Y, Hu Y S, et al. A waste biomass derived hard carbon as a high-performance anode material for sodium-ion batteries[J]. Journal of Materials Chemistry A, 2016, 4(34): 13046-13052.

[47] Wang H, Yu W, Shi J, et al. Biomass derived hierarchical porous carbons as high-performance anodes for sodium-ion batteries[J]. Electrochimica Acta, 2016, 188: 103-110.

[48] Li Y, Hu Y S, Titirici M M, et al. Hard carbon microtubes made from renewable cotton as high-performance anode material for sodium-ion batteries[J]. Advanced Energy Materials, 2016, 6(18): 1600659.

[49] Niu Q, Tang Q, Sun X, et al. Wood-based carbon tubes with low-tortuosity and open tubular structure for energy storage application[J]. Journal of Materials Science, 2022, 57(8): 5154-5166.

[50] Wang H G, Wu Z, Meng F L, et al. Nitrogen-doped porous carbon nanosheets as low-cost, high-performance anode material for sodium-ion batteries[J]. ChemSusChem, 2013, 6(1): 56-60.

[51] Thompson M, Xia Q, Hu Z, et al. A review on biomass-derived hard carbon materials for sodium-ion batteries[J]. Materials Advances, 2021, 2(18): 5881-5905.

[52] Molaiyan P, Reis G S D, Karuppiah D, et al. Recent progress in biomass-derived carbon materials for Li-ion and Na-ion batteries—A review[J]. 2023.

[53] Rakhymbay L, Bazybek N, Kudaibergenov K, et al. Present development and future perspectives on biowaste-derived hard carbon anodes for room temperature sodium-ion batteries[J]. Journal of Power Sources, 2024, 602: 234347.

[54] Huang S, Qiu X Q, Wang C W, et al. Biomass-derived carbon anodes for sodium-ion batteries[J]. New Carbon Materials, 2023, 38(1): 40-66.

[55] Yan M, Qin Y, Wang L, et al. Recent advances in biomass-derived carbon materials for sodium-ion energy storage devices[J]. Nanomaterials, 2022, 12(6): 930.

[56] Huang Y, Tang Z, Zhou S, et al. Renewable waste biomass-derived carbon materials for energy storage[J]. Journal of Physics D: Applied Physics, 2022, 55(31): 313002.

[57] Saurel D, Orayech B, Xiao B, et al. From charge storage mechanism to performance: A roadmap toward high specific energy sodium-ion batteries through carbon anode optimization[J]. Advanced Energy Materials, 2018, 8(17): 1703268.

[58] Huang Q, Song S, Chen Z, et al. Biochar-based materials and their applications in removal of organic contaminants from wastewater: state-of-the-art review[J]. Biochar, 2019, 1(1): 45-73.

[59] Zheng Y, Lu Y, Qi X, et al. Superior electrochemical performance of sodium-ion full-cell using poplar wood derived hard carbon anode[J]. Energy Storage Materials, 2019, 18: 269-279.

[60] Zhang G, Chen Y, Chen Y, et al. Activated biomass carbon made from bamboo as electrode material for supercapacitors[J]. Materials Research Bulletin, 2018, 102: 391-398.

[61] Hao E, Liu W, Liu S, et al. Rich sulfur doped porous carbon materials derived from ginkgo leaves for multiple electrochemical energy storage devices[J]. Journal of Materials Chemistry A, 2017, 5(5): 2204-2214.

[62] Cong L, Tian G, Luo D, et al. Hydrothermally assisted transformation of corn stalk wastes into high-performance hard carbon anode for sodium-ion batteries[J]. Journal of Electroanalytical Chemistry, 2020, 871: 114249.

[63] Yan P, Ai F, Cao C, et al. Hierarchically porous carbon derived from wheat straw for high rate lithium ion battery anodes[J]. Journal of Materials Science: Materials in Electronics, 2019, 30(15): 14120-14129.

[64] Ding J, Zhang Y, Huang Y, et al. Sulfur and phosphorus co-doped hard carbon derived from oak seeds enabled reversible sodium spheres filling and plating for ultra-stable sodium storage[J]. Journal of Alloys and Compounds, 2021, 851: 156791.

[65] Zhang Y, Li X, Dong P, et al. Honeycomb-like Hard carbon derived from pine pollen as high-performance anode material for sodium-ion batteries[J]. ACS Applied Materials & Interfaces, 2018, 10(49): 42796-42803.

[66] Ding J, Wang H, Li Z, et al. Peanut shell hybrid sodium ion capacitor with extreme energy–power rivals lithium ion capacitors[J]. Energy & Environmental Science, 2015, 8(3): 941-955.

[67] Bharti V, Gangadharan A, Rao T N, et al. Carbon soot over layered sulfur impregnated coconut husk derived carbon: An

efficient polysulfide suppressor for lithium sulfur battery[J]. Materials Today Communications, 2020, 22: 100717.

[68] Li F, Qin F, Zhang K, et al. Hierarchically porous carbon derived from banana peel for lithium sulfur battery with high areal and gravimetric sulfur loading[J]. Journal of Power Sources, 2017, 362: 160-167.

[69] Xiang J, Lv W, Mu C, et al. Activated hard carbon from orange peel for lithium/sodium ion battery anode with long cycle life[J]. Journal of Alloys and Compounds, 2017, 701: 870-874.

[70] Yu W, Wang H, Liu S, et al. N, O-codoped hierarchical porous carbons derived from algae for high-capacity supercapacitors and battery anodes[J]. Journal of Materials Chemistry A, 2016, 4(16): 5973-5983.

[71] Zhang G, Liu X, Wang L, et al. Recent advances of biomass derived carbon-based materials for efficient electrochemical energy devices[J]. Journal of Materials Chemistry A, 2022, 10(17): 9277-9307.

[72] Raheem A, Prinsen P, Vuppaladadiyam A K, et al. A review on sustainable microalgae based biofuel and bioenergy production: Recent developments[J]. Journal of Cleaner Production, 2018, 181: 42-59.

[73] Shao H, Ai F, Wang W, et al. Crab shell-derived nitrogen-doped micro-/mesoporous carbon as an effective separator coating for high energy lithium–sulfur batteries[J]. Journal of Materials Chemistry A, 2017, 5(37): 19892-19900.

[74] Lu M, Qian Y, Yang C, et al. Nitrogen-enriched pseudographitic anode derived from silk cocoon with tunable flexibility for microbial fuel cells[J]. Nano Energy, 2017, 32: 382-388.

[75] Qu Y, Guo M, Wang X, et al. Novel nitrogen-doped ordered mesoporous carbon as high-performance anode material for sodium-ion batteries[J]. Journal of Alloys and Compounds, 2019, 791: 874-882.

[76] Ogura T, Hoshino R, Date Y, et al. Visualization of microfloral metabolism for marine waste recycling[J]. Metabolites, 2016, 6(1): 7.

[77] Illa M P, Sharma C S, Khandelwal M. Catalytic graphitization of bacterial cellulose–derived carbon nanofibers for stable and enhanced anodic performance of lithium-ion batteries[J]. Materials Today Chemistry, 2021, 20: 100439.

[78] Zuo X, Chang K, Zhao J, et al. Bubble-template-assisted synthesis of hollow fullerene-like MoS_2 nanocages as a lithium ion battery anode material[J]. Journal of Materials Chemistry A, 2016, 4(1): 51-58.

[79] Sun Y, Xiao H, Li H, et al. Nitrogen/oxygen co-doped hierarchically porous carbon for high-performance potassium storage[J]. Chemistry – A European Journal, 2019, 25(30): 7359-7365.

[80] Du X, Zhang Z, Liu W, et al. Nanocellulose-based conductive materials and their emerging applications in energy devices - A review[J]. Nano Energy, 2017, 35: 299-320.

[81] Chen X, Mi H, Ji C, et al. Hierarchically porous carbon microfibers for solid-state supercapacitors[J]. Journal of Materials Science, 2020, 55(13): 5510-5521.

[82] Lian Y, Yang N, bai Y, et al. Nb_2O_5 quantum dots confined in multi-chamber yeast carbon for sodium ion hybrid capacitors[J]. Journal of Alloys and Compounds, 2022, 896: 163128.

[83] Cheng J, Zhang G, Wang P, et al. Confined red phosphorus in edible fungus slag-derived porous carbon as an improved anode material in sodium-ion batteries[J]. ACS Applied Materials & Interfaces, 2019, 11(51): 47948-47955.

[84] Moradi M, Kim J C, Qi J, et al. A bio-facilitated synthetic route for nano-structured complex electrode materials[J]. Green Chemistry, 2016, 18(9): 2619-2624.

[85] Pakseresht S, Al-Ogaili A W M, Cetinkaya T, et al. Prevention of side reactions with a unique carbon-free catalyst biosynthesized by a virus template for non-aqueous and quasi-solid-state Li–O_2 batteries[J]. Journal of Power Sources, 2021, 509: 230374.

[86] Xu L, Guo W, Zeng L, et al. V_3Se_4 embedded within N/P co-doped carbon fibers for sodium/potassium ion batteries[J]. Chemical Engineering Journal, 2021, 419: 129607.

[87] Zhang L, Wang W, Lu S, et al. Carbon anode materials: A detailed comparison between Na-ion and K-ion batteries[J]. Advanced Energy Materials, 2021, 11(11): 2003640.

[88] Gao Z, Zhang Y, Song N, et al. Biomass-derived renewable carbon materials for electrochemical energy storage[J]. Materials Research Letters, 2017, 5(2): 69-88.

[89] Zhao L F, Hu Z, Lai W H, et al. Hard carbon anodes: Fundamental understanding and commercial perspectives for Na-ion batteries beyond Li-ion and K-ion counterparts[J]. Advanced Energy Materials, 2021, 11(1): 2002704.

[90] Xie F, Xu Z, Guo Z, et al. Hard carbons for sodium-ion batteries and beyond[J]. Progress in Energy, 2020, 2(4): 042002.

[91] Lu H, Zhao X S. Biomass-derived carbon electrode materials for supercapacitors[J]. Sustainable Energy & Fuels, 2017, 1(6): 1265-1281.

[92] Han S W, Jung D W, Jeong J H, et al. Effect of pyrolysis temperature on carbon obtained from green tea biomass for superior lithium ion battery anodes[J]. Chemical Engineering Journal, 2014, 254: 597-604.

[93] Pariyar P, Kumari K, Jain M K, et al. Evaluation of change in biochar properties derived from different feedstock and pyrolysis temperature for environmental and agricultural application[J]. The Science of the Total Environment, 2020, 713: 136433.

[94] Chen C, Huang Y, Zhu Y, et al. Nonignorable influence of oxygen in hard carbon for sodium ion storage[J]. Acs Sustainable Chemistry & Engineering, 2020, 8(3): 1497-1506.

[95] Deng J, Li M, Wang Y. Biomass-derived carbon: Synthesis and applications in energy storage and conversion[J]. Green Chemistry, 2016, 18(18): 4824-4854.

[96] Ma Q, Han L, Huang G. Effect of water-washing of wheat straw and hydrothermal temperature on its hydrochar evolution and combustion properties[J]. Bioresource Technology, 2018, 269: 96-103.

[97] Canales-Flores R A, Prieto-García F. Activation methods of carbonaceous materials obtained from agricultural waste[J]. Chemistry & Biodiversity, 2016, 13(3): 261-268.

[98] Sajjadi B, Chen W Y, Egiebor N. A comprehensive review on physical activation of biochar for energy and environmental applications[J]. Reviews in chemical engineering, 2019, 35(6): 735-776.

[99] Gao Y P, Zhai Z B, Huang K J, et al. Energy storage applications of biomass-derived carbon materials: Batteries and supercapacitors[J]. New Journal of Chemistry, 2017, 41(20): 11456-11470.

[100] Zhong Y, Xia X, Deng S, et al. Popcorn inspired porous macrocellular carbon: Rapid puffing fabrication from rice and its applications in lithium–sulfur batteries[J]. Advanced Energy Materials, 2018, 8(1): 1701110.

[101] Zheng Z, Hu S, Yin W, et al. CO_2-etching creates abundant closed pores in hard carbon for high-plateau-capacity sodium storage[J]. Advanced Energy Materials, 2024, 14(3): 2303064.

[102] Tian W, Gao Q, Tan Y, et al. Bio-inspired beehive-like hierarchical nanoporous carbon derived from bamboo-based industrial by-product as a high performance supercapacitor electrode material[J]. Journal of Materials Chemistry A, 2015, 3(10): 5656-5664.

[103] Wang P, Ye H, Yin Y X, et al. Fungi-enabled synthesis of ultrahigh-surface-area porous carbon[J]. Advanced Materials, 2019, 31(4): 1805134.

[104] Lv W, Wen F, Xiang J, et al. Peanut shell derived hard carbon as ultralong cycling anodes for lithium and sodium batteries[J]. Electrochimica Acta, 2015, 176: 533-541.

[105] Jiang L, Sheng L, Chen X, et al. Construction of nitrogen-doped porous carbon buildings using interconnected ultra-small carbon nanosheets for ultra-high rate supercapacitors[J]. Journal of Materials Chemistry A, 2016, 4(29): 11388-11396.

[106] Yu C, Hou H, Liu X, et al. Old-loofah-derived hard carbon for long cyclicity anode in sodium ion battery[J]. International Journal of Hydrogen Energy, 2018, 43(6): 3253-3260.

[107] Yu Z, Zhao Z, Peng T. Coralloid carbon material based on biomass as a promising anode material for lithium and sodium storage[J]. New Journal of Chemistry, 2021, 45(16): 7138-7144.

[108] Hong K L, Qie L, Zeng R, et al. Biomass derived hard carbon used as a high performance anode material for sodium ion batteries[J]. Journal of Materials Chemistry A, 2014, 2(32): 12733.

[109] Shen S, Xia X, Zhong Y, et al. Implanting niobium carbide into trichoderma spore carbon: a new advanced host for sulfur cathodes[J]. Advanced Materials, 2019, 31(16): 1900009.

[110] Shen Y, Sun S, Yang M, et al. Typha-derived hard carbon for high-performance sodium ion storage[J]. Journal of Alloys and Compounds, 2019, 784: 1290-1296.

[111] Hou J, Cao C, Ma X, et al. From rice bran to high energy density supercapacitors: a new route to control porous structure of 3D carbon[J]. Scientific Reports, 2014, 4: 7260.

[112] Li Y, Zhang X, Yang R, et al. The role of H_3PO_4 in the preparation of activated carbon from NaOH-treated rice husk residue[J]. RSC Advances, 2015, 5(41): 32626-32636.

[113] Mohammed A A, Chen C, Zhu Z. Low-cost, high-performance supercapacitor based on activated carbon electrode materials derived from baobab fruit shells[J]. Journal of Colloid and Interface Science, 2019, 538: 308-319.

[114] Wan Y, Shi Y, Zhao D. Supramolecular aggregates as templates: Ordered mesoporous polymers and carbons[J]. Chemistry of Materials, 2008, 20(3): 932-945.

[115] Liang C, Li Z, Dai S. Mesoporous carbon materials: Synthesis and modification[J]. Angewandte Chemie International Edition, 2008, 47(20): 3696-3717.

[116] Zhu S, Zhao N, Li J, et al. Hard-template synthesis of three-dimensional interconnected carbon networks: Rational design, hybridization and energy-related applications[J]. Nano Today, 2019, 29: 100796.

[117] Ou J, Wang J, Zhao G, et al. Buckwheat derived nitrogen-rich porous carbon material with a high-performance Na-storage[J]. Journal of Porous Materials, 2020, 27(4): 1139-1147.

[118] Ji K, Liang G, Shen Y, et al. Ordered macroporous graphenic carbon-based framework materials and their low-temperature co-sacrificial template synthesis mechanism[J]. Cell Reports Physical Science, 2023, 4(2): 101283.

[119] Chen C, Wang H, Han C, et al. Asymmetric flasklike hollow carbonaceous nanoparticles fabricated by the synergistic interaction between soft template and biomass[J]. Journal of the American Chemical Society, 2017, 139(7): 2657-2663.

[120] Feng S, Li W, Wang J, et al. Hydrothermal synthesis of ordered mesoporous carbons from a biomass-derived precursor for electrochemical capacitors[J]. Nanoscale, 2014, 6(24): 14657-14661.

[121] Nicolae S A, Szilágyi P Á, Titirici M M. Soft templating production of porous carbon adsorbents for CO_2 and H_2S capture[J]. Carbon, 2020, 169: 193-204.

[122] Zheng Z, Zhao B, Guo Y, et al. Preparation of mesoporous batatas biochar via soft-template method for high efficiency removal of tetracycline.[J]. Science of the Total Environment, 2021, 787(15): 147397.

[123] He B, Feng L M, Hong et al. A generic F-doped strategy for biomass hard carbon to achieve fast and stable kinetics in sodium/potassium-ion batteries[J]. Chemical Engineering Journal, 2024, 490(15): 151636.

[124] Li Y, Shi J, Wu F, et al. Dual-functionalized Ca enables high sodiation kinetics for hard carbon in sodium-ion batteries[J]. ACS Applied Materials & Interfaces, 2024, 16(2): 2397-2407.

[125] Zhu Y, Huang Y, Chen C, et al. Phosphorus-doped porous biomass carbon with ultra-stable performance in sodium storage and lithium storage[J]. Electrochimica Acta, 2019, 321: 134698.

[126] Wu F, Zhang M, Bai Y, et al. Lotus seedpod-derived hard carbon with hierarchical porous structure as stable anode for sodium-ion batteries[J]. ACS Applied Materials & Interfaces, 2019, 11(13): 12554-12561.

[127] Tang Z, Zhang R, Wang H, et al. Revealing the closed pore formation of waste wood-derived hard carbon for advanced sodium-ion battery[J]. Nature Communications, 2023, 14(1): 6024.

[128] Li Y, Lu Y, Meng Q, et al. Regulating pore structure of

hierarchical porous waste cork-derived hard carbon anode for enhanced Na storage performance[J]. Advanced Energy Materials, 2019, 9(48): 1902852.

[129] Liu X W, Liu H Y, Yuan R L, et al. Potato-starch-based hard carbon microspheres: Preparation and application as an anode material for sodium-ion batteries[J]. Solid State Ionics, 2024, 406: 116475.

[130] Chen S, Tang K, Song F, et al. Porous hard carbon spheres derived from biomass for high-performance sodium/potassium-ion batteries[J]. Nanotechnology, 2022, 33(5): 055401.

[131] Yu L H, Zhang L L, He X D, et al. Study of stable sodium ion storage in porous carbon derived from puffball biomass[J]. 2024, 208: 117805.

[132] Lyu T, Liang L, Kang Shen P. Hollow porous carbon spheres for high initial coulombic efficiency and low-potential sodium ion storage[J]. Journal of Colloid and Interface Science, 2021, 604: 168-177.

[133] Khan M, Ahmad N, Lu K, et al. Nitrogen-doped carbon derived from onion waste as anode material for high performance sodium-ion battery[J]. Solid State Ionics, 2020, 346: 115223.

[134] Hu X, Fan X, Mou Z, et al. Controlled synthesis of multi-doped highly-disordered porous biomass carbon microsphere for ultra-stable and fast sodium storage[J]. Journal of Energy Storage, 2024, 83(1): 110619.

[135] Nagmani, Verma P, Puravankara S. Jute-fiber precursor-derived low-cost sustainable hard carbon with varying micro/mesoporosity and distinct storage mechanisms for sodium-ion and potassium-ion batteries[J]. Langmuir, 2022, 38(50): 15703-15713.

[136] Wang H, Chen H, Chen C, et al. Tea-derived carbon materials as anode for high-performance sodium ion batteries[J]. Chinese Chemical Letters, 2023, 34(4): 107465.

[137] Wang C, Huang J, Li J, et al. Revealing the effect of nanopores in biomass-derived carbon on its sodium-ion storage behavior[J]. ChemElectroChem, 2020, 7(1): 201-211.

[138] Tao S, Xu W, Zheng J, et al. Soybean roots-derived N, P Co-doped mesoporous hard carbon for boosting sodium and potassium-ion batteries[J]. Carbon, 2021, 178: 233-242.

[139] Sarma H R, Sun J, Hora Y, et al. Effect of carbonization behaviour of cotton biomass in electrodes for sodium-ion batteries[J]. ChemElectroChem, 2023, 10(14): e202300127.

[140] Zhang T Y, Zhang T, Wang F J, et al. High-efficiently doping nitrogen in kapok fiber-derived hard carbon used as anode materials for boosting rate performance of sodium-ion batteries[J]. Journal of Energy Chemistry, 2024, 96: 472-482.

[141] Yang D, Li S, Cheng D, et al. Nitrogen, Sulfur, and Phosphorus codoped hollow carbon microtubes derived from silver willow blossoms as a high-performance anode for sodium-ion batteries[J]. Energy & Fuels, 2021, 35(3): 2795-2804.

[142] Saikia D, Deka J R, Lu B J, et al. Pinecone-derived biomass carbons as anodes for lithium and sodium-ion batteries by template-assisted and chemically activated approaches[J]. Journal of Power Sources, 2023, 580(1): 233329.

[143] Muruganantham R, Wang F M, Liu W R. A green route N, S-doped hard carbon derived from fruit-peel biomass waste as an anode material for rechargeable sodium-ion storage applications[J]. Electrochimica Acta, 2022, 424: 140573.

[144] Tang Y, He J, Peng J, et al. Electrochemical behavior of the biomass hard carbon derived from waste corncob as a sodium-ion battery anode[J]. Energy & Fuels, 2024, 38(8): 7389-7398.

[145] Ghani U, Iqbal N, Aboalhassan A A, et al. One-step sonochemical fabrication of biomass-derived porous hard carbons; towards tuned-surface anodes of sodium-ion batteries[J]. Journal of Colloid and Interface Science, 2022, 611: 578-587.

[146] Sun Y J, Li X, Zhang Y, et al. One-step production of capacitive-dominated carbon anode derived from biomass for sodium-ion batteries[J]. Inorganic Chemistry Communications, 2022, 144: 109921.

[147] Li L, Sun M, Xu Z, et al. Hierarchical porous hard carbon derived from rice husks for high-performance sodium ion storage[J]. Colloids and Surfaces A: Physicochemical and Engineering Aspects, 2023, 661: 130927.

[148] Wang T, Liu L, Wei Y, et al. Agar-derived slope-dominated carbon anode with puparium like nano-morphology for cost-effective SIBs[J]. 2024, 20(20): 2309809.

[149] Zheng J, Yu K, Wang X, et al. Nitrogen self-doped porous carbon based on sunflower seed hulls as excellent double anodes for potassium/sodium ion batteries[J]. Diamond and Related Materials, 2023, 131: 109593.

[150] He L, Sun W, Sun K, et al. Nitrogen and sulfur co-doped hierarchically mesoporous carbon derived from biomass as high-performance anode materials for superior sodium storage[J]. Journal of Power Sources, 2022, 526: 231019.

[151] Zou X F, Dong C, Jin Y C, et al. Engineering of N, P co-doped hierarchical porous carbon from sugarcane bagasse for high-performance supercapacitors and sodium ion batteries[J]. 2023, 672(5): 131715.

[152] Aristote N T, Song Z R, Deng W T, et al. Effect of double and triple-doping of sulfur, nitrogen and phosphorus on the initial coulombic efficiency and rate performance of the biomass derived hard carbon as anode for sodium-ion batteries[J]. Journal of Power Sources, 2023, 558(28): 232517.

[153] Zhao R, Sun N, Xu B. Recent advances in heterostructured carbon materials as anodes for sodium-ion batteries[J]. Small Structures, 2021, 2(12): 2100132.

[154] Huang Y, Wang Y, Bai P, et al. Storage mechanism of alkali metal ions in the hard carbon anode: An electrochemical viewpoint[J]. ACS Applied Materials & Interfaces, 2021, 13(32): 38441-38449.

[155] Chen D, Zhang W, Luo K, et al. Hard carbon for sodium storage: mechanism and optimization strategies toward commercialization[J]. Energy & Environmental Science, 2021, 14(4): 2244-2262.

[156] Chu Y, Zhang J, Zhang Y, et al. Reconfiguring hard carbons with emerging sodium-ion batteries: A perspective[J]. Advanced Materials, 2023, 35(31): 2212186.

[157] Katsuyama Y, Nakayasu Y, Kobayashi H, et al. Rational route for increasing intercalation capacity of hard carbons as sodium-ion

battery anodes[J]. ChemSusChem, 2020, 13(21): 5762-5768.

[158] Kubota K, Shimadzu S, Yabuuchi N, et al. Structural analysis of sucrose-derived hard carbon and correlation with the electrochemical properties for lithium, sodium, and potassium insertion[J]. Chemistry of Materials, 2020, 32(7): 2961-2977.

[159] Wu C, Yang Y, Zhang Y, et al. Hard carbon for sodium-ion batteries: progress, strategies and future perspective[J]. Chemical Science, 2024, 15(17): 6244-6268.

[160] Meng Q, Lu Y, Ding F, et al. Tuning the closed pore structure of hard carbons with the highest Na storage capacity[J]. ACS Energy Letters, 2019, 4(11): 2608-2612.

[161] Olsson E, Cottom J, Au H, et al. Elucidating the effect of planar graphitic layers and cylindrical pores on the storage and diffusion of Li, Na, and K in carbon materials[J]. Advanced Functional Materials, 2020, 30(17): 1908209.

[162] Alvin S, Chandra C, Kim J. Extended plateau capacity of phosphorus-doped hard carbon used as an anode in Na- and K-ion batteries[J]. Chemical Engineering Journal, 2020, 391: 123576.

[163] Cao Y, Xiao L, Sushko M L, et al. Sodium ion insertion in hollow carbon nanowires for battery applications[J]. Nano Letters, 2012, 12(7): 3783-3787.

[164] Li R, Huang J, Xu Z, et al. Controlling the thickness of disordered turbostratic nanodomains in hard carbon with enhanced sodium storage performance[J]. Energy Technology, 2018, 6(6): 1080-1087.

[165] Song Z, Di M, Chen S, et al. Three-dimensional N/O co-doped hard carbon anode enabled superior stabilities for sodium-ion batteries[J]. Chemical Engineering Journal, 2023, 470: 144237.

[166] Zhao Y, Ye J, Zhang P, et al. Abnormal preferential oxygen functionalization on the surface of soft/hard carbon for sodium storage[J]. Applied Surface Science, 2022, 602: 154336.

[167] Lin Q, Zhang J, Lv W, et al. A functionalized carbon surface for high-performance sodium-ion storage[J]. Small, 2020, 16(15): e1902603.

[168] Liu Y, Dai H, Wu L, et al. A large scalable and low-cost sulfur/nitrogen dual-doped hard carbon as the negative electrode material for high-performance potassium-ion batteries[J]. Advanced Energy Materials, 2019, 9(34): 1901379.

[169] Zhu Z, Liang F, Zhou Z, et al. Expanded biomass-derived hard carbon with ultra-stable performance in sodium-ion batteries[J]. Journal of Materials Chemistry A, 2018, 6(4): 1513-1522.

[170] Yang J, Wang X, Dai W, et al. From micropores to ultra-micropores inside hard carbon: Toward enhanced capacity in room-/low-temperature sodium-ion storage[J]. Nano-Micro Letters, 2021, 13(1): 98.

[171] Yue L, Lei Y, Niu Y, et al. Recent advances of pore structure in disordered carbons for sodium storage: A mini review[J]. Chemical Record (New York, N. Y.), 2022, 22(10): e202200113.

[172] Chen X, Liu C, Fang Y, et al. Understanding of the sodium storage mechanism in hard carbon anodes[J]. Carbon Energy, 2022, 4(6): 1133-1150.

[173] Bommier C, Surta T W, Dolgos M, et al. New mechanistic insights on Na-ion storage in nongraphitizable carbon[J]. Nano Letters, 2015, 15(9): 5888-5892.

[174] Qiu S, Xiao L, Sushko M L, et al. Manipulating adsorption–insertion mechanisms in nanostructured carbon materials for high-efficiency sodium ion storage[J]. Advanced Energy Materials, 2017, 7(17): 1700403.

[175] Sun N, Guan Z, Liu Y, et al. Extended "Adsorption–Insertion" model: A new insight into the sodium storage mechanism of hard carbons[J]. Advanced Energy Materials, 2019, 9(32): 1901351.

[176] Chen X, Tian J, Li P, et al. An overall understanding of sodium storage behaviors in hard carbons by an "Adsorption-Intercalation/Filling" hybrid mechanism[J]. Advanced Energy Materials, 2022, 12(24): 2200886.

[177] Zhang B, Ghimbeu C M, Laberty C, et al. Correlation between microstructure and Na storage behavior in hard carbon[J]. Advanced Energy Materials, 2016, 6(1): 1501588.

[178] Tian Z, Zou Y, Liu G, et al. Electrolyte solvation structure design for sodium ion batteries[J]. Advanced Science, 2022, 9(22): 2201207.

[179] Zhen Y, Sa R, Zhou K, et al. Breaking the limitation of sodium-ion storage for nanostructured carbon anode by engineering desolvation barrier with neat electrolytes[J]. Nano Energy, 2020, 74: 104895.

[180] Dong R, Zheng L, Bai Y, et al. Elucidating the mechanism of fast Na storage kinetics in ether electrolytes for hard carbon anodes[J]. Advanced Materials, 2021, 33(36): 2008810.

[181] Yi X, Li X, Zhong J, et al. Unraveling the mechanism of different kinetics performance between ether and carbonate ester electrolytes in hard carbon electrode[J]. Advanced Functional Materials, 2022, 32(48): 2209523.

[182] Ponrouch A, Monti D, Boschin A, et al. Non-aqueous electrolytes for sodium-ion batteries[J]. Journal of Materials Chemistry A, 2014, 3(1): 22-42.

[183] Zhang J, Wang D W, Lv W, et al. Achieving superb sodium storage performance on carbon anodes through an ether-derived solid electrolyte interphase[J]. Energy & Environmental Science, 2017, 10(1): 370-376.

[184] Yin X, Wang Z, Liu Y, et al. Insight into the influence of ether and ester electrolytes on the sodium-ion transportation kinetics for hard carbon[J]. Nano Research, 2023, 16(8): 10922-10930.

[185] Wang K, Li M, Zhu Z, et al. Hard carbon with embedded graphitic nanofibers for fast-charge sodium-ion batteries[J]. Nano Energy, 2024, 124: 109459.

[186] Lan N, Shen Y, Li J, et al. Cell-shearing chemistry directed closed-pore regeneration in biomass-derived hard carbons for ultrafast sodium storage[J]. Advanced Materials, 2412989.

[187] Asfaw H D, Gond R, Kotronia A, et al. Bio-derived hard carbon nanosheets with high rate sodium-ion storage characteristics[J]. Sustainable Materials and Technologies, 2022, 32: e00407.

[188] Medina A, Alcántara R, Lavela P, et al. A facile method to transform pickled olive wastes into sulfur-doped carbon for sodium-ion battery electrode[J]. ChemSusChem, 2024, e202400708.

[189] Wan H, Ju X, He T, et al. Sulfur-doped porous carbon as high-

capacity anodes for lithium and sodium ions batteries[J]. Journal of Alloys and Compounds, 2021, 863: 158078.

[190] Zhao G, Yu D, Zhang H, et al. Sulphur-doped carbon nanosheets derived from biomass as high-performance anode materials for sodium-ion batteries[J]. Nano Energy, 2020, 67: 104219.

[191] Yan J, Li H, Wang K, et al. Ultrahigh phosphorus doping of carbon for high-rate sodium ion batteries anode[J]. Advanced Energy Materials, 2021, 11(21): 2003911.

[192] Wang P, Qiao B, Du Y, et al. Fluorine-doped carbon particles derived from lotus petioles as high-performance anode materials for sodium-ion batteries[J]. The Journal of Physical Chemistry C, 2015, 119(37): 21336-21344.

[193] Kong L, Li Y, Feng W. Fluorine-doped hard carbon as the advanced performance anode material of sodium-ion batteries[J]. Transactions of Tianjin University, 2022, 28(2): 123-131.

[194] Ghosh S, Barg S, Jeong S M, et al. Heteroatom-doped and oxygen-functionalized nanocarbons for high-performance supercapacitors[J]. Advanced Energy Materials, 2020, 10(32): 2001239.

[195] Han P, Cheng M, Luo D, et al. Selective etching of C-N bonds for preparation of porous carbon with ultrahigh specific surface area and superior capacitive performance[J]. Energy Storage Materials, 2020, 24: 486-494.

[196] Yang Y, Tang D M, Zhang C, et al. “Protrusions” or “holes” in graphene: which is the better choice for sodium ion storage?[J]. Energy & Environmental Science, 2017, 10(4): 979-986.

[197] Qiao Y, Ma M, Liu Y, et al. First-principles and experimental study of nitrogen/sulfur co-doped carbon nanosheets as anodes for rechargeable sodium ion batteries[J]. Journal of Materials Chemistry A, 2016, 4(40): 15565-15574.

[198] Yan Z, Yang Q W, Wang Q, et al. Nitrogen doped porous carbon as excellent dual anodes for Li- and Na-ion batteries[J]. Chinese Chemical Letters, 2020, 31(2): 583-588.

[199] Feng X, Bai Y, Zheng L, et al. Effect of different nitrogen configurations on sodium storage properties of carbon anodes for sodium ion batteries[J]. ACS applied materials & interfaces, 2021, 13(47): 56285-56295.

[200] Liu H, Jia M, Yue S, et al. Creative utilization of natural nanocomposites: nitrogen-rich mesoporous carbon for a high-performance sodium ion battery[J]. Journal of Materials Chemistry A, 2017, 5(20): 9572-9579.

[201] Wang D, Du G, Han D, et al. Porous flexible nitrogen-rich carbon membranes derived from chitosan as free-standing anodes for potassium-ion and sodium-ion batteries[J]. Carbon, 2021, 181: 1-8.

[202] Araujo P T, Terrones M, Dresselhaus M S. Defects and impurities in graphene-like materials[J]. Materials Today, 2012, 15(3): 98-109.

[203] Qie L, Chen W, Xiong X, et al. Sulfur-doped carbon with enlarged interlayer distance as a high-performance anode material for sodium-ion batteries[J]. Advanced Science, 2015, 2(12): 1500195.

[204] Wu X, Chen Y, Xing Z, et al. Advanced carbon-based anodes for potassium-ion batteries[J]. Advanced Energy Materials, 2019, 9(21): 1900343.

[205] Hou Z, Wang X, Ikeda T, et al. Interplay between nitrogen dopants and native point defects in graphene[J]. Physical Review B, 2012, 85(16): 165439.

[206] Li Y, Chen M, Liu B, et al. Heteroatom doping: An effective way to boost sodium ion storage[J]. Advanced Energy Materials, 2020, 10(27): 2000927.

[207] Jin Q, Li W, Wang K, et al. Experimental design and theoretical calculation for sulfur-doped carbon nanofibers as a high performance sodium-ion battery anode[J]. Journal of Materials Chemistry A, 2019, 7(17): 10239-10245.

[208] Qiao Y, Han R, Pang Y, et al. 3D well-ordered porous phosphorus doped carbon as an anode for sodium storage: structure design, experimental and computational insights[J]. Journal of Materials Chemistry A, 2019, 7(18): 11400-11407.

[209] Yang W, Yang W, Kong L, et al. Phosphorus-doped 3D hierarchical porous carbon for high-performance supercapacitors: A balanced strategy for pore structure and chemical composition[J]. Carbon, 2018, 127: 557-567.

[210] Lü H Y, Zhang X H, Wan F, et al. Flexible P-doped carbon cloth: Vacuum-sealed preparation and enhanced Na-storage properties as binder-free anode for sodium ion batteries[J]. ACS applied materials & interfaces, 2017, 9(14): 12518-12527.

[211] Liu T, Zhang F, Song Y, et al. Revitalizing carbon supercapacitor electrodes with hierarchical porous structures[J]. Journal of Materials Chemistry A, 2017, 5(34): 17705-17733.

[212] Xu Z, Deng W, Wang X. 3D hierarchical carbon-rich micro-/nanomaterials for energy storage and catalysis[J]. Electrochemical Energy Reviews, 2021, 4(2): 269-335.

[213] Hong W, Zhang Y, Yang L, et al. Carbon quantum dot micelles tailored hollow carbon anode for fast potassium and sodium storage[J]. Nano Energy, 2019, 65: 104038.

[214] Zhao G, Yu D, Chen C, et al. One-step production of carbon nanocages for supercapacitors and sodium-ion batteries[J]. Journal of Electroanalytical Chemistry, 2020, 878: 114551.

[215] Li Y, Xu S, Wu X, et al. Amorphous monodispersed hard carbon micro-spherules derived from biomass as a high performance negative electrode material for sodium-ion batteries[J]. Journal of Materials Chemistry A, 2015, 3(1): 71-77.

[216] Zhong X, Li Y, Zhang L, et al. High-performance sodium-ion batteries based on nitrogen-doped mesoporous carbon spheres with ultrathin nanosheets[J]. ACS Applied Materials & Interfaces, 2019, 11(3): 2970-2977.

[217] Tomas C de, Alabidun S, Chater L, et al. Doping carbon electrodes with sulfur achieves reversible sodium ion storage[J]. Journal of Physics: Energy, 2023, 5(2): 024006.

[218] Lian Y, Xin W, Zhang M, et al. Low-content Ni-doped CoS_2 embedded within N, P-codoped biomass-derived carbon spheres for enhanced lithium/sodium storage[J]. Journal of Materials Science, 2019, 54(11): 8504-8514.

[219] Chen F, Di Y, Su Q, et al. Vanadium-modified hard carbon spheres with sufficient pseudographitic domains as high-

performance anode for sodium-ion batteries[J]. Carbon Energy, 2023, 5(2): e191.

[220] Wang B, Wang H, Chen W, et al. Carbonized cotton fiber supported flexible organic lithium ion battery cathodes[J]. Journal of Colloid and Interface Science, 2020, 572: 1-8.

[221] Li Z, Guan Z, Guan Z, et al. Effect of deep cryogenic activated treatment on hemp stem-derived carbon used as anode for lithium-ion batteries[J]. Nanoscale Research Letters, 2020, 15(1): 193.

[222] Shen F, Zhu H, Luo W, et al. Chemically crushed wood cellulose fiber towards high-performance sodium-ion batteries[J]. ACS applied materials & interfaces, 2015, 7(41): 23291-23296.

[223] Pei L, Yang L, Cao H, et al. Cost-effective and renewable paper derived hard carbon microfibers as superior anode for sodium-ion batteries[J]. Electrochimica Acta, 2020, 364: 137313.

[224] Sun J, Rakov D, Wang J, et al. Sustainable free-standing electrode from biomass waste for sodium-ion batteries[J]. 2022, 9(16): e202200382.

[225] Ren Q, Wang J, Yan L, et al. Manipulating free-standing, flexible and scalable microfiber carbon papers unlocking ultra-high initial Coulombic efficiency and storage sodium behavior[J]. Chemical Engineering Journal, 2021, 425: 131656.

[226] Chen Y, Zhao X, He J, et al. Engineering stress-release structures based on biological swelling in carbon fibers for stable sodium ion storage[J]. ACS Applied Energy Materials, 2022, 5(5): 6091-6099.

[227] Gao J, Wang X, Lu X, et al. Coal-based hierarchically porous carbon nanofibers as high-performance anode for sodium-ion batteries[J]. ChemElectroChem, 2022, 9(15).

[228] Chen Y, Wu Y, Liao Y, et al. Tuning carbonized wood fiber via sacrificial template-assisted hydrothermal synthesis for high-performance lithium/sodium-ion batteries[J]. Journal of Power Sources, 2022, 546: 231993.

[229] Li X, Yang C, Wang S, et al. Comprehensive study on improving the sodium storage performance of low-defect biomass-derived carbon through S or N doping[J]. Diamond and Related Materials, 2022, 129: 109382.

[230] Ye J, Zhao H, Song W, et al. Enhanced electronic conductivity and sodium-ion adsorption in N/S co-doped ordered mesoporous carbon for high-performance sodium-ion battery anode[J]. Journal of Power Sources, 2019, 412: 606-614.

[231] Li Z, Bommier C, Chong Z S, et al. Mechanism of Na-ion storage in hard carbon anodes revealed by heteroatom doping[J]. Advanced Energy Materials, 2017, 7(18): 1602894.

[232] Li J, Wang L, Li L, et al. Metal sulfides@carbon microfiber metworks for boosting lithium ion/sodium ion storage via a general metal-aspergillus niger bioleaching strategy[J]. Acs Applied Materials & Interfaces, 2019, 11(8): 8072-8080.

[233] Zheng J G, Xiao F Y, Jin H J, et al. Facile fabrication of MoS_2 nanocrystals confined in waste leather derived N, P co-doped carbon fiber for long-lifespan of sodium/potassium ion batteries[J]. Journal of Physics and Chemistry of Solids, 2023, 172: 111080.

[234] Li B, Liu Y, Jin X, et al. Designed formation of hybrid nanobox composed of carbon sheathed $CoSe_2$ anchored on nitrogen-doped carbon skeleton as ultrastable anode for sodium-ion batteries[J]. Small, 2019, 15(42): 1902881.

[235] Chen W, Zhang X, Mi L, et al. High performance flexible freestanding anode with hierarchical 3D carbon-networks/Fe_7S_8/graphene for applicable sodium-ion batteries[J]. Advanced Materials, 2019, 31(8): 1806664.

[236] Wang Q, Zhang W, Guo C, et al. In situ construction of 3D interconnected FeS@Fe_3C@graphitic carbon networks for high-performance sodium-ion batteries[J]. Advanced Functional Materials, 2017, 27(41): 1703390.

[237] Zhang Y, Lv C, Wang X, et al. Boosting sodium-ion storage by encapsulating NiS (CoS) hollow nanoparticles into carbonaceous fibers[J]. ACS Applied Materials & Interfaces, 2018, 10(47): 40531-40539.

[238] Li D, Sun Y, Chen S, et al. Highly porous FeS/carbon fibers derived from Fe-carrageenan biomass: High-capacity and durable anodes for sodium-ion batteries[J]. ACS Applied Materials & Interfaces, 2018, 10(20): 17175-17182.

[239] Teng Y, Mo M, Li Y. Microtubular hard carbon derived from willow catkins as an anode material with enhanced performance for sodium-ion batteries[J]. Journal of Electrochemical Energy Conversion and Storage, 2018, 15(041010).

[240] Yu Z E, Lyu Y, Wang Y, et al. Hard carbon micro-nano tubes derived from kapok fiber as anode materials for sodium-ion batteries and the sodium-ion storage mechanism[J]. Chemical Communications, 2020, 56(5): 778-781.

[241] Liu H, Liu H, Di S, et al. Advantageous tubular structure of biomass-derived carbon for high-performance sodium storage[J]. ACS Applied Energy Materials, 2021, 4(5): 4955-4965.

[242] Rawat S, Mishra R K, Bhaskar T. Biomass derived functional carbon materials for supercapacitor applications[J]. Chemosphere, 2022, 286: 131961.

[243] Zhou Y, He J, Chen R, et al. Recent advances in biomass-derived graphene and carbon nanotubes[J]. Materials Today Sustainability, 2022, 18: 100138.

[244] Wu D H, Huang H, Ul Haq M, et al. Lignin-derived iron carbide/Mn, N, S-codoped carbon nanotubes as a high-efficiency catalyst for synergistically enhanced oxygen reduction reaction and rechargeable zinc-air battery[J]. Journal of Colloid and Interface Science, 2023, 647: 1-11.

[245] Wang Q, Ge X, Xu J, et al. Fabrication of microporous sulfur-doped carbon microtubes for high-performance sodium-ion batteries[J]. ACS Applied Energy Materials, 2018, 1(11): 6638-6645.

[246] Yang H, Yin J, Yang J T, et al. From macro to micro: Biomass-derived advanced carbon microtube assembly for sodium-ion batteries[J]. Nano Energy, 2024, 125: 109591.

[247] Tong M, Cao B, Li Y, et al. Biomass carbon combined antimony sulfide with various contents as anodes with improved cycle stability in the sodium ion batteries[J]. Journal of Alloys and Compounds, 2023, 936: 168270.

[248] Chen K, Li G, Wang Y, et al. High loading FeS_2 nanoparticles

anchored on biomass-derived carbon tube as low cost and long cycle anode for sodium-ion batteries[J]. Green Energy & Environment, 2020, 5(1): 50-58.

[249] Luo Y, Li X, Hao X, et al. Few layers 2D MoS_2/tubular sisal fiber-derived carbon composite: Enhanced cycling performance as anode material for sodium-ion batteries[J]. Journal of Energy Storage, 2023, 67: 107463.

[250] Li C, Li J, Zhang Y, et al. Heteroatom-doped hierarchically porous carbons derived from cucumber stem as high-performance anodes for sodium-ion batteries[J]. Journal of Materials Science, 2019, 54(7): 5641-5657.

[251] Qin D, Chen S. A sustainable synthesis of biomass carbon sheets as excellent performance sodium ion batteries anode[J]. Journal of Solid State Electrochemistry, 2017, 21(5): 1305-1312.

[252] Hu H Y, Xiao Y, Ling W, et al. A Stable biomass-derived hard carbon anode for high-performance sodium-ion full battery[J]. Energy Technology, 2021, 9(1): 2000730.

[253] Jiang K, Tan X, Zhai S, et al. Carbon nanosheets derived from reconstructed lignin for potassium and sodium storage with low voltage hysteresis[J]. Nano Research, 2021, 14(12): 4664-4673.

[254] Yue L, Xu W, Li K, et al. 3D nitrogen and sulfur equilibrium co-doping hollow carbon nanosheets as Na-ion battery anode with ultralong cycle life and superior rate capability[J]. Applied Surface Science, 2021, 546: 149168.

[255] Shen H, Zhao H, Kang M, et al. Sodium storage in coal/biomass-derived carbon/carbon 3D networks[J]. ChemElectroChem, 2019, 6(17): 4541-4544.

[256] Wang P, Wang H, Liang C, et al. Two-dimensional porous flake biomass carbon with large layer spacing as an anode material for sodium ion batteries[J]. Diamond and Related Materials, 2023, 131: 109601.

[257] Wang Y Y, Hou B H, Ning Q L, et al. Hierarchically porous nanosheets-constructed 3D carbon network for ultrahigh-capacity supercapacitor and battery anode[J]. Nanotechnology, 2019, 30(21): 214002.

[258] Zhang M, Li Y, Wu F, et al. Boost sodium-ion batteries to commercialization: Strategies to enhance initial Coulombic efficiency of hard carbon anode[J]. Nano Energy, 2021, 82: 105738.

[259] Aristote N T, Zou K, Di A, et al. Methods of improving the initial Coulombic efficiency and rate performance of both anode and cathode materials for sodium-ion batteries[J]. Chinese Chemical Letters, 2022, 33(2): 730-742.

[260] Aristote N T, Liu C, Deng X, et al. Sulfur-doping biomass based hard carbon as high performance anode material for sodium-ion batteries[J]. Journal of Electroanalytical Chemistry, 2022, 923: 116769.

[261] Xu C, Yang W, Ma G, et al. Edge-nitrogen enriched porous carbon nanosheets anodes with enlarged interlayer distance for fast charging sodium-ion batteries[J]. Small, 2022, 18(48): 2204375.

[262] Gao M, Xue Y, Zhang Y, et al. Growing Co–Ni–Se nanosheets on 3D carbon frameworks as advanced dual functional electrodes for supercapacitors and sodium ion batteries[J]. Inorganic Chemistry Frontiers, 2022, 9(15): 3933-3942.

[263] Yin Y, Zhang Y, Liu N, et al. Biomass-derived P/N-co-Doped carbon nanosheets encapsulate Cu_3P nanoparticles as high-performance anode materials for sodium-ion batteries[J]. Frontiers in Chemistry, 2020, 8: 316.

[264] Zhong G, Xu S, Chao J, et al. Biomass-derived nitrogen-doped porous carbons activated by magnesium chloride as ultrahigh-performance supercapacitors[J]. Industrial & Engineering Chemistry Research, 2020, 59(50): 21756-21767.

[265] Chen C, Huang Y, Meng Z, et al. N/O/P-rich three-dimensional carbon network for fast sodium storage[J]. Carbon, 2020, 170: 225-235.

[266] Mehmood A, Ali G, Koyutürk B, et al. Nanoporous nitrogen doped carbons with enhanced capacity for sodium ion battery anodes[J]. Energy Storage Materials, 2020, 28: 101-111.

[267] Kuai J, Xie J, Wang J D, et al. Comparison and optimization of biomass-derived hard carbon as anode materials for sodium-ion batteries[J]. Chemical Physics Letters, 2024, 842: 141214.

[268] Jeon I, Kim T, Seo J, et al. Enhanced electrochemical performance and interdiffusion behavior of sodium ions in onion-derived freeze-dried and KOH-activated carbon for sodium-ion battery anodes[J]. Applied Surface Science, 2024, 2024,648: 159023.

[269] Wang X K, Shi J, Mi L W, et al. Hierarchical porous hard carbon enables integral solid electrolyte interphase as robust anode for sodium-ion batteries[J]. Rare Metals, 2020, 39(9): 1053-1062.

[270] Zhu Y, Huang Y, Wang M, et al. Nitrogen and phosphorus co-doped 3D hierarchical porous carbon network with highly-reversible performance in sodium storage[J]. Ceramics International, 2019, 45(18, Part A): 24500-24507.

[271] Qiu D, Kang C, Li M, et al. Biomass-derived mesopore-dominant hierarchical porous carbon enabling ultra-efficient lithium ion storage[J]. Carbon, 2020, 162: 595-603.

[272] Chen Y, Liu H, Jiang B, et al. Hierarchical porous architectures derived from low-cost biomass equisetum arvense as a promising anode material for lithium-ion batteries[J]. Journal of Molecular Structure, 2020, 1221: 128794.

[273] Yang M, Kong Q, Feng W, et al. N/O double-doped biomass hard carbon material realizes fast and stable potassium ion storage[J]. Carbon, 2021, 176: 71-82.

[274] Liu Z, Wang J, Bi R, et al. Ultrasmall NiS_2 nanocrystals embedded in ordered macroporous graphenic carbon matrix for efficiently pseudocapacitive sodium storage[J]. Transactions of Tianjin University, 2023, 29(2): 89-100.

[275] Ghani U, Iqbal N, Li J, et al. Improved Na-ion kinetics of 1T MoS_2 nanopatterned porous hard carbon as an ultra-long life anode[J]. Electrochimica Acta, 2022, 432: 141130.

[276] Chen Y, Zhao Y, Liu H, et al. Crab shell-derived SnS_2/C and FeS_2/C carbon composites as anodes for high-performance sodium-ion batteries[J]. ACS Omega, 2023, 8(10): 9145-9153.

[277] Lu B, Deng D, Song J, et al. One-step in-situ synthesis of bimetallic-doped disordered carbons as anode for high-performance sodium-ion batteries[J]. Journal of Alloys and Compounds, 2024, 988: 174280.

[278] Guo W, Yu C, Li S, et al. Toward commercial-level mass-loading electrodes for supercapacitors: opportunities, challenges and perspectives[J]. Energy & Environmental Science, 2021, 14(2): 576-601.

[279] Lv Z, Yue M, Ling M, et al. Controllable design coupled with finite element analysis of low-tortuosity electrode architecture for advanced sodium-ion batteries with ultra-high mass loading[J]. Advanced Energy Materials, 2021, 11(17): 2003725.

[280] Guo W, Dun C, Marcus M A, et al. The emerging layered hydroxide plates with record thickness for enhanced high-mass-loading energy storage[J]. Advanced Materials, 2023, 35(19): 2211603.

[281] Fan Z, Song W, Yang N, et al. Insights into the phase purity and storage mechanism of nonstoichiometric $Na_{3.4}$ $Fe_{2.4}(PO_4)_{1.4}P_2O_7$ Cathode for high-mass-loading and high-power-density sodium-ion batteries[J]. Angewandte Chemie International Edition, 2024, 63(8): e202316957.